

Osteochondral Tissue Engineering with  
Induced Pluripotent Stem Cells

by

Shannon Kathleen O'Connor

Department of Biomedical Engineering  
Duke University

Date: \_\_\_\_\_  
Approved: \_\_\_\_\_

\_\_\_\_\_  
Farshid Guilak, Supervisor

\_\_\_\_\_  
Charles Gersbach

\_\_\_\_\_  
Bruce Klitzman

\_\_\_\_\_  
Jeffrey Lawson

\_\_\_\_\_  
George Truskey

Dissertation submitted in partial fulfillment of the  
requirements for the degree of Doctor of Philosophy in the  
Department of Biomedical Engineering in the  
Graduate School of Duke University

2018

ABSTRACT

Osteochondral Tissue Engineering with

Induced Pluripotent Stem Cells

by

Shannon Kathleen O'Connor

Department of Biomedical Engineering  
Duke University

Date: \_\_\_\_\_

Approved:

\_\_\_\_\_  
Farshid Guilak, Supervisor

\_\_\_\_\_  
Charles Gersbach

\_\_\_\_\_  
Bruce Klitzman

\_\_\_\_\_  
Jeffrey Lawson

\_\_\_\_\_  
George Truskey

An abstract of a dissertation submitted in partial fulfillment of the requirements for the degree of Doctor of Philosophy in the Department of Biomedical Engineering in the Graduate School of Duke University

2018

Copyright by  
Shannon Kathleen O'Connor  
2018

## **Abstract**

With growing numbers of increasingly younger patients suffering debilitating arthropathies, the need for simple models that recapitulate the complex interplay between distinct joint tissues, and grafts that emulate these joint structures in their biological properties and their strength have become more urgent. The *objective* of this study is to engineer constructs of multiple tissue types by controlling the morphogenetic factors that direct stem cell differentiation and tissue formation either exogenously or via transduction of expression vectors. Our *hypothesis* is that sequential changes in exogenous growth factor delivery and also scaffold-mediated inducible regulation of morphogenetic gene expression and signaling in 3D-constructs of murine iPSCs will lead to the formation of both bone and cartilage tissue types, both as separate tissues, and as osteochondral constructs. In the first study, osteochondral organoids were grown in a scaffold-free system from a single iPSC cell source, creating tissues containing a distinct core with the genetic and extracellular matrix profile of articular cartilage surrounded by a shell with the genetic and extracellular matrix profile of bone. In the second study, chondrogenic, osteogenic, and osteochondral tissue grafts were grown by scaffold-mediated lentiviral delivery of differentiation factors expressed both constitutively and in a temporally inducible manner. These constructs will provide an excellent platform to study diseases of the osteochondral junction, to screen pharmacologic therapies affecting both cartilage and bone tissue, and as a next step toward making an implantable osteochondral graft for the direct treatment of joint defects.

# Contents

Abstract .....	iv
List of Tables .....	viii
List of Figures .....	ix
Acknowledgements .....	xii
1. Introduction.....	1
2. Background .....	7
2.1 Chondrogenically induced pluripotent stem cells (iPSCs):.....	7
2.2 Osteochondral tissue engineering .....	9
2.3 Unmet need: osteochondral organoids.....	11
2.4 3D-Woven polymer scaffolds.....	12
2.5 Biomaterial-Mediated Gene Delivery.....	14
2.6 Temporally Controlled Biomaterial-Mediated Gene Delivery for Cell Differentiation and Tissue Formation.....	16
3. Chondrogenic Differentiation of Induced Pluripotent Stem Cells and Formation of Cartilaginous Extracellular Matrix Prevents Re-Induction of Pluripotency .....	18
3.1 Rationale and experimental plan .....	18
3.2 Methods.....	19
3.2.1 Chondrogenic differentiation of miPSCs via micromass formation, and purification of Col2-GFP miPSCs via flow cytometry.....	19
3.2.2 Cell culture: pellet formation, chondrogenic culture, endochondral ossification, and pluripotency induction .....	21
3.2.3 Gene expression analysis: RNA isolation and quantitative RT-PCR (qPCR).....	25
3.2.4 Histological analysis .....	27
3.2.5 MicroCT analysis .....	28
3.2.6 Biochemical analysis .....	29

3.2.7 Statistics .....	29
3.3 Results.....	29
3.3.1 Osteogenic induction after chondrogenesis .....	29
3.3.2 Chondrogenic outcomes.....	33
3.3.3 Doxycycline induction effect on multipotency .....	36
3.3.4 Doxycycline induction effect on pluripotency in 2D vs. 3D culture .....	41
3.4 Discussion: conclusions, limitations, and implications.....	46
3.4.1 Creation of an iPSC-derived osteochondral organoid .....	47
3.4.2 Creation of a robust osteochondral construct.....	48
3.4.3 Prevention of re-induction of pluripotency with cartilaginous extracellular matrix.....	49
4. Cartilage and Bone Tissue Engineering on 3D-Woven Scaffolds with Induced Pluripotent Stem Cells .....	51
4.1 Rationale and experimental plan .....	51
4.2 Methods.....	55
4.2.1 Chondrogenic differentiation of miPSCs via micromass formation, and purification of Col2-GFP miPSCs via flow cytometry.....	55
4.2.2 Lentivirus production.....	60
4.2.3 Production of 3D-woven PCL scaffold.....	61
4.2.4 Cell culture: scaffold construct formation and culture.....	61
4.2.5 Flow cytometry analysis of transduction efficiency.....	63
4.2.6 Gene expression analysis: RNA isolation and quantitative RT-PCR (qPCR).63	
4.2.7 Histological analysis .....	65
4.2.8 microCT analysis .....	67
4.2.9 ELISA and biochemical analysis.....	67
4.2.10 Statistics .....	68

4.3 Results.....	68
3.3.1 Osteogenic scaffold constructs.....	68
3.3.2 Chondrogenic scaffold constructs.....	75
4.4 Discussion: conclusions, limitations, and implications.....	80
4.4.1 Applications of bone, cartilage, and osteochondral tissue grafts.....	81
4.4.2 Applications of tissue constructs created without exogenous growth factor delivery .....	82
5. Conclusions and future applications.....	84
5.1 Disease modeling in a dish.....	85
5.2 Implantation of functional osteochondral grafts in animal models .....	86
References .....	88
Biography .....	99

## List of Tables

Table 3.1 qPCR primer probes.....	26
Table 4.1 Primer probes for qPCR.....	65

## List of Figures

Figure 2.1 miPSC chondrogenesis. ....	9
Figure 2.2 3D-woven scaffolds.....	14
Figure 2.4 Temporal control of gene expression, cell differentiation, and tissue formation. ....	17
Figure 3.1 Differentiation and purification of hESC-CMs. ....	18
Table 3.1 qPCR primer probes. ....	26
Figure 3.2 Flow sort analysis. ....	30
Figure 3.3 qPCR shows expected increase in osteogenic gene expression during osteogenic induction. ....	32
Figure 3.4 Histology and microCT demonstrate a shell of calcified tissue after osteogenic induction. ....	33
Figure 3.5 PCR shows expected increase in chondrogenic gene expression during chondrogenic induction, and decrease during osteogenic induction. ....	34
Figure 3.6 Histology demonstrates presence of cartilage matrix proteins throughout the timeline. ....	35
Figure 3.7 qPCR shows increase in osteogenic gene expression after dox treatment. ....	36
Figure 3.8 Histological and microCT show treatment with dox had little effect on osteogenic protein expression or mineralization. ....	37
Figure 3.9 qPCR shows decrease in chondrogenic gene expression after dox treatment. ....	38
Figure 3.10 Histological analysis shows treatment with dox had little effect on chondrogenic protein expression.....	39
Figure 3.11 Biochemical analysis of pellets. ....	40
Figure 3.12 MicroCT evaluation showed dox treatment had little effect on mineralization. ....	41
Figure 3.13 Colony pluripotency assay.....	43
Figure 3.14 Confocal image of pluripotent colony.....	44

<b>Figure 3.15 qPCR shows that doxycycline treatment does not restore pluripotency gene expression in pellet constructs after osteochondral induction. ....</b>	<b>45</b>
<b>Figure 4.1 Study design: osteogenic and chondrogenic tissue engineering on PCL 3D-woven scaffold with miPSCs. ....</b>	<b>53</b>
<b>Figure 4.2 Study design: experimental groups. ....</b>	<b>55</b>
<b>Figure 4.3 Flow sort analysis. ....</b>	<b>57</b>
<b>Figure 4.4 Alcian blue staining of micromasses. ....</b>	<b>58</b>
<b>Table 4.1 Primer probes for qPCR. ....</b>	<b>65</b>
<b>Figure 4.5 qPCR shows expected increase in osteogenic gene expression during osteogenic induction. ....</b>	<b>69</b>
<b>Figure 4.6 qPCR of hBMP2 shows expression in groups transduced with hBMP2, and no amplification in non-transduced groups. ....</b>	<b>70</b>
<b>Figure 4.7 qPCR shows increase in chondrogenic gene expression from day 0 during osteogenic induction, with smaller increases than in chondrogenic groups, as expected. ....</b>	<b>71</b>
<b>Figure 4.8 MicroCT imaging demonstrates mineralized tissue distributed through the scaffold. ....</b>	<b>72</b>
<b>Figure 4.9 MicroCT evaluation of bone volume demonstrated mineralization in all osteo groups, with significantly higher bone volumes in the BMP2 constitutive and the osteochondral groups. ....</b>	<b>73</b>
<b>Figure 4.10 MicroCT evaluation of bone volume (BV) and bone volume over tissue volume (BV/TV) demonstrated mineralization in all osteo groups, with significantly higher bone volumes in the BMP2 constitutive and the osteochondral groups. ....</b>	<b>73</b>
<b>Figure 4.11 MicroCT evaluation of bone mineral density demonstrated mineralization in all osteo groups. ....</b>	<b>74</b>
<b>Figure 4.12 ELISA assay demonstrates early expression of BMP-2 from constitutive and inducible constructs, which tapers off over time. ....</b>	<b>75</b>
<b>Figure 4.13 qPCR shows increase in chondrogenic gene expression during chondrogenic induction, with smaller increases than in chondrogenic groups, as expected. ....</b>	<b>76</b>
<b>Figure 4.14 qPCR shows increase in osteogenic gene expression from day 0 during chondrogenic induction, with smaller increases than in chondrogenic groups, as expected. ....</b>	<b>77</b>

**Figure 4.15 Biochemical analysis: ELISA assay demonstrates early expression of TGF- $\beta$ 3 from constitutive and inducible constructs, which tapers off over time. Collagen content shows significantly higher values in the TGF- $\beta$ 3 constitutive groups. ....78**

**Figure 4.16 Confocal microscopy (left) and fluorescence microscopy (right) demonstrates surface topology of fluorescent cells on the scaffold after 28 days of culture. ....79**

## **Acknowledgements**

Primarily, I would like to thank my PhD advisor, Dr. Farshid Guilak for the opportunity to work and learn in his labs at Duke University, Washington University in St. Louis, and Shriners Hospital for Children. From my first rotation before medical school 9 years ago through today, it has been quite a journey, and I am grateful for his support, mentorship, scientific guidance, and academic insight. Rocky Tuan was right when he told me in college that if I was really serious about musculoskeletal tissue engineering, I had to work with Farsh. As I head into my next chapter as a physician scientist, I hope to make him proud.

I would like to thank everyone who served on my preliminary examination and dissertation defense committee: Dr. Charles Gersbach, Dr. Bruce Klitzman, Dr. Jeffrey Lawson, and Dr. George Truskey. I am grateful for their feedback and scientific guidance over the years.

During the long hours at the lab bench and in the cell culture hood, I remember the words of wisdom of those who have been my great scientific teachers over the years. Dr. Francis Lefcort, from Montana State University in Bozeman, who taught me to read my first journal article, and guided me through my first small project in a real lab during my last summer in high school. She showed me how to make cells fluoresce, and I was hooked. Dr. Kalina Hristova, from Johns Hopkins University who, when I asked at a scholarship interview in high school how to find a lab to join, and all the other professors at the table told me the doors I could knock on and all the people I would need to talk to, simply

said, “come by tomorrow afternoon and we’ll get you started.” I would come by most days (and nights) for the next four years, and I learned from her and from Dr. Edwin Li and from Dr. Lijuan Huang how to think about science, how to work carefully, consistently, and cleanly, and how to troubleshoot. They were patient with me, and they taught me patience in science, and the great joy of contributing something to the scientific community. Thank you for teaching me.

At the encouragement of Dr. Hristova, I had two wonderful summer research experiences in college outside of her lab, and learned great lessons that I carried through my thesis research. To Dr. Eva-Kathrin Sinner, Dr. Ingo Köper, and Dr. Wolfgang Knoll of the Max Planck Institute for Polymer Research in Mainz, Germany, for showing me a very different model of scientific lab work, and for providing me an environment where I could collaborate with different labs, learn new techniques while teaching others what I knew, to work independently and also to lead a team. Thank you for this complex exposure to a balanced scientific life. And thank you to my students in Mainz: Clemens Krost, Manuela Kratochwil, and Christian Hoffman, who taught me to teach, and sparked a joy for teaching that remains lit. To Dr. Rocky Tuan, Dr. Juan Taboas, and Dr. Thomas Lozito who were all at NIAMS at the NIH back in the summer of 2008. From these great mentors, I learned about tissue engineering, the complexities of designing large *in vitro* studies with multiple outcome measures, and how fun and exciting engineering new tissues could be. These were great lessons, as were those gained from long conversations with Dr. Tuan, Chief of

NIAMS and a professional singer, about the vital importance of continuing to play my violin at the highest level I could, because of how indescribably important it would be to my science. And it has. To the people in each of these labs, who value answering a question as the most important calling, and inspired me to dedicate my life to such a pursuit, thank you.

And to the members of the Guilak lab, both at Duke, and the new lab at Washington University thank you for letting me join the team! I would like to thank everyone in the lab for their help, guidance, and for challenging me; but an especial thank you to Dr. Amy McNulty, my first mentor, who showed me the ropes, encouraged me, and gave me a sense of how I could contribute to and learn from the Guilak lab. To Dr. Vince Willard, who taught me numerous tricks and techniques of cell culture of tissues, and who talked through all my early experimental designs. Thank you for your kind and insightful mentorship over the years. To Team Awesome— Dakota Katz, Logan Groneck, and Sara Oswald, thank you for all your hard work, for challenging me to answer all the questions and to simplify the scientific stories, and for your support these last few years. It has been an honor to work with them.

I would like to thank my family. To my parents, William and Teresa O'Connor, who have loved and supported me my whole life, and gave me the tools from a young age to be able to take on such a long journey; they taught me to delight in the small joys, to work hard, to love hard, to plug into a community, and to take on daunting challenges if they might make a positive impact. When I wanted

to “do research” in high school, they drove me to Bozeman every week to learn from someone who knew what that was. And they gave me my violin. To them and to my brothers Brendan and Quinlan O’Connor—my own personal team of lawyers— thank you for always being there for me.

Finally, I would like to thank my fiancé, Alec Rose. I am grateful for his unceasing help and support amidst the challenges and delights of this journey, and for his numerous trips to visit me during the years of daily cell culture. I could not be more excited to begin our married life together.

It takes a village to raise a graduate student; and what an incredible village I have. Thank you all.

# 1. Introduction

Osteoarthritis (OA) is a painful, debilitating disease characterized by progressive degenerative changes in articular cartilage and other joint tissues. Currently, there are few treatment options for end-stage OA other than total joint replacement with a metal and plastic prosthesis, but wear limits their lifespan to only 10-15 years. The field of tissue engineering seeks to develop new methods to regenerate cartilage made from cells and biocompatible materials to potentially last a lifetime. Significant advances have been made in the field to develop the three main components for tissue engineering: scaffold materials and design; cellular programming and cell sources; and delivery of cell signaling molecules. *The goal of this project is to apply novel techniques in tissue engineering to construct functional cartilage and bone tissue.*

To study the biology of this debilitating disease, it is important to study the normal physiology of the tissues affected, and to further study the differences between the normal tissue and diseased tissue. Our lab created a system to study cartilage made from miPSCs<sup>1</sup> as large step toward modeling osteoarthritis in an *in vitro* system. Osteoarthritis is a disease of both the articular cartilage and the bone, and an *in vitro* organoid system modeling the osteochondral junction does not yet exist with iPSCs, but would be a powerful tool for understanding normal physiology of the joint, for modeling OA and other diseases of the osteochondral junction, such as osteochondritis dissecans, and for potential drug screening, even in a patient-specific manor. *One of our objectives for this study is*

*to create an osteochondral organoid system. Our first hypothesis for this work is that after differentiation of a cartilage construct, endochondral ossification can be induced to differentiate part of the construct into osteogenic tissue.*

For these constructs, induced pluripotent stem cells (iPSCs) were used. As iPSCs provide a virtually unlimited source of potentially patient-specific cells that can be reprogrammed into a pluripotent state then differentiated into any cell type, these cells solve many of the current problems in the field, including the need for large quantities of cells and the risk of rejection of non-autologous cells. They also invite the possibility of differentiation into two cell types in one construct, namely cartilage and bone for an osteochondral construct or graft.

With an eye toward translation and direct implantation of an osteochondral graft, these cells must be seeded onto a scaffold strong enough to withstand forces of normal human activity, wear slowly over time, and be porous enough to allow for tissue growth. Our lab developed a 3-dimensional woven scaffold with mechanical properties similar to those of native articular cartilage. When woven with poly( $\epsilon$ -caprolactone) (PCL), an FDA-approved biocompatible polymer, the scaffold supports chondrogenesis and degrades slowly (less than 5% degradation at 2 years) into byproducts that are entirely cleared from the body.

Work in our lab and the Gersbach lab has shown that this scaffold can be coated with an immobilized lentivirus for gene transduction: delivery of transforming growth factor  $\beta$ 3 (TGF- $\beta$ 3), a powerful chondrogenic inducer, via

scaffold-mediated viral transduction can induce growth of neocartilage tissue with human mesenchymal stem cells (hMSCs); preliminary data suggests that similar delivery of bone morphogenetic protein 2 (BMP-2), a powerful osteogenic inducer, produces mineralized bone-like tissue with hMSCs. Also, we have shown that exogenous delivery of these factors to iPSCs is the final step in chondrogenic (TGF- $\beta$ 3) and osteogenic (BMP-2) tissue formation. To engineer chondrogenic and osteogenic tissue, we propose lentiviral delivery of TGF- $\beta$ 3 and BMP-2 respectively. **Our second hypothesis is that scaffold-mediated viral transduction of TGF- $\beta$ 3 and BMP-2 into iPSCs will yield robust chondrogenic and osteogenic constructs from a single scaffold type and single cell population.**

### **Significance**

**Limitations of standard of care for cartilage injury and disease:** The treatments for injuries and diseases affecting articular cartilage pose important unmet challenges to the medical community. Damage to articular cartilage is a significant clinical problem with over 50% of orthopaedic injuries involving cartilage in synovial joints. Osteoarthritis (OA), a degenerative joint disease characterized by articular cartilage degradation and subchondral osteophyte formation, affects 53 million adults, 23 million of whom suffer during activities of daily living, with an economic burden of over \$40 billion per year in the USA.<sup>2,3</sup> Approximately 25% of the population older than age 60 years suffers significant pain and disability caused by OA.<sup>4</sup> Further, OA accounts for nearly one quarter of disability in activities of

daily living in older adults.<sup>5</sup> Once damaged, articular cartilage has a limited capacity for intrinsic repair<sup>6</sup> such that injuries and cartilage defects can lead to progressive damage, joint degeneration, and pain. Metal and polymer-based joint replacements have provided extraordinary relief from pain and renewed activity level for those with OA; however, these devices last only 10-15 years, limiting the options as our growing aging population lives longer, more active lives. There have been numerous efforts to achieve cell-based repair of cartilage defects, which if left untreated, can progress to OA.<sup>7</sup> To date, several techniques have used autologous chondrocytes clinically to enhance knee repair;<sup>8-10</sup> however, this approach faces numerous challenges including inadequate supply of chondrocytes, their limited regenerative potential with age or disease, graft hypertrophy, and graft delamination.<sup>11, 12</sup> Additionally, the harvest of autologous cartilage for the cell implantation procedure carries significant iatrogenic risk for the patient. The harvest of even non-load-bearing cartilage is associated with the onset of articular cartilage degeneration and osteoarthritic changes in the joint.<sup>13</sup> Other current treatment options include joint lavage, tissue debridement, abrasion arthroplasty, the transplantation of autologous or allogeneic osteochondral grafts, or commonly the microfracture of the subchondral bone.<sup>14-25</sup> Microfracture entails penetration of the subchondral bone to induce flow of the bone marrow, and presumably stem cells, into the tissue defect to form a clot which will hopefully remodel into cartilage. Although this procedure yields initial clinical success with improvement noted up to 24 months after surgery, the outcome deteriorates after

the initial postoperative period.<sup>26-31</sup> In particular, microfracture results in the formation of fibrocartilage, rather than hyaline cartilage which is necessary to maintain long-term cartilage function.

Therefore current procedures have yielded promising initial clinical results, but have long-term limitations due to the formation of fibrous tissue, apoptosis, and further cartilage degeneration.<sup>32-34</sup> Many of these limitations can be attributed to the lack of two specific components for tissue regeneration: 1) the proper biologic signals for guiding cell differentiation, hyaline cartilage formation, and integration with the underlying bone, and 2) the proper scaffolding biomaterial to support physiologic loading, retain the cells at the site of implantation, guide and constrain the growth of the tissue, and integrate with the host cartilage. Therefore our goal is to develop an approach for *in situ* tissue engineering that combines our novel 3D-woven polymer scaffolds<sup>35-39</sup> with spatially-defined, inducible gene delivery of morphogenetic factors<sup>40-47</sup> to specifically address these two limitations in a single device that possesses biomimetic cartilage properties as well as controlled cell-instructive signals.

### **Approach**

The **objective** of this study is to engineer constructs of multiple tissue types by controlling the morphogenetic factors that direct stem cell differentiation and tissue formation either exogenously or via transduction of expression vectors. This study will build on our preliminary studies described below by delivering lentiviral vectors encoding differentiation factors, and by designing these factors to be

temporally inducible. Our ***hypothesis*** is that sequential changes in exogenous growth factor delivery and also scaffold-mediated inducible regulation of morphogenetic gene expression and signaling in 3D-constructs of murine iPSCs will lead to the formation of both bone and cartilage tissue types.

## **2. Background**

### **2.1 Chondrogenically induced pluripotent stem cells (iPSCs):**

Recently, our laboratory has successfully developed methods to induce chondrogenic differentiation of iPSCs derived from mouse tail fibroblasts via viral transduction of the Yamanaka factors Oct4, Sox2, Klf4, and Myc.<sup>48, 49</sup> Reprogramming continues with growth on feeder cells, colony selection based on morphology, nucleofection with a Col2-GFP plasmid, further selection based on GFP expression, and feeder cell subtraction. Importantly, these differentiated cells are purified from undifferentiated iPSCs using a GFP reporter for type II collagen, a strong marker of chondrogenesis, and thus greatly minimizing chances of aberrant differentiation of iPSCs. We created dozens of murine iPSC lines that have been characterized and frozen, such that we will not conduct viral transduction experiments at this stage for these proposed experiments. Thawed cells are grown for 24 hours on 0.1% gelatin. After resuspension, micromass cultures are created and grown in 10% serum with LIF for 24 hours. Serum is then replaced with serum-free chondrogenic differentiation medium every 3 days for the next 15 days; BMP-4 and dexamethasone are added during days 3-5 of micromass culture. Micromasses are then digested with collagenase type II, pronase, and DNase I, and prepared for cell sorting via flow cytometry based on GFP expression. Approximately 10-20% of cells are GFP+ and therefore collagen II positive. Pure GFP+ cells are plated for rapid expansion (as are GFP- cells and

unsorted cells both used as controls) in chondrogenic differentiation medium with 10% FBS and bFGF on gelatin-coated plates, and passaged every 2-3 days. To maintain chondrogenicity, cells are cultured with TGF- $\beta$ 3 for 28 days.<sup>50, 51</sup>

We have demonstrated that during the final 28 days of culture with TGF- $\beta$ 3, cells can be grown in 3D pellet culture, and subsequently produce robust neocartilage (**Fig. 1A**). Staining for pluripotency markers prior to differentiation is shown (**B**); and demonstrates (**C**) the chondrocytic phenotype of these GFP+ cells, which express high levels of glycosaminoglycans (GAGs) and collagen II (both present in high levels in native cartilage tissue), but little collagen type I (an osteogenic marker) or collagen type X (a marker of hypertrophy during endochondral ossification). In the long term, the potential to harvest adult cells from individual patients and reprogram the cells for induction of chondrogenesis could diminish rejection potential of non-autologous transplantation, provide a patient-specific platform for osteoarthritis drug screening,<sup>1</sup> as well as provide an abundant source of cells for creating large cartilage constructs.

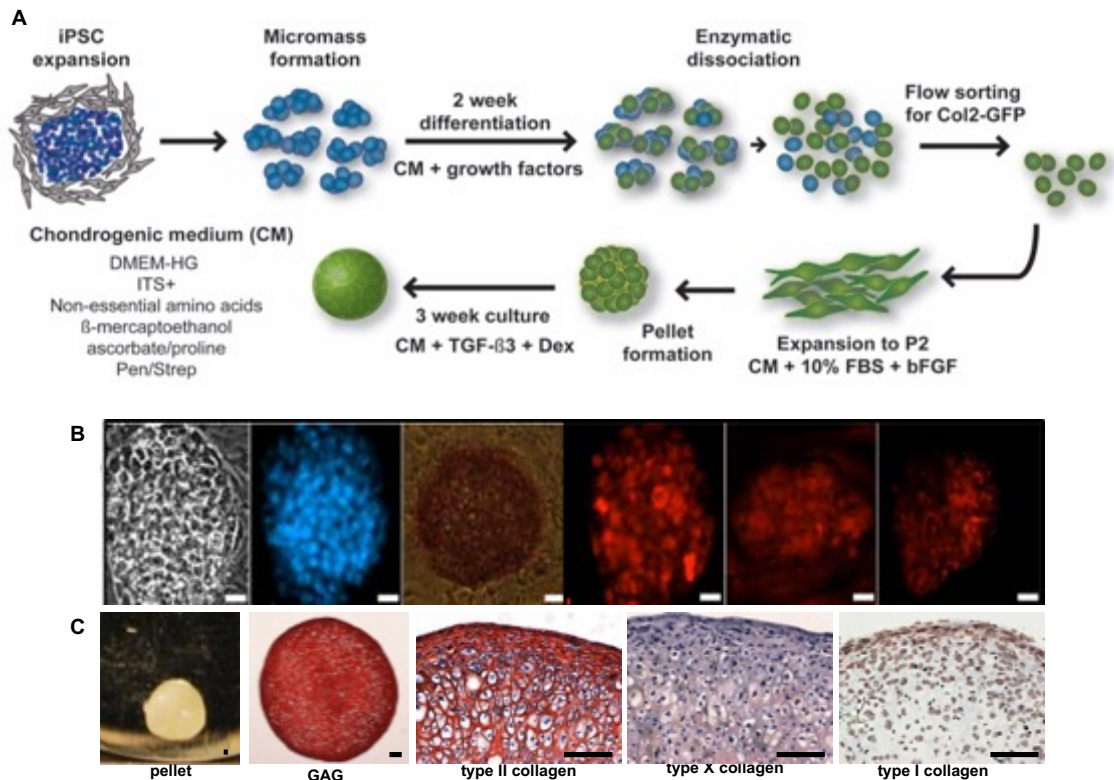


**Figure 2.1 miPSC chondrogenesis.** Reproduced with permission from reference 49, copyright PNAS 2012. A) Cartilage tissue engineering with iPSCs. B) Pluripotency markers of colonies. Left to right, scale=20μm: bright field, DAPI, alkaline phosphatase, nanog, Oct4/Pou5f1, SSEA1. C) Histology of pellets from Col2-GFP-sorted murine iPSCs. Left to right, scale=100μm: pellet, Safranin-O/Fast Green/Hematoxylin, type II, type X, and type I collagen. (Note: IHC and GAG staining show positive staining in red.)<sup>49</sup>

## 2.2 Osteochondral tissue engineering

In recent years, there have been many novel and interesting osteochondral tissue implants created with the goal of treating cartilage defects with implants that can be anchored into the subchondral bone, and many have utilized human mesenchymal stem cells (hMSCs) as their cell source. A recent paper demonstrated that freeze-dried and crosslinked mineralized salmon

collagen and jellyfish collagen in combination with an alginate hydrogel was sufficient to yield osteogenic and chondrogenic differentiation of hMSCs.<sup>52</sup> Another interesting study showed successful transfection of MSCs in a biphasic manner, with alginate hydrogels embedded with nanohydroxyapatite complexed with plasmids encoding genes for BMP2 and TGF- $\beta$ 3.<sup>53</sup> Cell-free scaffolds have also been designed recently; these are designed to be implanted at the osteochondral junction after microfracture, such that bone marrow cells will populate the scaffold and differentiate based on biological or polymer-based cues on the scaffold, such as collagen and hydroxyapatite,<sup>54</sup> or polyglycolic acid-hyaluronan.<sup>55</sup>

These studies represent interesting and useful steps toward the goal of translational, implantable osteochondral constructs; constructs made from hydrogels such as these, however, lack the mechanical properties necessary to support a load-bearing joint *in vivo*. Also, each of these studies utilizes hMSCs which, they show, do not maintain properties of articular cartilage in their chondrogenic layers, but rather undergo hypertrophy after 2-3 weeks of culture. Additionally, although MSCs have been demonstrated to be clinically useful in the treatment of osteonecrosis post-tumor resection in long-term studies,<sup>56</sup> as well as in non-unions,<sup>57</sup> MSCs are highly variable in their healing, differentiation, and proliferation capacities, depending on their donor's health, sex, and age. Since allogeneic MSC transplants are rarely an option, challenges arise when older or unhealthy patients present with a clinical need of MSC therapies. The

clinical need is great for the development of osteochondral constructs differentiated from iPSCs, which can be generated from multiple sources of healthy, abundant, and autologous cell types. Further, we have demonstrated in miPSCs, and others have demonstrated in hiPSC chondrogenesis much lower levels of Collagen Type X present in longer-term chondrogenic cultures,<sup>58-62</sup> suggesting a possible stable source of non-hypertrophic, articular cartilage.<sup>63</sup>

### **2.3 Unmet need: osteochondral organoids**

Recent years have shown an increase in development of disease-in-a-dish and organ-on-a chip models to study organ development, complex interactions between normal organ systems, disease models, and drug efficacy in high-throughput systems for patient-specific personalized medicine applications. A few such systems have been developed for the study of cartilage tissue, including cartilage from miPSCs.<sup>1</sup> Others have created complex multi-compartmental osteochondral tissues on a chip from hMSCs.<sup>64-66</sup> The need still exists for a simple, osteochondral organoid model system. Organoids, as defined by Lancaster and Knoblich, are self-organizing three-dimensional tissues derived from pluripotent stem cells or isolated organ progenitors that differentiate into an organ-like tissue to form a structure similar to the organ *in vivo*.<sup>67</sup> An osteochondral organoid system could provide unique opportunities to study basic biological interactions at the bone-cartilage interface, as well as the ability to test drugs that have differential effects on cartilage and bone, such as growth

factors,<sup>68</sup> hormones, cytokines, and other pharmaceuticals. An osteochondral organoid system could also be derived from cells with genetic mutations for osteochondral diseases, such as osteoarthritis and osteochondritis dissecans, for potential drug screening, even in a patient-specific manner. Organoids made for modeling osteoarthritis would need to recapitulate the properties of cartilage and bone in their function, gene expression, and specific extracellular matrix formation. They would also need to be spatially organized similarly to the osteochondral junction, with the surface of the bone in direct contact with the surface of the cartilage. One of our goals in this study is to create such a system.

## **2.4 3D-Woven polymer scaffolds**

As described above, biomaterial scaffolds that support tissue growth and maturation while providing necessary mechanical properties for tissue function and integrity are necessary to improve upon current methods for osteochondral regeneration. To address this need, we have developed 3D-woven scaffolds with biomimetic mechanical properties similar to those of native articular cartilage as the basis for composite tissue-engineered constructs (**Fig. 2**).<sup>35-37</sup> With this technique, pore size and geometry may be controlled by manipulating machine variables during the weaving process. Directional mechanical properties may be controlled by independently varying constituent fibers in any of the three directions. Anisotropy can be controlled by changing diameter, material, or spacing of each individual fiber. The placement of individual fibers and pores throughout the depth

of the scaffold permits inhomogeneous construct architectures that mimic the osteochondral tissue structure. Because there is no crimping or bending of fibers during fabrication, there is reduced fiber buckling relative to typical 2D weaving processes. This process results in increased strength and stiffness of 3D-woven fabrics in both compression and tension, and prevents crimping when the 3D-woven fabrics are molded into curved geometries that can replicate the native geometry of the joint.

The 3D-woven scaffolds were made by weaving yarns in three orthogonal directions (**Fig. 2**). PCL was selected because of its structural and mechanical properties. Specifically, PCL is a biocompatible, FDA-approved material<sup>69, 70</sup> that supports chondrogenesis<sup>71</sup> and degrades very slowly (i.e., less than 5% degradation at 2 years, as measured by mass loss) into byproducts that are entirely cleared from the body.<sup>72, 73</sup> Mechanical properties of the 3D-woven scaffold with and without embedded tissue growth have been well-characterized and are consistent, such that this proposal will not re-measure these properties. The 3D-woven PCL scaffolds were constructed from ~600 multi-filament yarns (24  $\mu\text{m}$  diameter per filament; 44 filaments/yarn) that were woven in three orthogonal directions using 11 total fiber layers (5 warp, 6 weft).<sup>37</sup> By varying the weaving parameters, PCL scaffolds can be made with pore sizes ranging from 150 to 1000  $\mu\text{m}$ , porosities ranging from 50 to 75%, and cartilage-mimetic compressive mechanical properties that can be maintained for more than 6 weeks in standard *in vitro* culture conditions.<sup>35, 36</sup>

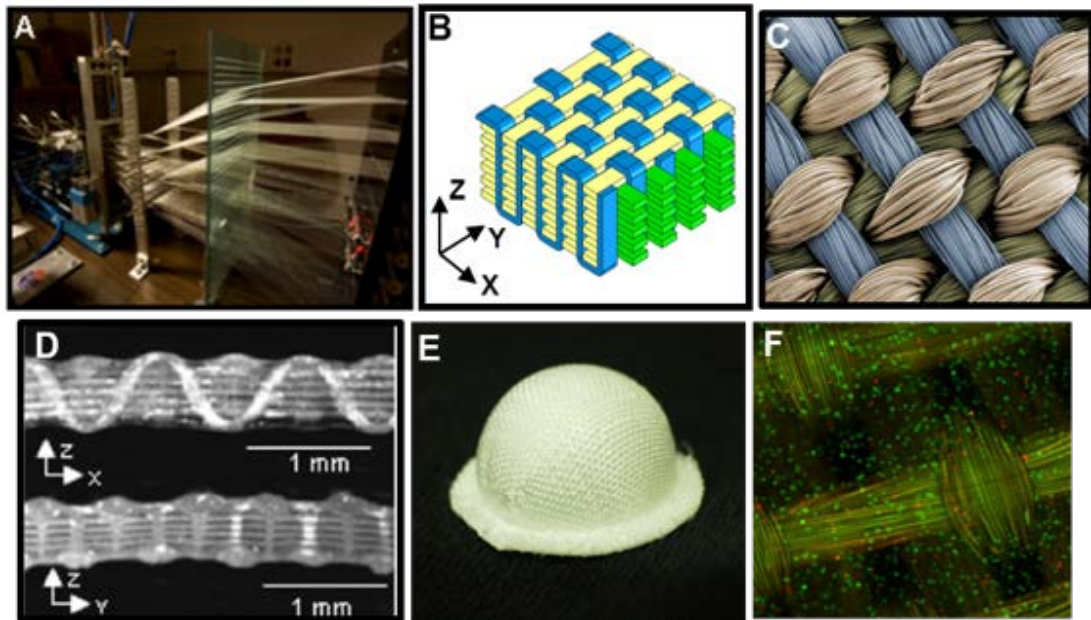


**Figure 2.2 3D-woven scaffolds.** Reproduced and adapted with permission from reference 37, copyright Nature Materials 2007 (B,C,D,F). (A) Custom-built weaving machine used to produce scaffolds; (B) scaffold structure showing three orthogonal fiber directions; (C) SEM micrographs showing x-y view of the scaffold; (D) photomicrographs of scaffold cross-sections showing the fiber architecture in x-z and y-z directions; (E) 3D-woven fabric molded in the shape of a hemispherical hip surface; (F) Calcein AM staining of cells in 2% agarose seeded onto woven scaffold.<sup>35-37</sup>

## 2.5 Biomaterial-Mediated Gene Delivery

Conventional methods for gene therapy involve *in vitro* gene delivery to cultured cells or *in vivo* delivery by direct injection of gene carriers. However, both of these approaches are often limited by inefficient transgene delivery and/or poor specificity. Recent attempts to overcome these limitations include biomaterial-mediated gene delivery, wherein the gene carrier is immobilized to, or encapsulated within, a biomaterial scaffold.<sup>46, 74, 75</sup> The hybrid gene-activated biomaterial is then seeded with cells *in vitro* or implanted. By co-localizing the gene delivery vehicle and cell adhesion, this method enhances gene transfer and specifically targets cells at the biomaterial interface, thereby reducing the risks

associated with direct injection of the gene carrier. Therefore, this approach provides several advantages over conventional gene delivery modalities, including reduced cytotoxicity and immunogenicity of freely diffusible gene carriers, eliminated or reduced risk of ectopic transgene expression in neighboring tissues, improved stability of the gene carrier, and controlled levels of gene transfer and expression. Biomaterial-mediated gene delivery has been used recently in a variety of successful model studies and in generating musculoskeletal tissues.<sup>76-88</sup> Importantly, our preliminary results suggest that growth factors secreted using this method act in an autocrine manner, as evidenced by site-specific differentiation of MSCs into osteogenic or chondrogenic lineages.

In order to engineer structurally complex tissues that replicate the organization of natural tissues, we have developed methods for controlled gene transfer within the 3D-woven scaffolds. The Gersbach lab previously showed that enveloped retroviral and lentiviral vectors interact electrostatically with biomaterial surfaces coated with the cationic polymer poly-L-lysine (PLL)<sup>44</sup> and this approach was subsequently used to engineer mineralized tissues on fibrous collagen scaffolds.<sup>76</sup> In our lab's recent publication,<sup>89</sup> we have extended this approach to our 3D-woven PCL scaffolds to engineer osteochondral tissues. After weaving, the scaffold was incubated in viral supernatant, leading to site-specific virus binding to the PLL-coated fibers. These scaffolds were then washed and seeded with human MSCs, leading to efficient lentiviral transduction of cells on PLL-coated fibers. Notably, >70% of the cells were transduced when the complete scaffold was

coated with PLL and incubated with GFP-encoding virus before cell seeding, demonstrating the high efficiency of gene transfer with this system.

## **2.6 Temporally Controlled Biomaterial-Mediated Gene Delivery for Cell Differentiation and Tissue Formation**

Gene delivery of morphogenetic factors is essential for guiding proper cell differentiation and tissue development, but prolonged and uncontrolled production of these factors is undesirable and can lead to hypertrophy or osteophyte formation.<sup>90, 91</sup> In order to control the dynamics of tissue development, the Gersbach and Guilak labs have previously used doxycycline-inducible vectors to control morphogenetic factors driving bone formation *in vitro* and *in vivo* (**Fig. 3A-E**).<sup>41</sup> These studies used a two-vector tet-off system, but more recently a single tet-on lentiviral vector has been engineered for low levels of leaky expression and high levels of induction<sup>92-96</sup> that was used for this work (**Fig. 3F**).

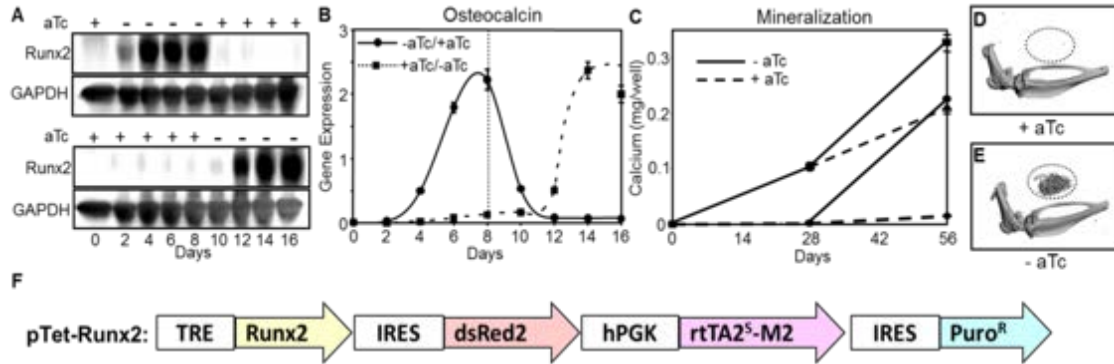


**Figure 2.4 Temporal control of gene expression, cell differentiation, and tissue formation.** Reproduced and adapted with permission from reference 41, copyright Gene Therapy 2006. A tetracycline (aTc)-inducible retroviral expression system (tet-off) was used to control the levels of the master osteoblastic transcription factor Runx2 in primary skeletal myoblasts. Expression of (A) Runx2 and (B) its downstream target osteocalcin could be modulated by adding or removing aTc from the culture media, as detected by western blot and qRT-PCR, respectively. (C) Similarly, the Runx2-mediated formation of mineralized tissue formation by these cells could be controlled by aTc presence in the culture media. (D-E) Genetically engineered myoblasts were implanted into the hind limbs of mice and mineralized tissue formation could be controlled by administering aTc in the drinking water.<sup>41</sup> (F) This single dox-on lentiviral vector contains a morphogenetic factor Runx2 that is co-expressed with the red fluorescent protein dsRed2 via an internal ribosomal entry site (IRES) under the control of the tet-responsive element (TRE). The enhanced reverse tetracycline transactivator (rtTA2<sup>S</sup>-M2) and the selectable puromycin-resistance are expressed from the constitutive PGK promoter.<sup>41</sup>

### 3. Chondrogenic Differentiation of Induced Pluripotent Stem Cells and Formation of Cartilaginous Extracellular Matrix Prevents Re-Induction of Pluripotency

#### 3.1 Rationale and experimental plan

Mouse iPSCs expressed GFP under the control of the *Col2a1* promoter,<sup>97</sup> which allowed for fluorescence-activated cell sorting of chondrogenically differentiated cells as part of a multi-stage cartilage tissue engineering strategy.<sup>50</sup> Following sort and expansion, pellets were formed to perform experiments detailed below, and illustrated in Figure 3.1. iPSCs contain a doxycycline-inducible lentiviral vector for the pluripotency factors Oct4, Sox2, Klf4, and c-Myc.

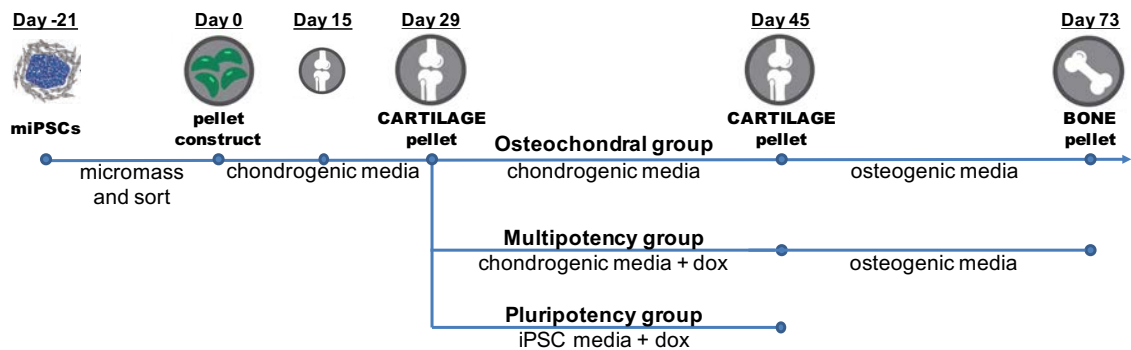


**Figure 3.1 Differentiation and purification of hESC-CMs.** Pellets were formed and grown for 29 days in chondrogenic media (with TGF- $\beta$ 3). Pellets were then either maintained in chondrogenic media or in chondrogenic media with dox for 16 days. All pellets were then switched to osteogenic media (with BMP2), and grown for 28 days. To test the potential for re-induction of pluripotency in an additional experimental group, after 29 days of chondrogenic induction, pellets in the third group were switched to iPSC media with dox for 16 days.

## 3.2 Methods

### 3.2.1 Chondrogenic differentiation of miPSCs via micromass formation, and purification of Col2-GFP miPSCs via flow cytometry

miPSCs were derived at Duke University in accordance with a protocol approved by the Duke IACUC. Mouse tail fibroblasts from 8 to 10 week old mice were transduced for 24 hours with a single doxycycline-inducible lentiviral vector to control the transgenic expression of mouse cDNA for Sox2, Oct4 (*pou5f1*), Klf4, and c-Myc.<sup>98</sup> After 2 weeks of culture, individual colonies were manually selected and grown on Mouse Embryonic Fibroblasts (MEFs) as feeder cells in iPSC media without doxycycline. The Col2-GFP reporter plasmid<sup>97</sup> was enzymatically linearized and purified. After feeder subtraction, miPSCs were nucleofected with the linearized plasmid, and plated on neomycin-resistant MEFs, and cultured with G418 between 2 and 12 days posttransfection. Clonal expansion of individually-selected G418-resistant clones was performed on feeder cells. Clones were differentiated using micromass culture for selection of a clone with the largest increase in GFP+ cell count after induction of chondrogenesis.<sup>50</sup>

Mouse embryonic fibroblasts (PMEF, Millipore) were expanded and treated with 10 µg/mL mitomycin-C (Sigma-Aldrich) for 2–3 h to prevent proliferation and then cultured on 0.1% gelatin coated dishes at confluence to provide a feeder layer. miPSCs were cultured on this MEF feeder layer in iPSC media containing DMEM-HG (Gibco), 20% lot-selected FBS (Atlanta Biologicals), MEM nonessential

amino acids (NEAA, Gibco),  $\beta$ -mercaptoethanol (Gibco), gentamicin (Gibco), and mouse leukemia inhibitory factor (LIF, Millipore ESGRO).

After expansion on MEF feeder cells, feeder subtraction was performed in two 45min incubation periods, separated by 24 hours of culture on 0.1% gelatin coated plates. After passage, cells were resuspended at a concentration of  $2 \times 10^7$  cells/mL, and 10 $\mu$ L, or  $2 \times 10^5$  cells, were pipetted into each well of a 48-well cell culture plate. After 2 hours of incubation, 0.5mL of iPSC media with 10% serum and no LIF was added to each well. After 24 hours, media was replaced with serum free chondrogenic differentiation medium, with DMEM-HG (Gibco), NEAA (Gibco),  $\beta$ -mercaptoethanol (Gibco), ITS+ (BD), penicillin-streptomycin (Gibco), 50  $\mu$ g/mL L-ascorbic acid 2-phosphate (Sigma), and 40  $\mu$ g/mL L-proline (Sigma). Micromasses were cultured for 15 days. On days 3-5 of culture, 50 ng/mL mBMP-4 (R&D Systems) and 100 nM dexamethasone were added to the chondrogenic medium. Micromasses were then digested for 1 hour at 37°C using 0.4% collagenase type II (Worthington), 1320 PKU/mL pronase (Calbiochem), and 10  $\mu$ g/mL DNase I (Worthington) and pipetted every 15min during incubation. Cells were centrifuged, incubated with 0.25% trypsin-EDTA for 5 min, and resuspended in sort medium containing DMEM-HG, 2% FBS, DNase I, 10 mM HEPES (Gibco), 2x Penicillin/Streptomycin/Fungizone, and 5  $\mu$ M propidium iodide (Biolegend).<sup>50</sup> Cells were sorted based on GFP expression using the 100  $\mu$ m nozzle of an Aria II flow sorter (BD BioSciences, Washington University Flow Core).

### **3.2.2 Cell culture: pellet formation, chondrogenic culture, endochondral ossification, and pluripotency induction**

After sort, cells were expanded on gelatin coated plates at  $1 \times 10^4$  cells/cm<sup>2</sup> in chondrogenic differentiation media with 4ng/mL hbFGF (Roche) and 10% FBS. Cells were passaged every 3 days for two passages using 0.05% trypsin EDTA (Sigma). After the second passage, cells were resuspended in chondrogenic media, and  $2.5 \times 10^5$  cells in 0.5mL media were added to 15mL conical tubes (Corning). Tubes were centrifuged at 200g for 5min, followed by incubation at 37°C. Chondrogenic media contained 10ng/mL TGF- $\beta$ 3 and 100nM dexamethasone, in addition to DMEM-HG (Gibco), NEAA (Gibco),  $\beta$ -mercaptoethanol (Gibco), ITS+ (BD), penicillin-streptomycin (Gibco), 50  $\mu$ g/mL L-ascorbic acid 2-phosphate (Sigma), and 40  $\mu$ g/mL L-proline (Sigma).

Pellets were cultured in chondrogenic media for 29 days, with complete media changes every 3 days, and then split into three experimental groups. To form osteochondral pellets, one group continued to be cultured in chondrogenic media for 16 additional days, and media was then switched to osteogenic media for an additional 28 days. Osteogenic media contained 12.5ng/mL BMP2 (RnD), 10% FBS, DMEM-HG (Gibco), NEAA (Gibco),  $\beta$ -mercaptoethanol (Gibco), penicillin-streptomycin (Gibco), 50  $\mu$ g/mL L-ascorbic acid 2-phosphate (Sigma), dexamethasone, and 10mM  $\beta$ -glycerophosphate (Sigma).

To test multipotency potential, one group was cultured in chondrogenic media for 29 days, and then 10  $\mu$ g/mL doxycycline (Sigma) was added to the

media for the next 16 days of culture. On day 45, media was changed to osteogenic media without doxycycline.

To test pluripotency potential, one group was cultured in chondrogenic media for 29 days, and then switched to iPSC media for 16 days with 10 µg/mL doxycycline (Sigma), 20% FBS, DMEM-HG (Gibco), NEAA (Gibco), β-mercaptoethanol (Gibco), Gentamicin (Gibco), and mouse LIF (EMD Millipore). In parallel, some pellets were dissociated at day 29, plated in monolayer, and switched to iPSC media with 10 µg/mL doxycycline for 16 days. To dissociate the cells from the pellet matrix, pellets were digested for 1 hour and 15min at 37°C using 0.4% collagenase type II (Worthington), 1320 PKU/mL pronase (Calbiochem), 10 µg/mL DNase I (Worthington), 5% FBS, and DMEM-HG, and pipetted every 15min during incubation. Cells from each pellet were washed, divided in two, and resuspended in iPSC media. Half the cells from each pellet were plated on a feeder layer of MEFs (described earlier) with daily media changes, and the other half of the cells from each pellet were plated into a 2i cell-free system: plates were coated with laminin (Sigma L2020) according to the manufacturer's instructions. Instead of using feeder cells, two molecules were added to the iPSC media: 1µM PD0325901 (Cayman Chemical) and 3µM CHIR99021 (Cayman Chemical). This system does not induce pluripotency if the cells have started to differentiate, it just prevents differentiation in pluripotent cells. The maintenance of pluripotency by the laminin-2i system has been shown to last for 8 passages, and the molecules remain active at 37C for only 24 hours, so

frozen aliquots were thawed just before addition to the media, and media was changed daily. Both the MEF system and the 2i-laminin system yielded similar numbers of morphologically similar colonies in the groups given doxycycline in monolayer.

Pellets that were given doxycycline in iPSC media for 16 days of construct-induction were then dissociated (as described above), and half the cells from each pellet were plated on a feeder layer of MEFs, and the other half of the cells from each pellet were plated into a 2i cell-free system. This was designated passage 0. Simultaneously, groups that had been given doxycycline in iPSC media for 16 days of monolayer-induction were passaged. As each group became confluent, cells were passaged, either onto MEFs or the 2i system. This experiment was performed with at least 3 samples per group, with 4 groups: GFP+ pellet-induced, GFP+ monolayer-induced, GFP- pellet-induced, and GFP- monolayer-induced. The halves of the pellet-induced groups that were grown on MEFs showed little growth, and grew within the MEF layer. These were passaged, but the cells passaged in the 2i system were used for the Colony Pluripotency Assay, so no MEFs would be present upon staining. One of the GFP- pellets in the 2i system stopped proliferating, and was only passaged to p5. All other groups were passaged to p7.

To perform the colony pluripotency assay, 4-well chambered culture slides (Falcon/Corning) were coated with laminin, and  $5 \times 10^4$  cells were plated into each well and cultured for 5 days. For alkaline phosphate staining, the alk phos staining

kit II was used (Stemgent), and manufacturer's instructions were followed for brightfield staining. These slides were mounted with Prolong Gold antifade mountant with DAPI (Invitrogen). These slides were imaged on the Cytation 5 both in brightfield and DAPI fluorescence, and later overlaid using MatLab.

For other pluripotency proteins, wells were rinsed 3x in PBS, then fixed in 4% paraformaldehyde in PBS with 0.1% Tween for 20min at room temperature. Wells were rinsed 3x in PBS, then permeabilized for 20min at room temperature in 0.1-0.55% Triton X-100 in PBS: transcription factors Nanog and Oct4 use 0.55% Triton X-100 in PBS and membrane protein SSEA-1 use 0.1% Triton X-100 in PBS; for all three together use 0.1% Triton X-100 in PBS. Wells were then rinsed 4x in PBS with 0.1% Triton-X. Wells were blocked in Blocking Buffer (10% FCS in PBS) for 40min at room temperature. Primary antibodies were incubated overnight at 4°C in pre-cooled Blocking Buffer (all Abcam 1:100, Nanog 80892, Oct4 27985, SSEA-1 16285). Wells were then rinsed 4x in PBS with 0.1% Triton-X. Secondary antibodies were incubated 1 hour 15min at 4°C in the dark in Blocking Buffer (all Invitrogen, for Nanog, 1:1000 Alexa Fluor Plus 488 (GFP) A-32731, for Oct4, 1:600 Alexa Fluor 568 (RFP) A-11057, for SSEA-1, 1:1000, Alexa Fluor 647 (Cy5) A-32728). Wells were then rinsed 2x in PBS with 0.1% Triton-X, well sides were removed from slides, and slides were mounted in Prolong Gold with DAPI (Invitrogen).<sup>99-102</sup>

In addition to processing a well for each sample, additional wells were seeded with GFP+ monolayer-induced samples that were given no primary antibodies, but all of the secondary antibodies, to test for nonspecific binding.

Wells were imaged on a Cytation 5 system using filter cubes specific for DAPI, GFP, RFP, and Cy5. Images were taken of each well in their entirety at 10x (tiled and stitched together), with intensity, gain, and exposure set constant for each filter cube. Whole wells were assessed, and smaller, representative images are presented here. Additional images were taken at 40x to appreciate the localization of the antibodies to their transcription factors and membrane protein.

Mycoplasma test samples were collected regularly throughout the cell and tissue culture experiments and tests were performed by an independent core facility at Washington University. DAPI staining for the colony pluripotency assay further demonstrated negative mycoplasma results.

### **3.2.3 Gene expression analysis: RNA isolation and quantitative RT-PCR (qPCR)**

Pellets were briefly rinsed with PBS -/- (Gibco) and transferred to cryotubes with 5 sterile glass beads and 350 $\mu$ L lysis buffer. Cryotubes were placed in a bead beater for mechanical disruption of constructs. Lysate was transferred to new Eppendorf tubes and frozen at -80°C until RNA isolation. RNA isolation was performed according to manufacturer instructions (Total RNA Purification Plus Micro Kit, Norgen). RNA concentrations and RINe values were measured using an Agilent 2200 TapeStation System (Agilent Technologies), with a ladder run on

each gel. cDNA synthesis was performed using SuperScript IV First-Strand Synthesis System (ThermoFisher), in parallel with a No Template Control (NTC). PCR was performed with Taqman Gene Expression Assay probes (ThermoFisher) (Table 3.1), and Taqman Fast Advanced Master Mix. Samples from each group were divided across plates, and the NTC was run with each probe. NTC showed no amplification for any probes after 55 cycles. All samples were run in triplicate. Data analysis was performed with the  $\Delta\Delta CT$  method, and displayed as fold changes, where  $RT = 2^{-(\Delta\Delta CT)}$ . Both GAPDH and HPRT were tested for use as the endogenous control gene with similar results; GAPDH was chosen for further data analysis. All samples were compared to miPSCs.

**Table 3.1 qPCR primer probes.**

<b>Gene</b>	<b>Name</b>	<b>Probe</b>
Col1a2	Type I collagen	Mm00483888_m1
Col2a1	Type II collagen	Mm01309565_m1
Col10a1	Type 10 collagen	Mm00487041_m1
Acan	Aggrecan	Mm00545794_m1
Sox9	sex determining region Y-box 9	Mm00448840_m1
GAPDH	Glyceraldehyde 3-phosphate dehydrogenase	Mm99999915_g1
Prg4	Lubricin	Mm01284582_m1
Bglap	Osteocalcin	Mm03413826_mH
Runx2	Runt-related transcription factor 2	Mm00501584_m1
Sp7	Osterix	Mm04209856_m1
HPRT	hypoxanthine guanine phosphoribosyl transferase	Mm00446968_m1
Oct4/Pou5F1	Octamer-binding transcription factor 4	Mm03053917_g1
Nanog	Nanog homeobox	Mm01617762_g1
Sox2	sex determining region Y-box 2	Mm03053810_s1
Ibsp	Bone sialoprotein	Mm00492555_m1
Alpl	Alkaline phosphatase	Mm00475834_m1

### 3.2.4 Histological analysis

For histology, pellets were fixed in 10% Neutral Buffered Formalin for 16 hours, dehydrated, paraffin embedded, and sectioned at 8  $\mu$ m thickness. Safranin-O/fast green/hematoxylin staining was stained under standard protocols using osteochondral sections from mouse knee joints as controls. Von Kossa staining was performed according to manufacturer instructions (Abcam); the control joint for this was a knee joint dissected from an 11-day old mouse. This skeletally-immature age allowed for fixation, embedding, and sectioning of the joint without decalcification. Masson's Trichrome staining was performed according to manufacturer's instructions (Abcam) using osteochondral sections from mouse shoulder joints as controls.

For immunohistochemistry, sections were treated with xylene and ethanol in decreasing concentrations. For type II collagen (Iowa II-II6B3, 1:1 in goat serum), type VI collagen (Fitzgerald 70R-CR009x, 1:1000 in 1% BSA), and type X collagen (Sigma c7974, 1:400), epitope retrieval was performed with Digest-All 3 Pepsin (Invitrogen) at room temperature for 5min, then treated with methanol-peroxidase, blocked for 30min (goat serum for type X collagen, goat serum with the addition of cold fish gelatin for type II collagen, and for type VI collagen, 2% goat serum, 1% BSA, 0.1% Triton X-100, 0.05% Tween 20, 0.01M PBS (pH 7.2)), then incubated for an hour at room temperature in primary antibody. Secondary antibody incubation was 30min at room temperature (ab97021 for type II collagen and type X collagen, and ab6720 for type VI collagen, 1:500), followed by HRP

Streptavidin treatment and AEC Red Single (Histostain Plus, Invitrogen), counterstained with hematoxylin, and mounted with Vectamount (Vector Labs). Osteochondral sections from mouse knee joints were used as controls. For type I collagen (8D4A1, Chondrex, 1:200, biotinylated), epitope retrieval was performed with pepsin incubation at 37°C for 20min, then treated with methanol-peroxidase, and blocked for 30min (goat serum) before primary incubation. Mouse hip cartilage from 10 day old mice and mouse patellar tendon were used as negative and positive controls, respectively.

Final histology images were taken on a VS120 microscope imaging system at 20x magnification, with consistent bright field settings for each stain.

### **3.2.5 MicroCT analysis**

Pellets were serially dehydrated to 70% ethanol. Kim wipes soaked in 70% ethanol were placed at the bottom of 15mL conical tubes, which were laid on their sides, and pellets were placed on the sides of the conical tubes for microCT imaging using a Skyscan Bruker microCT. Consistent settings were used to image pellets and calibration phantoms. After reconstruction, phantoms were used to determine threshold values for mineralization. In order to determine tissue volume and bone mineral density, sections of pellets were outlined both by hand and with an automated program, both yielding similar results. Tissue volume, bone volume, and bone mineral density values were calculated using CTAnalyser software (Bruker). Images were generated in CTVox software (Bruker).

### **3.2.6 Biochemical analysis**

Pellets were digested in papain at 65°C for 16 hours. dsDNA was measured with PicoGreen dsDNA Quantitation kit (Invitrogen). Sulfated glycosaminoglycans were measured with the DMB assay, and total collagen was measured with the hydroxyproline assay.<sup>103</sup> To quantify calcium content, pellets were decalcified by incubating in 5% formic acid for 30 minutes. Calcium concentration was measured using the Calcium Colorimetric Assay Kit (Fisher).

### **3.2.7 Statistics**

Experimental data reported as mean  $\pm$  SEM was compared using Student's t-test, a one-way ANOVA followed by a post-hoc Tukey's test, or a two-way ANOVA. Data was analyzed with JMP with a significance level set to  $\alpha=0.05$ .

## **3.3 Results**

### **3.3.1 Osteogenic induction after chondrogenesis**

After chondrogenic induction of miPSCs via micromass culture and the addition of BMP-4 and dexamethasone during days 3-5, cells were sorted via flow cytometry, and ~17% expressed GFP under the control of the Col2 promoter. An additional 35% of cells that did not express GFP under the control of the Col2

promoter were sorted as well (GFP- hereafter), and cultured in parallel for comparison.

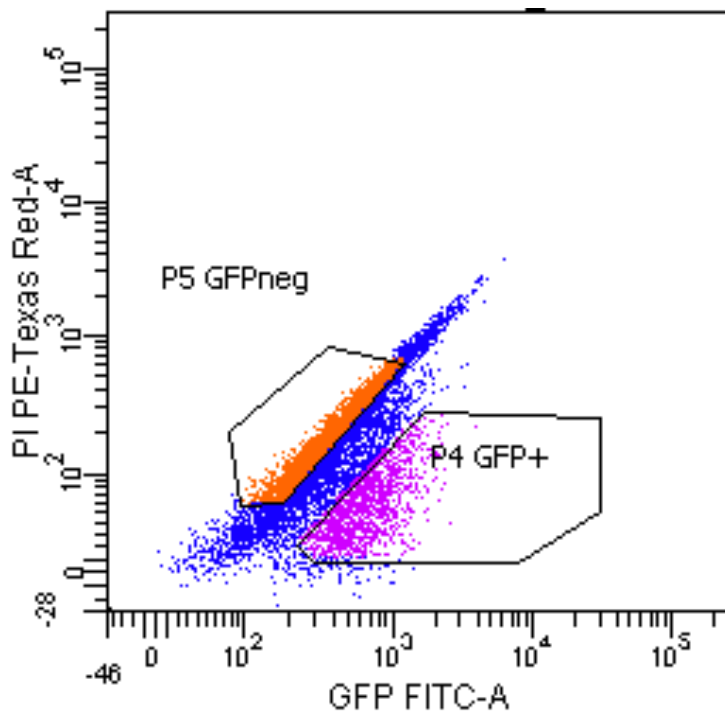


**Figure 3.2 Flow sort analysis.** Flow data was gated on miPSCs without the Col2-GFP reporter plasmid, and differentiated in micromass in parallel with the Col2-GFP-containing cells. ~17% of cells were GFP+, and 35% of cells were sorted as GFP- for further culture.

Cells were expanded for two passages in monolayer in the presence of 10% FBS and 4 ng/mL bFGF. Subsequently, cells were passaged, centrifuged to form pellets, and cultured for 45 days in chondrogenic media with TGF- $\beta$ 3. After 45 days, some constructs were harvested for subsequent assays, and in others, the

media was changed to osteogenic media with BMP-2 and cultured for an additional 28 days before harvest.

Although not shown in the figures presented here, constructs were made with GFP- cells and cultured in parallel. These pellets were smaller, had weaker protein staining for chondrogenic extracellular matrix proteins at 29 days of chondrogenic culture, and less chondrogenic gene expression than their GFP+ counterparts.

Samples were taken for RNA isolation at multiple timepoints during the study: frozen stocks of miPSCs (day -21); GFP+ cells after 2 passages (day 0); pellets after 15 days of pellet chondrogenesis (day 15); pellets after 29 days of pellet chondrogenesis (day 29); pellets after 45 days of pellet chondrogenesis (day 45); and pellets after a subsequent 28 days of osteogenic induction (day 73). Osteogenic gene expression demonstrates a dramatic increase between the chondrogenic culture period and the osteogenic period, for the genes *Ibsp*, *Sp7*, *Runx2*, *Bglap*, *Alpl*, and *Col1a2* (Figure 3.3). Note that alkaline phosphatase (*Alpl*) is a marker of pluripotency in addition to osteogenesis, reflected in the markedly

decreased expression of this gene during chondrogenesis in comparison to miPSCs (day -21).

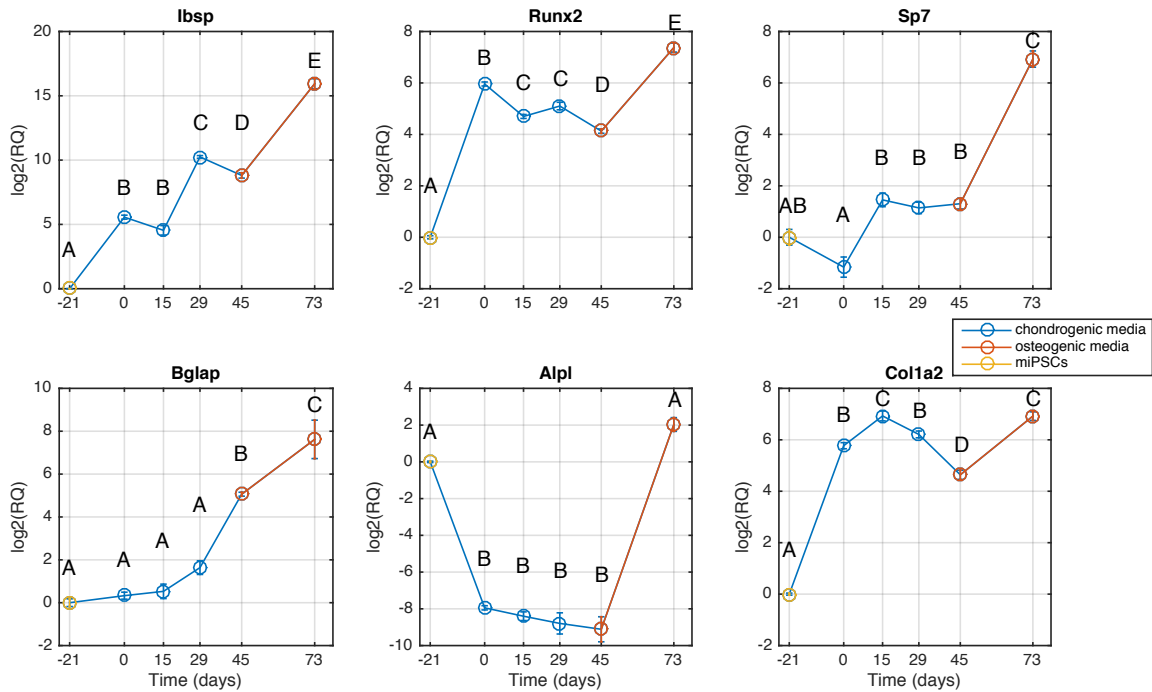


**Figure 3.3 qPCR shows expected increase in osteogenic gene expression during osteogenic induction.** Data points and error bars demonstrate mean ± SEM. RQ = Relative Quantification, or fold change. The reference gene is GAPDH. Groups not labelled with the same letter are significantly different by one-way ANOVA with post-hoc Tukey-Kramer analysis with  $p < 0.05$ .

Pellets were harvested on day 45 and day 73 for histological analysis before and after osteogenic induction. Immunohistochemical analysis of Collagen Type I showed a lack of Collagen Type I after chondrogenic induction, but a shell of Collagen Type I on the outside edge of the pellets after 28 days of osteogenesis. Von Kossa staining for calcification showed a lack of calcification on day 45, but a

shell of mineralization on day 73, which was further demonstrated via microCT analysis. Masson's Trichrome staining also demonstrated a thin layer of red collagen coating the outside of the pellets on day 73 that was not present at day 45 (Figure 3.4).

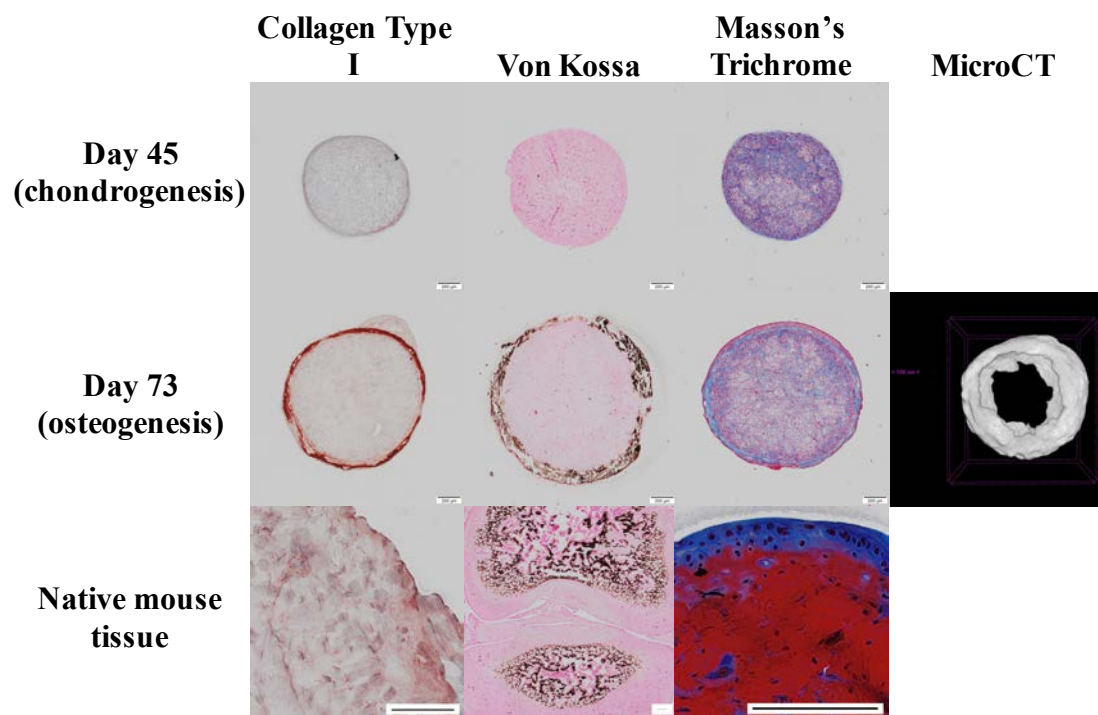


**Figure 3.4 Histology and microCT demonstrate a shell of calcified tissue after osteogenic induction.** Collagen Type I (red), Von Kossa (calcification in brown), Masson's Trichrome (cartilage in blue, collagen in red) of pellets, MicroCT (calcification in grayscale). Mouse controls show native mouse tendon, non-decalcified young mouse knee, and adult mouse shoulder. Scale bars are 200µm in pellet histology samples, and 100µm in mouse tissue controls and microCT images.

### 3.3.2 Chondrogenic outcomes

Pellets were also taken down at the same timepoints to measure chondrogenic gene and protein expression. Chondrogenic genes Col2a1, Sox9,

Acan, and Prg4 rise from baseline, and tend to peak after a few weeks in chondrogenic culture. After osteogenic induction, each of these chondrogenic genes decreases in expression.

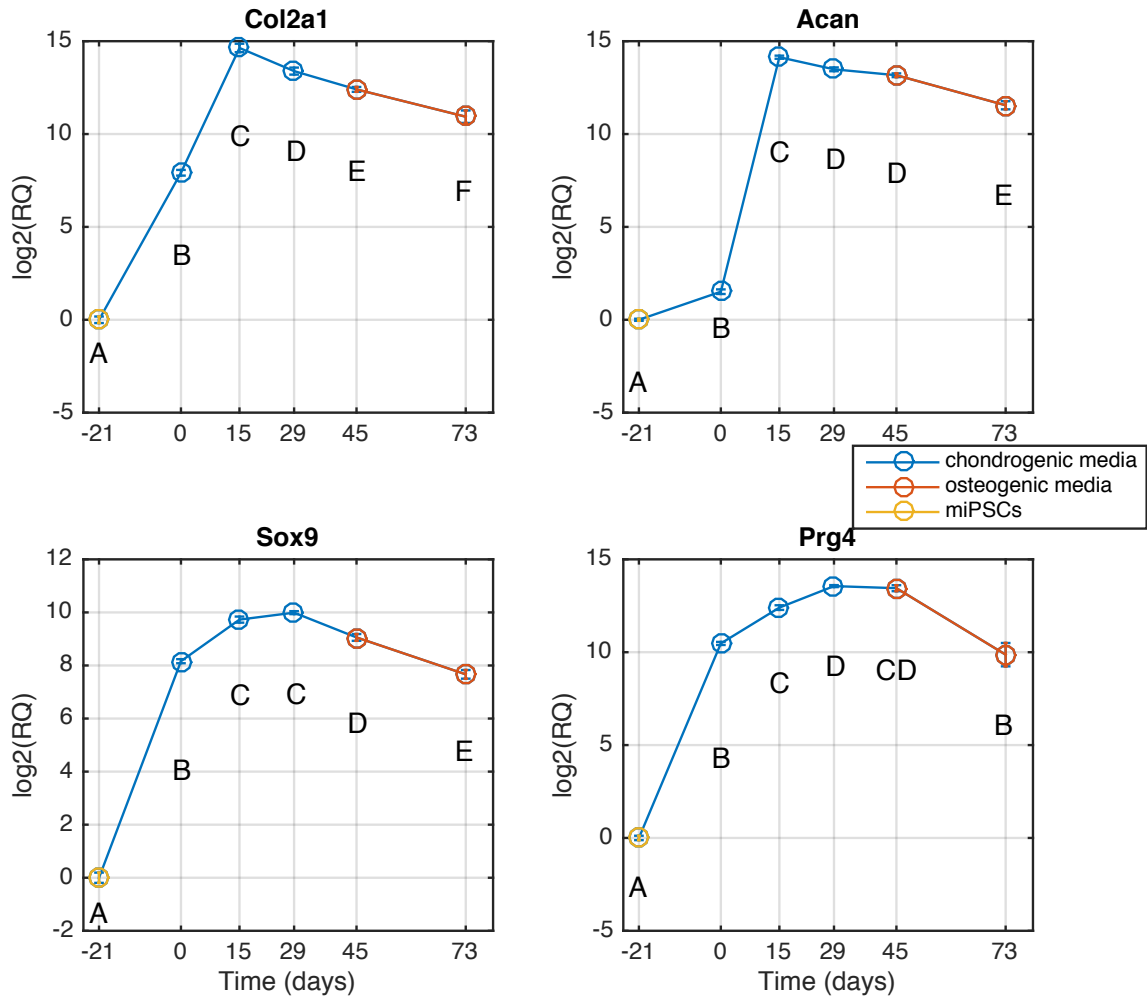


**Figure 3.5 PCR shows expected increase in chondrogenic gene expression during chondrogenic induction, and decrease during osteogenic induction.** Data points and error bars demonstrate mean  $\pm$  SEM. RQ = Relative Quantification, or fold change. The reference gene is GAPDH. Groups not labelled with the same letter are significantly different by one-way ANOVA with post-hoc Tukey-Kramer analysis with  $p < 0.05$ .

Immunostaining was performed at days 29 and 45 of chondrogenesis, and day 73 after osteogenic induction. Type II Collagen, Type VI Collagen, and glycosaminoglycans are present at each of these time points, and a morphologically dis-similar layer is present on the outside of these pellets on day 73. Little of the hypertrophic protein Type X Collagen is present at any time point.

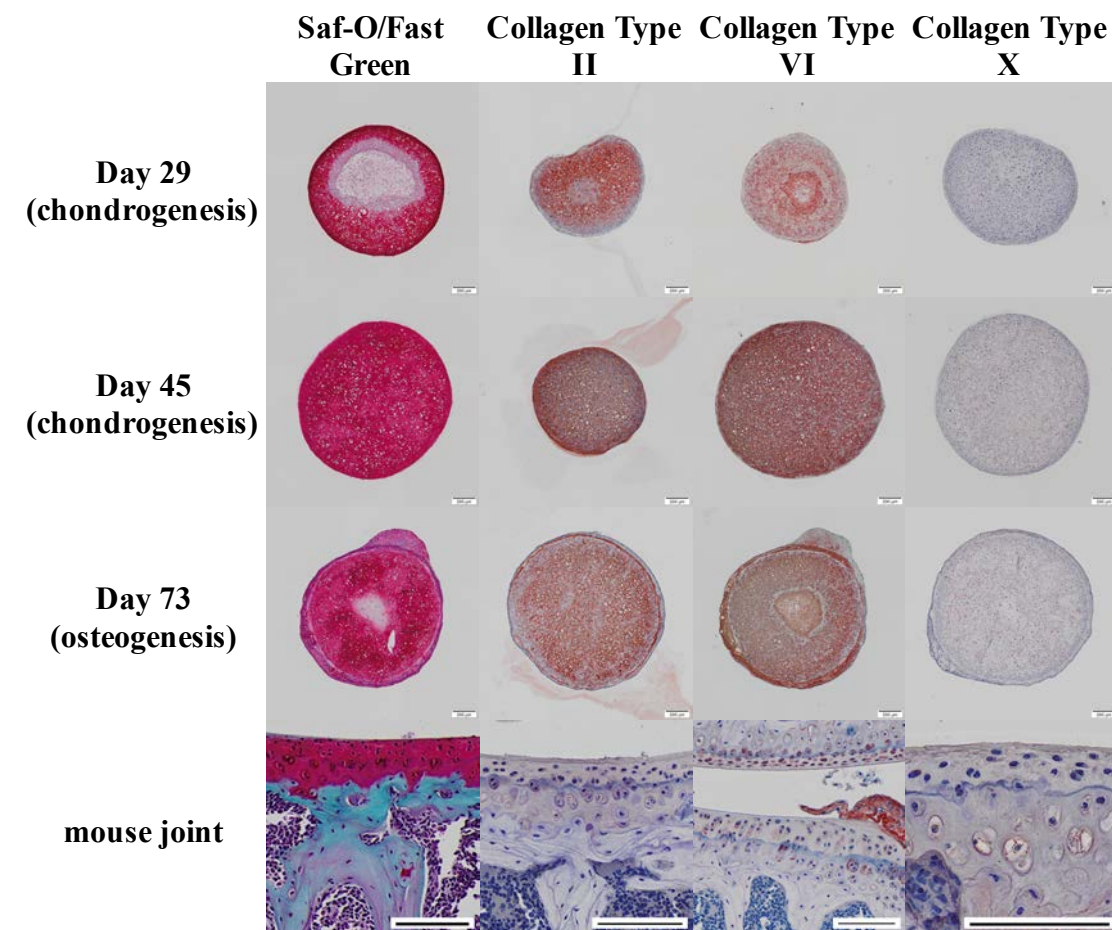


**Figure 3.6 Histology demonstrates presence of cartilage matrix proteins throughout the timeline.** Safranin-O/fast green stain for glycosaminoglycans (GAG in red), and immunohistochemical analysis of Collagen Type II, VI, and X (in red) of pellets, and of native mouse knee joints. Scale bars are 200µm in pellets samples, and 100µm in mouse tissue controls.

### 3.3.3 Doxycycline induction effect on multipotency

iPSCs contain a doxycycline- inducible lentiviral vector for the pluripotency factors Oct4, Sox2, Klf4, and c-Myc (the Yamanaka factors). To determine whether re-induction of the Yamanaka factors would affect the osteogenic potential of these pellets, pellets underwent 29 days of chondrogenic induction with TGF- $\beta$ 3, followed by 16 days of culture with the addition of doxycycline in the media, and subsequent 28 days of osteogenic induction without doxycycline. This experiment was run in parallel with the previous experiment to allow for a direct comparison of groups before and after dox-induction, and with or without dox-induction. Dox-induction prior to osteogenic induction had no significant effect on osteogenic gene expression.

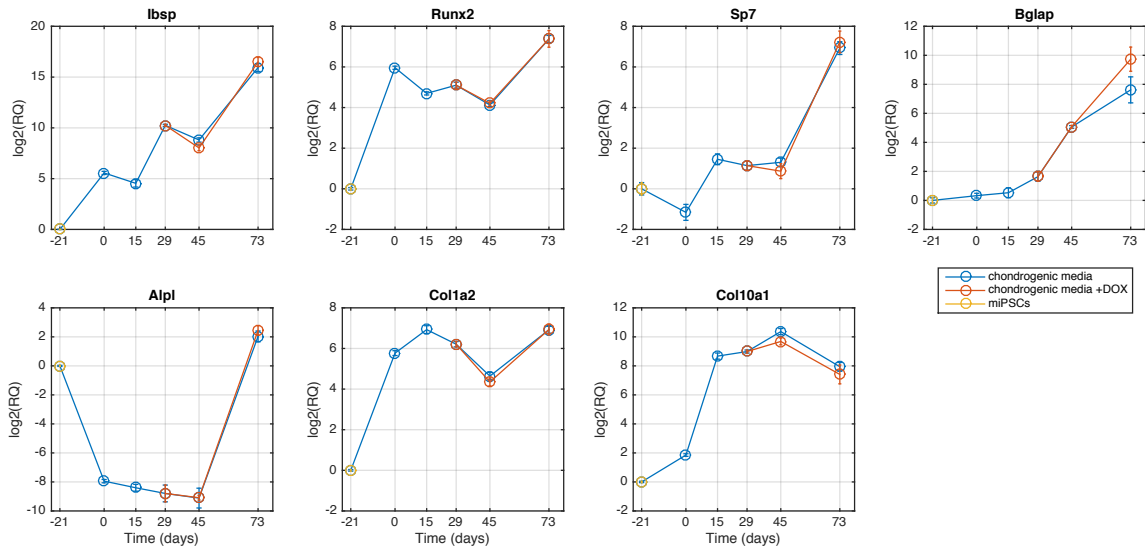


**Figure 3.7 qPCR shows increase in osteogenic gene expression after dox treatment.** Data points and error bars demonstrate mean  $\pm$  SEM. RQ = Relative Quantification, or fold change. The reference gene is GAPDH. A two-way ANOVA by days 45 and 73 and with and without dox treatment demonstrated a significant effect of osteogenic induction, but not of dox treatment with  $p < 0.05$ .

Histologically, there was little difference between groups given dox and groups not given dox before or after osteogenic induction.

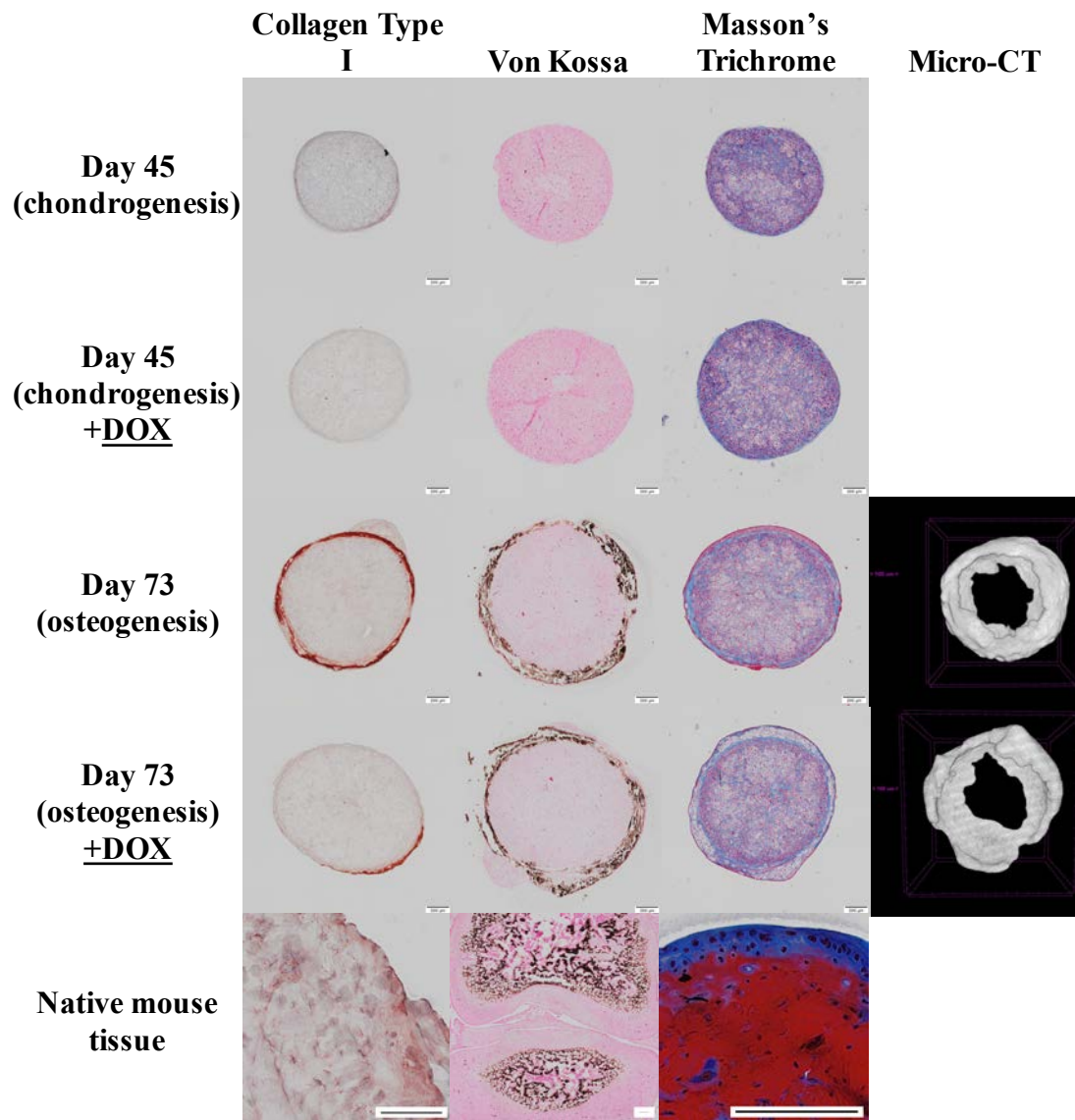


**Figure 3.8** Histological and microCT show treatment with dox had little effect on osteogenic protein expression or mineralization. Mouse controls show native mouse tendon, non-decalcified young mouse knee, and adult mouse shoulder. Scale bars are 200µm in pellet histology samples, and 100µm in mouse tissue controls and microCT images.

Interestingly, chondrogenic gene expression decreased after 16 days of dox induction, and remained lower after osteogenic induction. Dox-induction prior to osteogenic induction had no significant effect on chondrogenic gene expression.

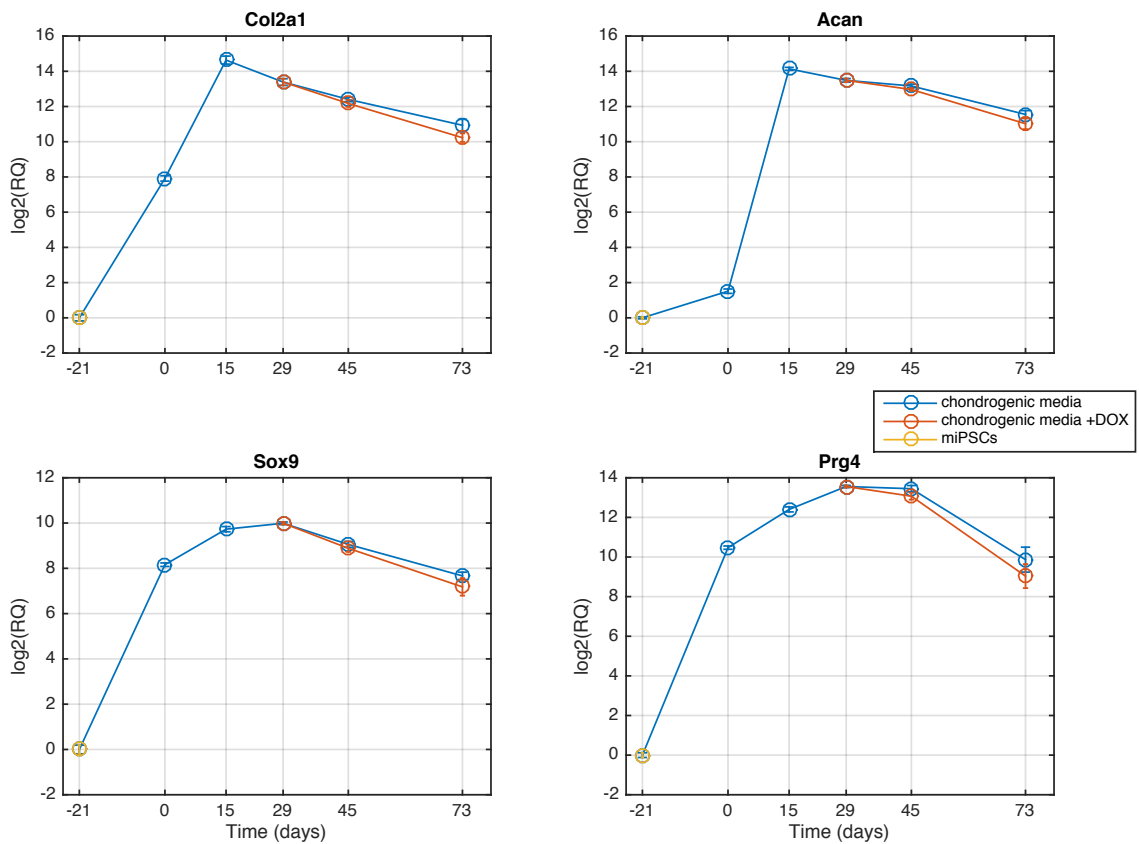


**Figure 3.9 qPCR shows decrease in chondrogenic gene expression after dox treatment.** Data points and error bars demonstrate mean ± SEM. RQ = Relative Quantification, or fold change. The reference gene is GAPDH. A two-way ANOVA by days 45 and 73 and with and without dox treatment demonstrated a significant effect of osteogenic induction on chondrogenic genes, but not of dox treatment with  $p < 0.05$ .

Histologically, there was little difference between groups given dox and groups not given dox before or after osteogenic induction.

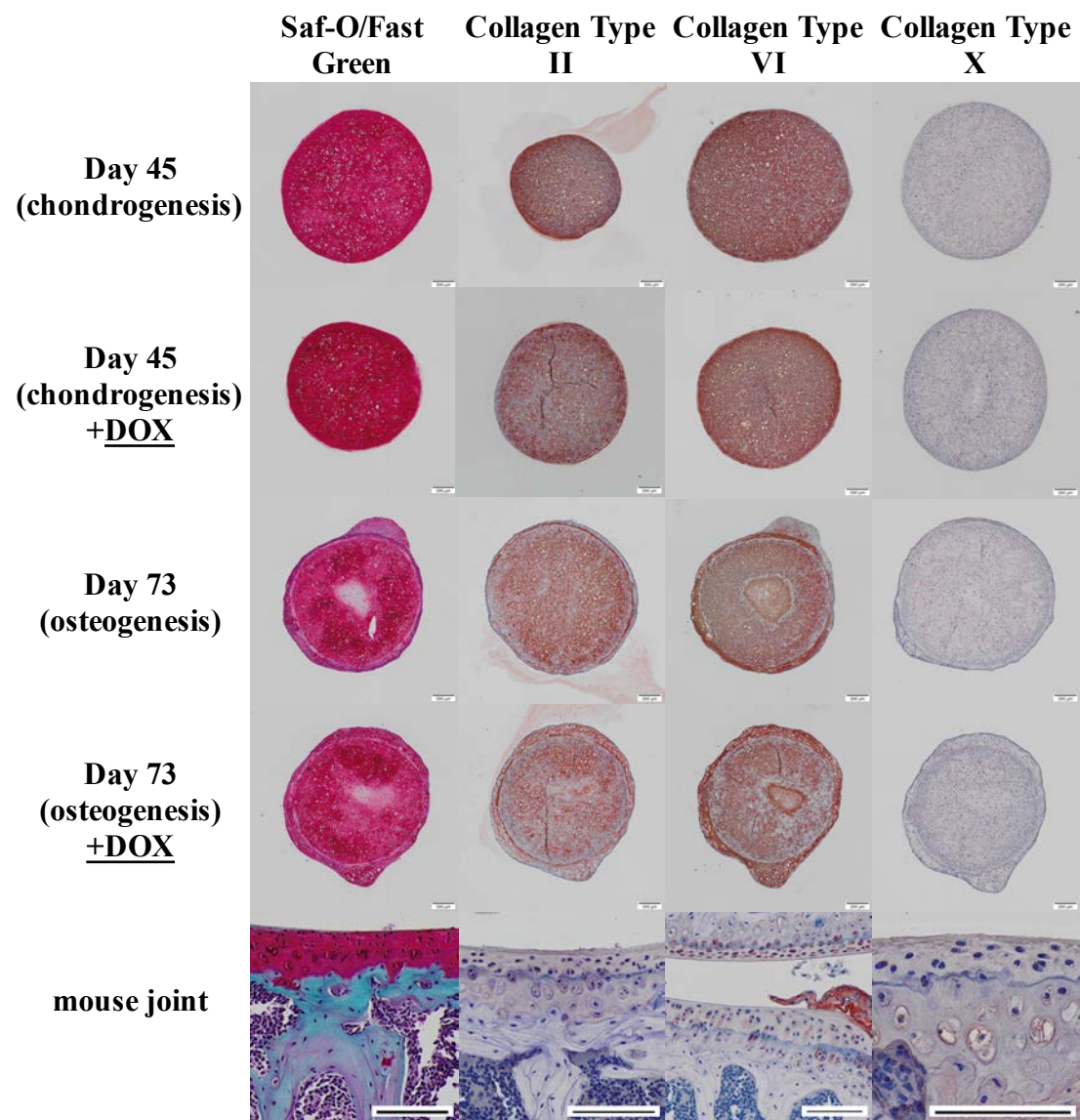


**Figure 3.10** Histological analysis shows treatment with dox had little effect on chondrogenic protein expression. Safranin-O/fast green stain for glycosaminoglycans (GAG in red), and immunohistochemical analysis of Collagen Type II, VI, and X (in red) of pellets, and of native mouse knee joints. Scale bars are 200µm in pellets samples, and 100µm in mouse tissue controls.

On biochemical analysis, dox treatment increased DNA content, suggesting an increase in proliferation of cells in constructs given doxycycline. Osteogenic induction also significantly increased DNA content. GAG content decreased significantly after osteogenic induction, but collagen content was not affected by osteogenic induction. GAG and collagen content normalized to DNA content were not significantly affected by doxycycline. Calcium content increased after osteogenic induction, but dox induction did not affect calcium content.

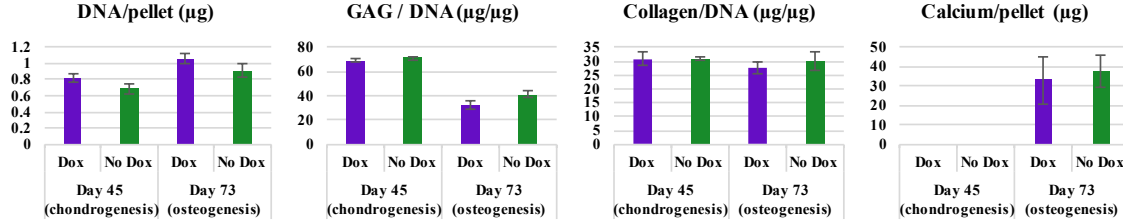


**Figure 3.11 Biochemical analysis of pellets.** Dox treatment significantly increased DNA content before and after osteogenesis, but not collagen or GAG content. Osteogenesis significantly increased calcium content and DNA content, significantly decreased GAG content, and had no effect on total collagen content. Data points and error bars demonstrate mean  $\pm$  SEM. Significance determined by two-way ANOVA with  $p < 0.05$ .

MicroCT evaluation demonstrated shells of mineralization around cores without any mineral content. Total tissue volume increased with dox induction, but bone mineral density, bone volume, and BV/TV were not affected by dox treatment.

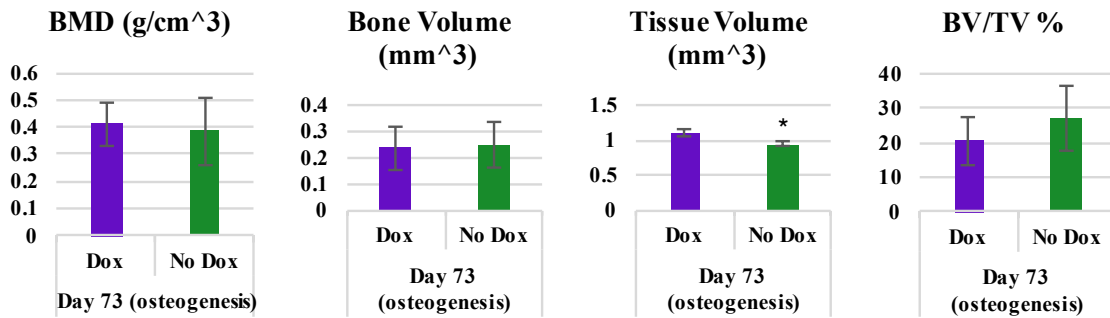


**Figure 3.12 MicroCT evaluation showed dox treatment had little effect on mineralization.** N=4 per group. Data points and error bars demonstrate mean  $\pm$  SEM. Significance determined by two-way ANOVA with  $p < 0.05$ .

### 3.3.4 Doxycycline induction effect on pluripotency in 2D vs. 3D culture

In addition to the experimental groups described above, additional groups were designed to determine the pluripotency potential of cells after chondrogenic induction, both in constructs and in monolayer. After 29 days of chondrogenesis, these pellets were changed to iPSC media with doxycycline for 16 days. During the original induction of pluripotency from mouse tail fibroblasts in this cell line, these cells were given the same iPSC media, with 14 days of doxycycline induction, at the same concentration as in this experiment. After 16 days of dox induction in iPSC media, these pellets were dissociated and cultured in monolayer in a 2i system without feeder cells, and passaged 5-8 times. These cells grew in monolayer, but they never formed colonies characteristic of stem cells. Interestingly, the GFP<sup>+</sup> cells expanded more rapidly and consistently than their GFP<sup>-</sup> counterparts; some of the GFP<sup>-</sup> cells stopped proliferating after 4 passages (not shown) and others continued to proliferate, but all of the GFP<sup>+</sup> cells were

passed 7-8 times. In parallel, on day 29 of chondrogenic pellet culture, other constructs were dissociated and plated in monolayer before 16 days of dox induction in iPSC media. These cells were then passed 7-8 times before colony pluripotency assay was performed.

Cells that were treated with dox in monolayer after dissociation from chondrogenic pellet culture all formed colonies characteristic of iPSCs, and stained for pluripotency factors Nanog, Oct4, SSEA1, and Alkaline Phosphatase. Cells that were treated with dox in pellet cultured and subsequently dissociated and passed continued to grow in monolayer without forming colonies, and did not stain for Nanog, Oct4, or SSEA1. Interestingly, some of these cells did stain positive for alkaline phosphatase, which is also an osteogenic protein. As a fluorescent antibody negative control, GFP+ monolayer dox groups were plated that were given no primary antibodies but all the secondary antibodies, and these indeed showed no nonspecific binding (Figure 3.13).

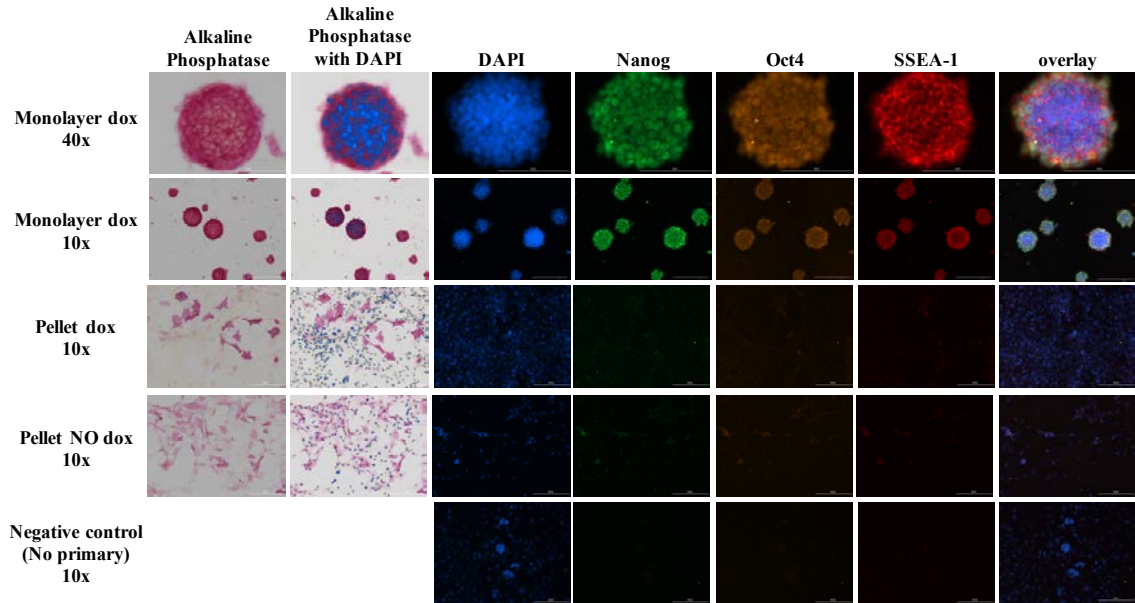


**Figure 3.13 Colony pluripotency assay.** Doxycycline treatment in cells dissociated from chondrogenic pellets and grown in monolayer demonstrate re-induction of pluripotency. Pellets treated with dox and then dissociated do not show markers of pluripotency. Cells in monolayer were grown under 2i conditions for at least 7 passages. Scale bars in 40x images are 200 $\mu$ m, and scale bars in 10x images are 100 $\mu$ m.

Additional images were taken at 40x on a confocal microscope to better appreciate the localization of the antibodies to their transcription factors and membrane protein in the GFP+ monolayer-induction group (Figure 3.14).

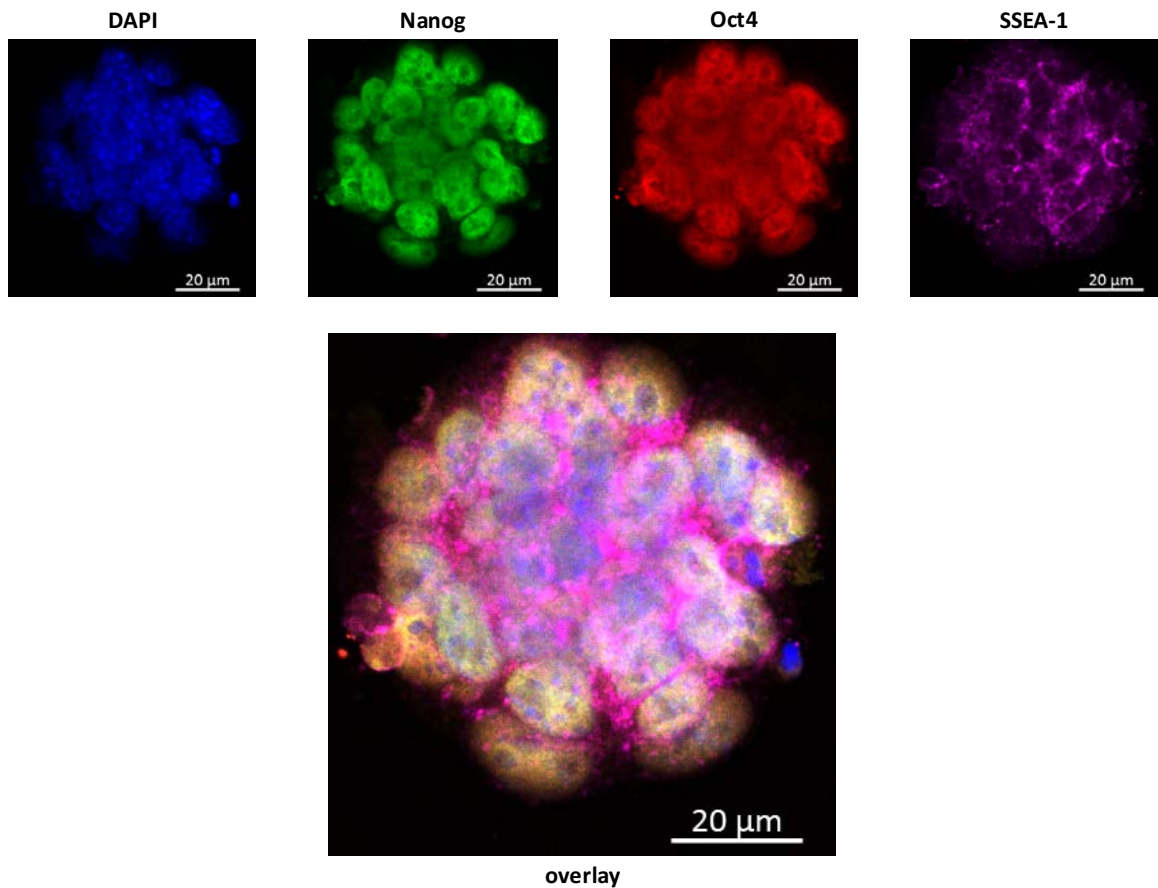


**Figure 3.14 Confocal image of pluripotent colony.** Doxycycline treatment in cells dissociated from chondrogenic pellets and grown in monolayer demonstrate re-induction of pluripotency. Cells dissociated from pellets and treated with doxycycline in monolayer were positive for pluripotency markers.

Finally, pluripotency genes Nanog, Sox2, Oct4, and Alpl were measured via qPCR on each of these pellet groups and compared to miPSCs. Dox treatment, whether given in chondrogenic media or iPSC media, did not restore gene expression of Nanog, Sox2, or Alpl to their original levels. Interestingly, RNA expression of Oct4 in pellets given chondrogenic media with or without dox did recover just above miPSC levels on day 45 (Figure 3.14). Pluripotency, however, is determined by the simultaneous expression of all of these genes, and further

confirmed by their protein expression with a colony pluripotency assay. The complete picture demonstrates that while these cells were capable of re-induction of pluripotency after chondrogenic induction in a pellet construct and subsequent dox induction in monolayer, they were resistant to pluripotency induction in pellet form.

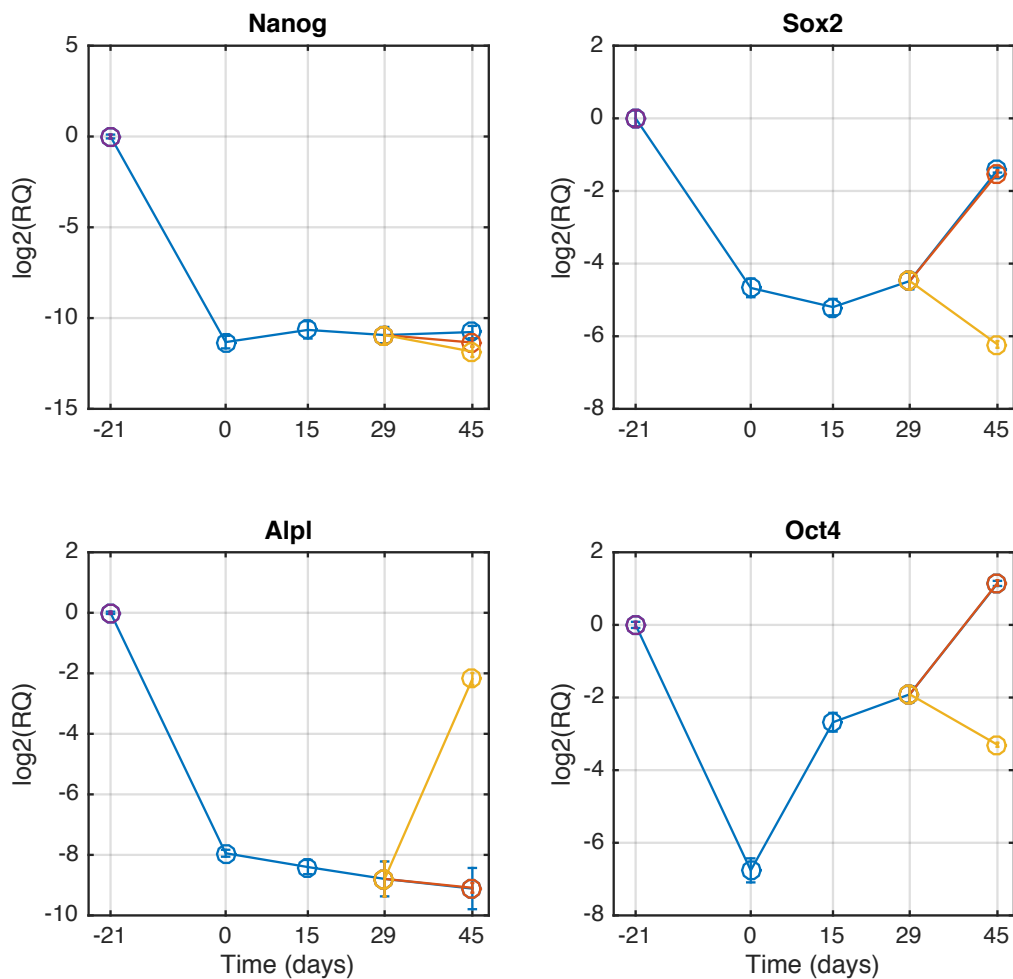


**Figure 3.15 qPCR shows that doxycycline treatment does not restore pluripotency gene expression in pellet constructs after osteochondral induction.** Data points and error bars demonstrate mean  $\pm$  SEM. RQ = Relative Quantification, or fold change. The reference gene is GAPDH. Groups not labelled with the same letter are significantly different by one-way ANOVA with post-hoc Tukey-Kramer analysis with  $p < 0.05$ . Letters are not referring to dox-treated groups.

### **3.4 Discussion: conclusions, limitations, and implications**

In this study, we successfully generated chondrogenic and osteogenic tissue in a single construct from a single cell source. We demonstrated that constructs of neocartilage created from miPSCs can be subsequently osteogenically differentiated via endochondral ossification. Using this platform, we tested two tissue engineering challenges, showing chondrogenic extracellular matrix (ECM) can prevent re-induction of iPSC pluripotency or multipotency in murine cartilage. The impact of this study is two-fold: for translational tissue engineering applications, it implies that a robust chondrogenic matrix may prevent dedifferentiation upon implantation, which has been a critical barrier to iPSC implantation in patients. Additionally, the creation of this novel iPSC-derived osteochondral organoid has great potential as a platform for studying normal and pathological interactions between bone and cartilage at the osteochondral junction, as well as for therapeutic screening in disease models of osteochondral disorders.

The potential for this platform is further illustrated below, but there are limitations in this model as well. Primarily, this pellet platform has a cartilage core surrounded by a bone shell, which does not recapitulate gross anatomy. Additionally, while the construct includes chondrogenic and osteogenic tissue, the joint as an organ includes many additional tissue types, including the meniscus and surrounding ligaments, the synovium, and the surrounding synovial fluid, only somewhat modeled by the media conditions present in this model system. Finally,

the process demonstrated here requires months of continuous cell and tissue culture. With these challenges come the opportunities to advance the model and to study the osteochondral junction. Incorporating other joint tissues into this model could create a more complex organoid structure, capable of answering more complex developmental questions. Optimizing the process to decrease cell culture time would allow for answering these questions in a more efficient timeframe. As the model stands, interesting questions can be explored, including the study of the development and physiology of the osteochondral junction, and the study of the cross-talk between the cartilage and the bone in osteoarthritis and other bone and cartilage diseases.

#### **3.4.1 Creation of an iPSC-derived osteochondral organoid**

Organoids have been created and established for several systems, including intestine, kidney, brain, retina, and liver buds.<sup>67</sup> The potential use of these systems expands from understanding normal physiology to disease modeling, drug testing, and ultimately to organ replacement technologies. There are many pharmaceuticals prescribed that are shown to have an effect on joints, but are difficult to study, including blood pressure medications (ie losartan), and hormonal therapies. Furthermore, numerous infectious diseases lead to arthritis, but other than treating the primary infection, little is done clinically to prevent long-term joint damage. This osteochondral organoid could be an excellent platform to study the interaction of microbial infections on joints to better understand how to treat

arthropathies of many origins. Furthermore, by creating organoids from iPSCs, the model created in this study has all the advantages of that cell type: iPSCs can be genetically modified, or derived from patients who have rare genetically-caused diseases, to better understand the pathology created by these conditions, and to screen drugs targeting pathology specific to that mutation. For the osteochondral system created here, debilitating diseases such as osteoarthritis and osteochondritis dissecans can be studied further, and high-throughput drug screening can be performed demonstrating effects on both bone and cartilage.

#### **3.4.2 Creation of a robust osteochondral construct**

Histological and qPCR analysis of iPSC-derived chondrogenic pellets demonstrate the presence of a robust cartilage matrix, demonstrating gene and protein expression specifically similar to articular cartilage, even through 45 days of pellet culture. Notably, tissue engineering with other cell types such as MSCs and ASCs tend to show such a profile in the first couple of weeks, but then begin to undergo hypertrophy, as evidenced by high gene and protein expression of Type X Collagen. A recent single-cell RNA seq screening of Chondrogenically-induced MSCs demonstrated an increase of Collagen Type X over 100,000 fold from day zero (not yet published), whereas the data from this study compared to its own day zero never went higher than a 1300 fold increase at day 45. This much lower expression of hypertrophic markers in iPSC-derived chondrogenic tissue is consistent in hiPSC literature as well,<sup>58-62</sup> suggesting a possible stable source of

non-hypertrophic, articular cartilage for tissue engineering applications.<sup>63</sup> A head-to-head study of MSCs grown in parallel with iPSCs looking specifically at differences in the mechanism of hypertrophic induction would be an interesting future study. A recent study found that in the context of fracture healing, cartilage to bone transformation transdifferentiate through the hypertrophic state while transiently expressing pluripotency genes;<sup>104</sup> this type of physiology in our model of endochondral ossification could explain the rise in Oct4 expression near the end of our culture period. Further study of this pathway in our model system would help elucidate the process of endochondral ossification.

### **3.4.3 Prevention of re-induction of pluripotency with cartilaginous extracellular matrix**

After sufficient induction of chondrogenesis in a tissue construct, re-induction of pluripotency was possible in dissociated cells subsequently grown in monolayer; but under the same conditions in their chondrogenic tissue construct, pluripotency was not re-induced. One of the most exciting potential applications of iPSCs is their ability to be created from a patient's own cells, and re-differentiated and grown into a tissue for re-implantation, potentially with all the advantages of an autologous transplantation, without rejection of the implanted tissue. However, to date, only one tissue construct has been re-implanted in a human patient. The second patient enrolled in that study was not given the implant because of chromosomal anomalies that concerned the researchers for potential of re-induction of pluripotency and possible teratoma formation.<sup>105</sup>

These findings are consistent with previous reports indicating that the pluripotency and differentiation potential of stem cells in a 3D environment are dependent on the physical properties of the ECM, such as matrix stiffness and elasticity,<sup>106, 107</sup> matrix softness,<sup>108, 109</sup> and cellular adhesivity.<sup>110</sup> Synergistic effects of the characteristically high stiffness in cartilage ECM, and specific receptor-ligand interactions between cells and their collagen matrix may be responsible for these results. Further study is needed to determine the precise ECM properties that provide these characteristics to iPSCs.

## **4. Cartilage and Bone Tissue Engineering on 3D-Woven Scaffolds with Induced Pluripotent Stem Cells**

### **4.1 Rationale and experimental plan**

As introduced above, the next objective was to create osteochondral grafts for cartilage defect repair. An optimal tissue-engineered construct for cartilage defect repair requires a sufficiently strong scaffold, that wears slowly, is biocompatible, and supports extracellular matrix formation. Additionally, the cell source for the construct must be pluripotent, or at least multipotent, to form both bone and cartilage tissue types; and non-immunogenic. iPSCs can be harvested from the patient, and can make both bone and cartilage tissue. The construct must also be self-sufficient, and support endogenous chondrogenic and osteogenic signaling. To realize this requirement, an ideal construct would have controlled production of relevant growth factors, to allow for local delivery, regulated growth, and decreased culture time. Such control can be achieved through viral transduction of expression vectors, including constitutive expression vectors for continued differentiation and growth, and inducible expression vectors for controlled growth factor expression. Finally, a construct for cartilage defect repair must allow for proper anchoring into the subchondral bone, and thus must have both chondrogenic and mineralized tissue present.

A new mouse iPSC line was used and transduced with the pluripotency factors Oct4, Sox2, Klf4, and c-Myc via a transiently expressed sendai-viral vector.

The sendai virus is a single-stranded negative-sense RNA virus that replicates in the cytoplasm, and thus does not integrate into the cell genome.

Mouse iPSCs expressed GFP under the control of the *Col2a1* promoter,<sup>97</sup> which allowed for fluorescence-activated cell sorting of chondrogenically differentiated cells as described above.<sup>50</sup> Lentiviruses encoding TGF- $\beta$ 3, BMP-2, or GFP (control) were produced in 293T cells, then immobilized on the 3-D woven poly( $\epsilon$ -caprolactone) (PCL) scaffold with poly-L-lysine. Lentiviruses for TGF- $\beta$ 3 and BMP-2 were created under constitutive promoters, as well as doxycycline-inducible (TetOn) promoters. Cells were seeded onto the bioactive scaffolds and cultured in chondrogenic or osteogenic media conditions for 28 days before histological, gene expression, biochemical, and micro-computed tomography analyses.

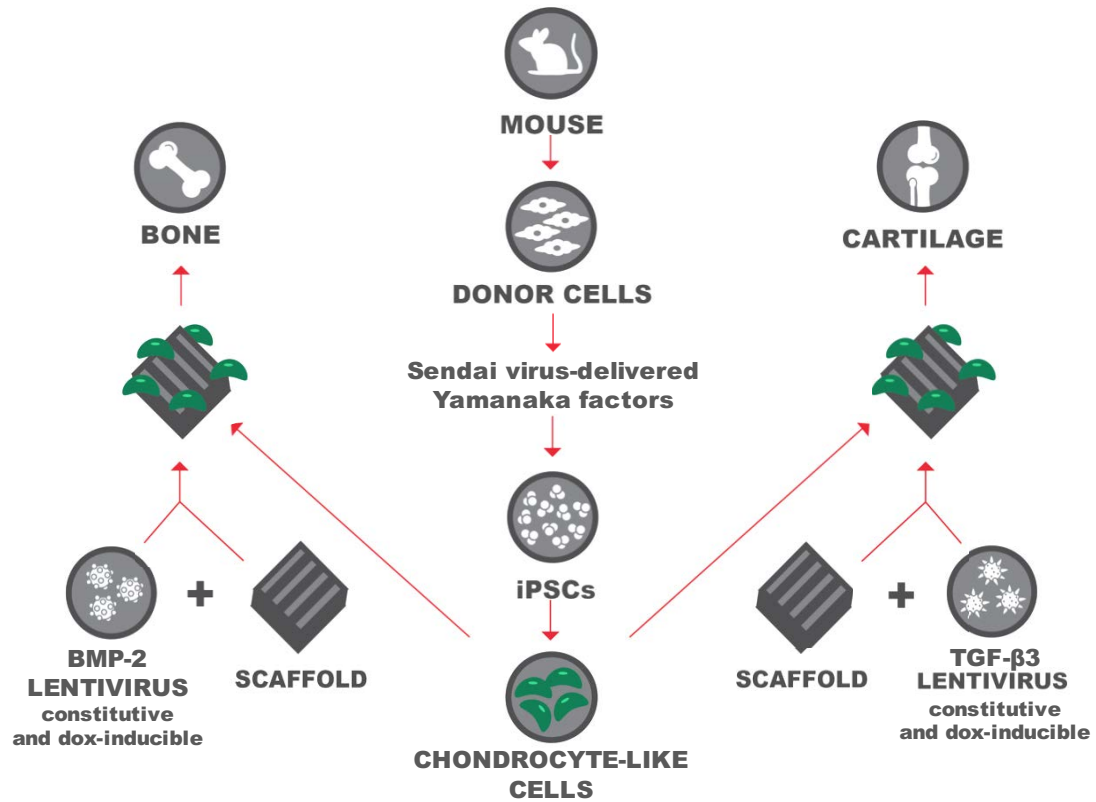


**Figure 4.1 Study design: osteogenic and chondrogenic tissue engineering on PCL 3D-woven scaffold with miPSCs.** After chondrogenic differentiation, lentiviruses encoding constitutive and doxycycline-inducible TGF- $\beta$ 3, BMP-2, or GFP (control) were immobilized on 3D-woven scaffolds made from PCL. Bioactive scaffolds were seeded with chondrogenically differentiated and sorted iPSCs, and cultured for 28 days.

With the goal of producing chondrogenic, osteogenic, and osteochondral tissue constructs, multiple experimental groups were incorporated into this study. Constructs made with the GFP control viral vector were grown in four different media conditions: chondrogenic media with and without TGF- $\beta$ 3, and osteogenic media with and without BMP2, serving as virally-transduced controls. Constitutive viruses for TGF- $\beta$ 3 and BMP2 were given chondrogenic and osteogenic media respectively, without exogenous growth factors. Inducible viruses for TGF- $\beta$ 3 and

BMP2 were given chondrogenic and osteogenic media respectively, without exogenous growth factors. To discern the necessary time-course of growth factor expression, doxycycline was added to the media in these groups for three different lengths of time: 3 days of doxycycline followed by 25 days without; 15 days of doxycycline followed by 13 days without; and 28 days of doxycycline. As additional non-transduced controls, scaffolds without immobilized virus were seeded with the same number of cells, and given chondrogenic media with or without TGF- $\beta$ 3, and osteogenic media with or without BMP2. All osteogenic constructs were flipped over every 3 days to encourage consistent mineralization throughout the construct. Finally, to create a biphasic osteochondral construct, chondrogenic media with BMP2 was given to constructs which were cultured without flipping for 28 days and, as a control, chondrogenic media with BMP2 was given to additional constructs which were flipped every three days for 28 days.

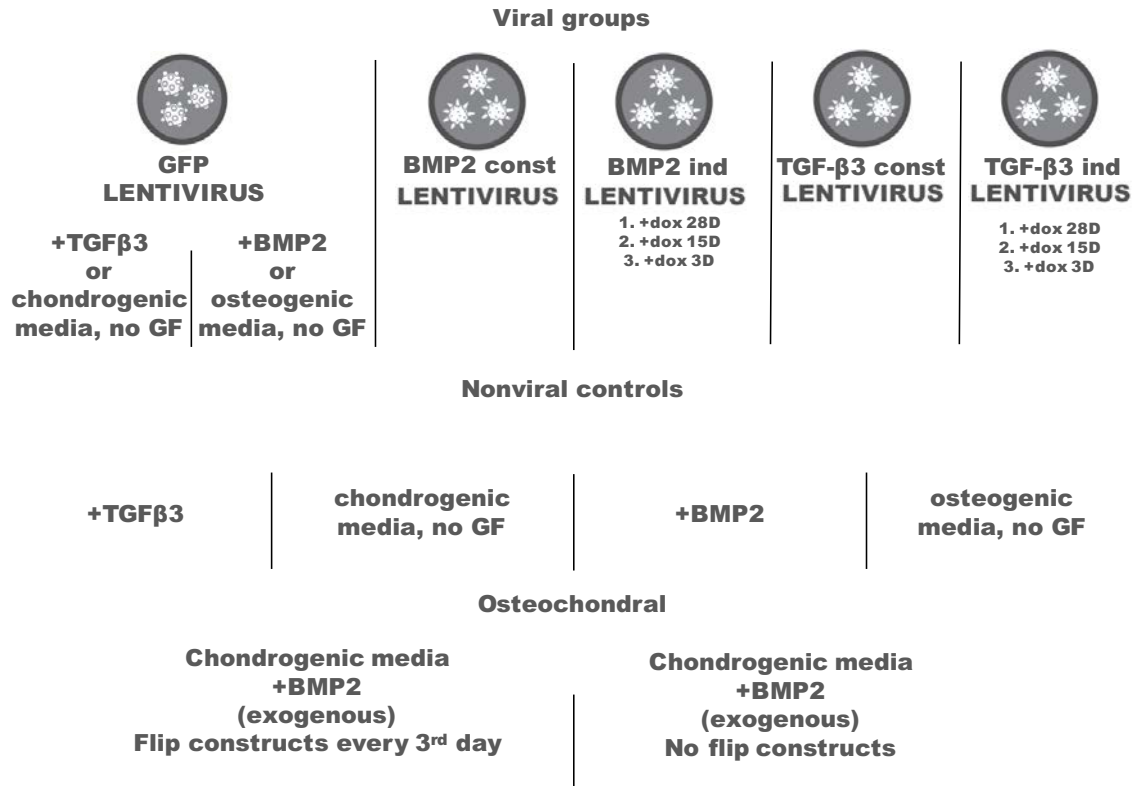


**Figure 4.2 Study design: experimental groups.** To create osteogenic, chondrogenic, and osteochondral scaffold-based constructs with the same cell source, five lentiviral vectors were made for this study, and multiple media conditions were used, with 18 total groups cultured. The inducible viral vector is based on a TetOn system, such that doxycycline induces expression of the growth factors TGF-β3 or BMP2. Const = constitutive; Ind = inducible; GF = growth factor.

## 4.2 Methods

### 4.2.1 Chondrogenic differentiation of miPSCs via micromass formation, and purification of Col2-GFP miPSCs via flow cytometry

miPSCs were purchased from the University of Colorado iPSC Core. Line miPSC002.07 was derived from mouse primary fibroblasts (C57Bl/6N Taconic). The cells were tested for expression of standard pluripotency markers (similar to

C57BL/6 ES cells) as determined by QRT-PCR and immunostaining, and shown to differentiate into cells of all three germ layers using an in vitro differentiation assay (Embryoid Body (EB) Differentiation Assay).

Mouse embryonic fibroblasts (PMEF, Millipore) were expanded and treated with 10 µg/mL mitomycin-C (Sigma-Aldrich) for 2–3 h to prevent proliferation and then cultured on 0.1% gelatin coated dishes at confluence to provide a feeder layer. Once received at Washington University in St Louis, cells were expanded on MEF feeder cells in iPSC media. The Col2GFP reporter plasmid<sup>97</sup> was grown from a glycerol stock of *e. coli* containing the plasmid, and was sequenced from three separate colonies with consistent results. The plasmid was enzymatically linearized with a restriction enzyme; linearization was verified via gel electrophoresis, and gel extraction and DNA purification were performed, followed by concentration of the linearized plasmid with a SpeedVac system. miPSCs underwent feeder subtraction, and half of these cells were re-plated on feeder vells to use as a control for micromass chondrogenesis. The other half of feeder-subtracted cells were split into two groups, which were nucleofected in parallel, one with the Col2-GFP reporter construct, and one with a pMaxGFP linearized plasmid as a visual control. Cells were re-plated on feeder cells, and selected for transfected clones with G418 given days 2-12 post-transfection. 46 individual colonies were manually selected for clonal expansion and freezing, with 12 colonies left in culture, along with the non-nucleofected control. These colonies were differentiated in micromass, and the most chondrogenic reporter line was

chosen based on GFP positive percentages after flow sort (Figure 4.3), alcian blue staining of micromasses (Figure 4.4), and safo-fast-green staining of pellets after 21 days of chondrogenic culture (not shown).

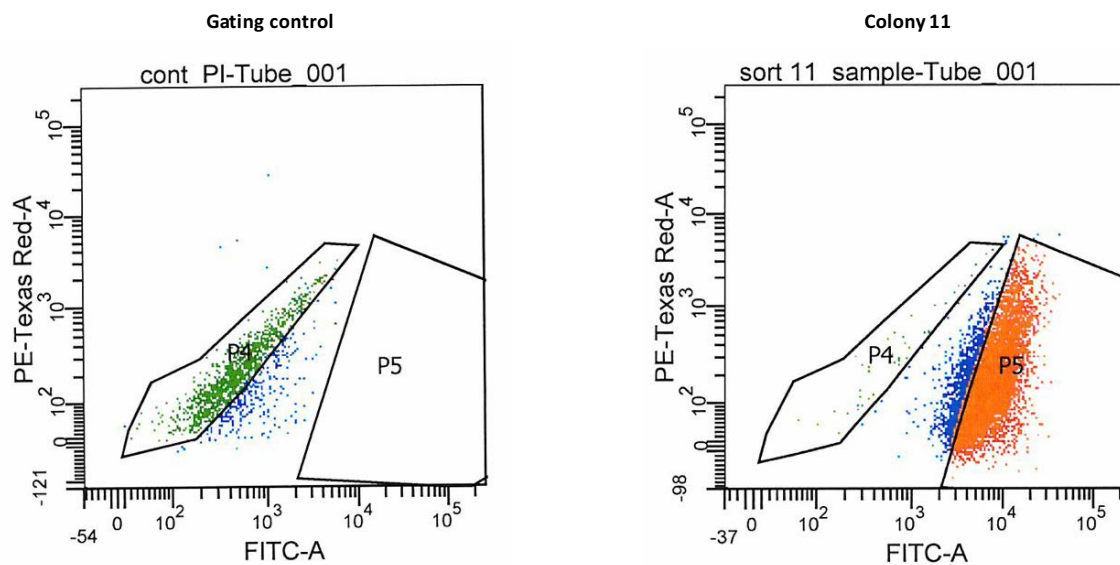


**Figure 4.3 Flow sort analysis.** Flow data was gated on miPSCs without the Col2-GFP reporter plasmid, and differentiated in micromass in parallel with the Col2-GFP-containing cells. ~63% of cells were GFP+ compared to gating control without the reporter.

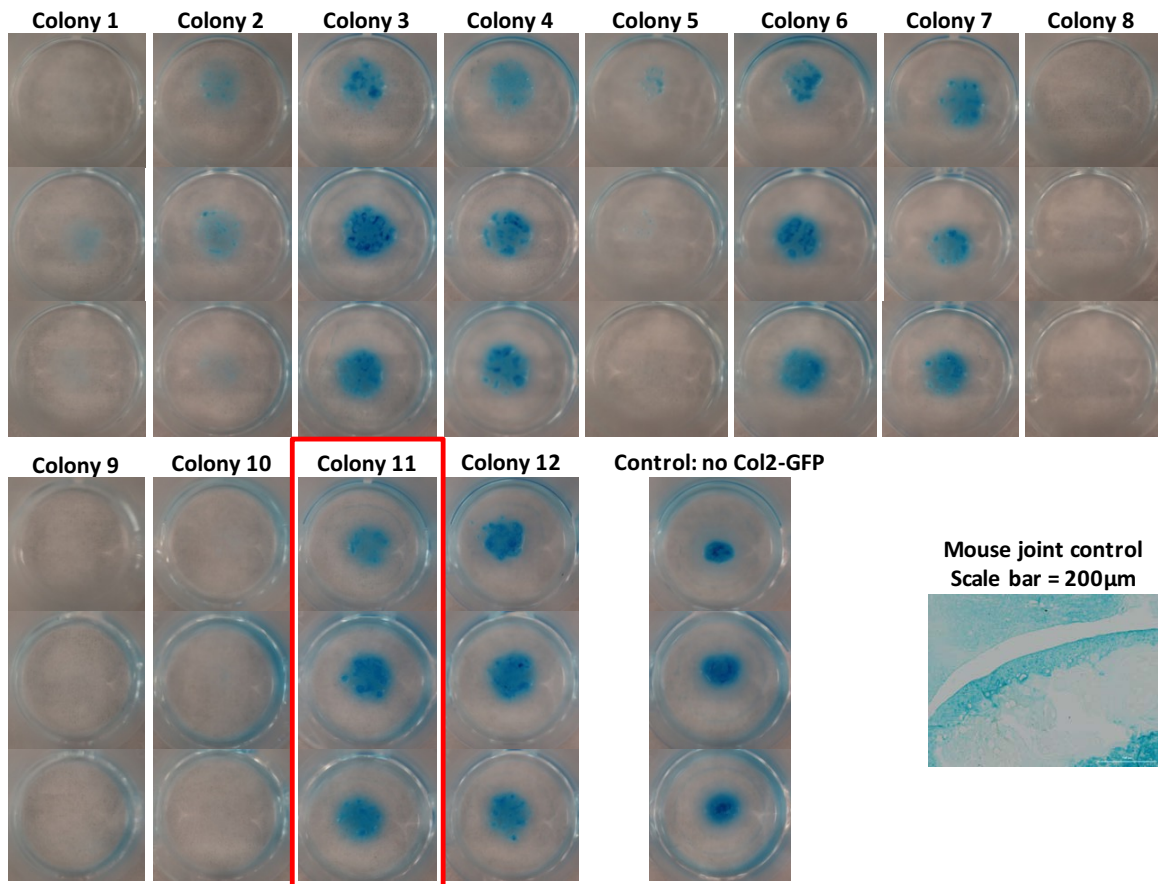


**Figure 4.4 Alcian blue staining of micromasses.** Alcian blue staining for GAG (blue) was performed after micromass differentiation on three micromasses from each Col2-GFP reporter-containing colony, as well as the non-transfected control. Colony 11 (highlighted in red) was chosen for this study based on alcian blue staining, GFP+ percentage after sort, and subsequent pellet chondrogenesis. Mouse joint control is shown.

After selection of one clonal reporter line, MEFs were cultured on 0.1% gelatin coated dishes and miPSCs were cultured in iPSC media containing DMEM-HG (Gibco), 20% lot-selected FBS (Atlanta Biologicals), MEM nonessential amino acids (NEAA, Gibco),  $\beta$ -mercaptoethanol (Gibco), gentamicin (Gibco), and mouse leukemia inhibitory factor (LIF, Millipore ESGRO).

After expansion on MEF feeder cells, feeder subtraction was performed in two 45min incubation periods, separated by 24 hours of culture on 0.1% gelatin coated plates. After passage, cells were resuspended at a concentration of  $2 \times 10^7$  cells/mL, and 10 $\mu$ L, or  $2 \times 10^5$  cells, were pipetted into each well of a 48-well cell culture plate. After 2 hours of incubation, 0.5mL of iPSC media with 10% serum and no LIF was added to each well. After 24 hours, media was replaced with serum free chondrogenic differentiation medium, with DMEM-HG (Gibco), NEAA (Gibco),  $\beta$ -mercaptoethanol (Gibco), ITS+ (BD), penicillin-streptomycin (Gibco), 50  $\mu$ g/mL L-ascorbic acid 2-phosphate (Sigma), and 40  $\mu$ g/mL L-proline (Sigma). Micromasses were cultured for 15 days. On days 3-5 of culture, 50 ng/mL mBMP-4 (R&D Systems) and 100 nM dexamethasone were added to the chondrogenic medium. Micromasses were then digested for 1 hour at 37°C using 0.4% collagenase type II (Worthington), 1320 PKU/mL pronase (Calbiochem), and 10  $\mu$ g/mL DNase I (Worthington) and pipetted every 15min during incubation. Cells were centrifuged, incubated with 0.25% trypsin-EDTA for 5 min, and resuspended in sort medium containing DMEM-HG, 2% FBS, DNase I, 10 mM HEPES (Gibco), 2x Penicillin/Streptomycin/Fungizone, and 5  $\mu$ M propidium iodide (Biolegend).<sup>50</sup> Cells were sorted based on GFP expression using the 100  $\mu$ m nozzle of an Aria II flow sorter (BD BioSciences, Washington University Flow Core).

#### 4.2.2 Lentivirus production

Lentiviral production methods of constitutive and inducible systems have been previously described by our lab.<sup>89, 96</sup> All plasmids were obtained from the Addgene Plasmid Repository. The cDNA for TGF- $\beta$ 3 and BMP-2 were obtained from HEK-293T cells via RT-PCR and cloned into a lentiviral transfer vector [Addgene Plasmid 12250<sup>111</sup> modified with a multiple-cloning site downstream of the EF-1 $\alpha$  promoter]. Virus driving overexpression of eGFP was produced using either Addgene Plasmid 21320<sup>112</sup> or 11645<sup>113</sup> modified to contain an EF1- $\alpha$ -eGFP cassette. The dox-inducible lentiviral vector (TMPrtTA, provided by the Danos Lab) is a single “tet-on” vector that constitutively co-expresses an improved reverse tetracycline-controlled transcriptional activator.<sup>92, 95, 114</sup> The dox-inducible vector was modified to include an IRES-puromycin expression cassette. The cDNA for TGF- $\beta$ 3 and BMP-2 were cloned into the modified TMPrtTA vector as well.<sup>95</sup> To produce VSV-G pseudotyped LV, 4.2e6 HEK-293T cells were plated onto each 10-cm dish in DMEM–high glucose supplemented with l-glutamine, sodium pyruvate, and 10% FBS (D-10 medium). The following day, cells on each dish were cotransfected with the appropriate lentiviral transfer plasmid (20  $\mu$ g), the second-generation packaging plasmid, psPAX2 (Addgene 12260, 15  $\mu$ g), and the pMD2.G (Addgene 12259, 6  $\mu$ g) envelope plasmid via calcium phosphate precipitation.<sup>115</sup> After an overnight incubation, transfection medium was removed and replaced with 12 mL of fresh 293T medium. The raw lentiviral supernatant was cleared of producer cells via centrifugation and stored

at  $-80\text{ }^{\circ}\text{C}$  until future use. Prior to scaffold immobilization, LV was concentrated via centrifugation in 100kDa MWCO filters (Millipre, Cork, Ireland).

#### **4.2.3 Production of 3D-woven PCL scaffold**

Using a custom-built weaving machine, scaffolds were woven from multifilament PCL yarns (EMS-Griltech, Domat, Switzerland) as previously described.<sup>37</sup> 7 layers of yarns, three warp and four weft, were axially oriented in alternating x and y directions with a third set of fibers passing through all the layers of the structure (z-direction). Scaffolds were treated with 4N NaOH for 16 hours to increase hydrophilicity, rinsed in DI water, dried, and heat set for 10 min at  $57^{\circ}\text{C}$ . 4mm biopsy punches were used to create scaffold cylinders. Disks were then ethylene-oxide sterilized in 24 well ultra-low attachment plates (Corning, Corning, NY), and then soaked overnight in 0.002% PLL (Sigma) prior to use in tissue engineering experiments.

#### **4.2.4 Cell culture: scaffold construct formation and culture**

After sort, cells were expanded on gelatin coated plates at  $1 \times 10^4$  cells/cm<sup>2</sup> in chondrogenic differentiation media with 4ng/mL hbFGF (Roche) and 10% FBS. Cells were passaged every 3 days for two passages using 0.05% trypsin EDTA (Sigma). After the second passage, cells were resuspended in expansion media at a concentration of  $3 \times 10^7$  cells per mL. Scaffolds were transferred to new 24 well ultra-low attachment plates, and concentrated LV was pipetted onto each

scaffold for the viral groups. Scaffolds were incubated at room temperature for one hour, rinsed in PBS, and then seeded with  $3 \times 10^5$  cells each. Constructs were incubated for 1 hour at 37°C, followed by the addition of 1mL media to each well. Chondrogenic media contained 100nM dexamethasone, in addition to DMEM-HG (Gibco), NEAA (Gibco),  $\beta$ -mercaptoethanol (Gibco), ITS+ (BD), penicillin-streptomycin (Gibco), 50  $\mu$ g/mL L-ascorbic acid 2-phosphate (Sigma), and 40  $\mu$ g/mL L-proline (Sigma), with or without 10ng/mL TGF- $\beta$ 3. Osteogenic media contained 10% FBS, DMEM-HG (Gibco), NEAA (Gibco),  $\beta$ -mercaptoethanol (Gibco), penicillin-streptomycin (Gibco), 50  $\mu$ g/mL L-ascorbic acid 2-phosphate (Sigma), dexamethasone, and 10mM  $\beta$ -glycerophosphate (Sigma), with or without 12.5ng/mL BMP2 (RnD). Osteochondral media contained 50ng/mL BMP2 (RnD), 1% FBS, 100nM dexamethasone, DMEM-HG (Gibco), NEAA (Gibco),  $\beta$ -mercaptoethanol (Gibco), ITS+ (BD), penicillin-streptomycin (Gibco), 50  $\mu$ g/mL L-ascorbic acid 2-phosphate (Sigma), and 40  $\mu$ g/mL L-proline (Sigma), 10mM  $\beta$ -glycerophosphate (Sigma). Every 3 days, 500 $\mu$ L was taken from each scaffold and frozen for ELISA analysis, and replaced with 500-600 $\mu$ L fresh media (depending on evaporation). For doxycycline-inducible vector systems, 1 $\mu$ g/mL doxycycline (Sigma) was added to the media for 3 days, 15 days, or 28 days, depending on the experimental group.

Mycoplasma test samples were collected regularly throughout the cell and tissue culture experiments and tests were performed by an independent core

facility at Washington University. DAPI staining for the colony pluripotency assay further demonstrated negative mycoplasma results.

#### **4.2.5 Flow cytometry analysis of transduction efficiency**

To determine transduction efficiency, 3 scaffolds from each group at both day 14 and day 28 of culture from groups with fluorescent protein expression (constitutive BMP2 (dsRed), constitutive TGF $\beta$ 3 (dsRed), and eGFP) were digested for 1 hour and 15min at 37°C using 0.4% collagenase type II (Worthington), 1320 PKU/mL pronase (Calbiochem), and 10  $\mu$ g/mL DNase I (Worthington) and pipetted every 15min during incubation. Cells were centrifuged, incubated with 0.25% trypsin-EDTA for 5 min, and resuspended in sort medium containing DMEM-HG, 2% FBS, DNase I, 10 mM HEPES (Gibco), 2x Penicillin/Streptomycin/Fungizone, and 5  $\mu$ M propidium iodide (Biolegend).<sup>50</sup> Cells were analysed based on GFP expression or dsRed expression using the 100  $\mu$ m nozzle of an Aria II flow sorter (BD BioSciences, Washington University Flow Core).

#### **4.2.6 Gene expression analysis: RNA isolation and quantitative RT-PCR (qPCR)**

Whole scaffolds or scaffolds cut in half were placed in cryovials and flash-frozen in liquid nitrogen prior to storage at -80°C until RNA isolation. In a sterile culture hood, scaffolds were individually minced and placed in a 1.7mL Eppendorf

tube. 1mL trizol was added followed by 2 sterile glass beads. Tubes were placed in a bead beater for mechanical disruption of constructs, followed by 30 minutes of rocking in a cold room. Samples were centrifuged and lysate was transferred to new Eppendorf tubes and frozen at -80°C until RNA isolation. RNA isolation was performed via chloroform purification and separation (Trizol, Invitrogen), followed by column purification of the aqueous layer (Total RNA Purification Plus Micro Kit, Norgen). RNA concentrations and RINe values were measured using an Agilent 2200 TapeStation System (Agilent Technologies), with a ladder run on each gel. cDNA synthesis was performed using SuperScript IV First-Strand Synthesis System (ThermoFisher), in parallel with a No Template Control (NTC). PCR was performed with Taqman Gene Expression Assay probes (ThermoFisher) (Table 4.1), and Taqman Fast Advanced Master Mix. Samples from each group were divided across plates, and the NTC was run with each probe. NTC showed no amplification for any probes after 55 cycles. All samples were run in triplicate. Data analysis was performed with the  $\Delta\Delta CT$  method, and displayed as fold changes, where  $RT = 2^{-(\Delta\Delta CT)}$ . GAPDH was used as the endogenous control gene. All samples were compared to cells flash frozen on the day of scaffold seeding (day 0).

**Table 4.1 Primer probes for qPCR.**

<b>Gene</b>	<b>Name</b>	<b>Probe</b>
Col1a2	Type I collagen	Mm00483888_m1
Col2a1	Type II collagen	Mm01309565_m1
Col10a1	Type 10 collagen	Mm00487041_m1
Acan	Aggrecan	Mm00545794_m1
Sox9	sex determining region Y-box 9	Mm00448840_m1
GAPDH	Glyceraldehyde 3-phosphate dehydrogenase	Mm99999915_g1
Prg4	Lubricin	Mm01284582_m1
Bglap	Osteocalcin	Mm03413826_mH
Runx2	Runt-related transcription factor 2	Mm00501584_m1
Sp7	Osterix	Mm04209856_m1
TGF- $\beta$ 3	Transforming Growth Factor Beta 3	Hs01086000_m1
BMP2	Bone morphogenetic protein 2	Hs00154192_m1

#### **4.2.7 Histological analysis**

For histology, scaffolds were fixed in 10% Neutral Buffered Formalin for 16 hours, dehydrated, paraffin embedded, and sectioned at 8  $\mu$ m thickness. Safranin-O/fast green/hematoxylin staining was stained under standard protocols using osteochondral sections from mouse knee joints as controls. Von Kossa staining was performed according to manufacturer instructions (Abcam); the control joint for this was a knee joint dissected from an 11-day old mouse. This skeletally-immature age allowed for fixation, embedding, and sectioning of the joint without decalcification. Masson's Trichrome staining was performed according to manufacturer's instructions (Abcam) using osteochondral sections from mouse shoulder joints as controls.

For immunohistochemistry, sections were treated with xylene and ethanol in decreasing concentrations. For type II collagen (Iowa II-II6B3, 1:1 in goat serum), type VI collagen (Fitzgerald 70R-CR009x, 1:1000 in 1% BSA), and type X collagen (Sigma c7974, 1:400), epitope retrieval was performed with Digest-All 3 Pepsin (Invitrogen) at room temperature for 5min, then treated with methanol-peroxidase, blocked for 30min (goat serum for type X collagen, goat serum with the addition of cold fish gelatin for type II collagen, and for type VI collagen, 2% goat serum, 1% BSA, 0.1% Triton X-100, 0.05% Tween 20, 0.01M PBS (pH 7.2)), then incubated for an hour at room temperature in primary antibody. Secondary antibody incubation was 30min at room temperature (ab97021 for type II collagen and type X collagen, and ab6720 for type VI collagen, 1:500), followed by HRP Streptavidin treatment and AEC Red Single (Histostain Plus, Invitrogen), counterstained with hematoxylin, and mounted with Vectamount (Vector Labs). Osteochondral sections from mouse knee joints were used as controls. For type I collagen (8D4A1, Chondrex, 1:200, biotinylated), epitope retrieval was performed with pepsin incubation at 37°C for 20min, then treated with methanol-peroxidase, and blocked for 30min (goat serum) before primary incubation. Mouse hip cartilage from 10 day old mice and mouse patellar tendon were used as negative and positive controls, respectively.

Final histology images were taken on a VS120 microscope imaging system at 20x magnification, with consistent bright field settings for each stain.

#### **4.2.8 microCT analysis**

Scaffold constructs were serially dehydrated to 70% ethanol. Kim wipes soaked in 70% ethanol were placed at the bottom of 15mL conical tubes, which were laid on their sides, and scaffolds were placed on the sides of the conical tubes for microCT imaging using a Skyscan Bruker microCT. Consistent settings were used to image pellets and calibration phantoms. After reconstruction, phantoms were used to determine threshold values for mineralization. In order to determine tissue volume and bone mineral density, sections of scaffolds were outlined with an automated program. Tissue volume, bone volume, and bone mineral density values were calculated using CTAnalyser software (Bruker). Images and videos were generated in CTVox software (Bruker).

#### **4.2.9 ELISA and biochemical analysis**

ELISAs measuring human BMP-2 and human TGF- $\beta$ 3 were performed according to manufacturer's instructions (DuoSet ELISA kits, R&Dsystems). Only active TGF- $\beta$ 3 can be measured; in addition to measuring active TGF- $\beta$ 3 from the media samples, media was activated and measured, giving concentration measurements of active, total, and inactive (latent) TGF- $\beta$ 3 in media samples.

Scaffolds were digested in papain at 58°C for 16 hours. dsDNA was measured with PicoGreen dsDNA Quantitation kit (Invitrogen). Sulfated glycosaminoglycans were measured with the DMB assay, and total collagen was

measured with the hydroxyproline assay.<sup>103</sup> To quantify calcium content, scaffold constructs were decalcified by incubating in 5% formic acid for 30 minutes. Calcium concentration was measured using the Calcium Colorimetric Assay Kit (Fisher).

#### **4.2.10 Statistics**

Experimental data reported as mean  $\pm$  SEM was compared using Student's t-test, a one-way ANOVA followed by a post-hoc Tukey's test, or a two-way ANOVA. Data was analyzed with JMP with a significance level set to  $\alpha=0.05$ .

### **4.3 Results**

#### **3.3.1 Osteogenic scaffold constructs**

After several days of osteogenic culture, the bottom of each well began to accumulate mineral content, with more obvious mineralization accumulating in groups with exogenous, constitutive, or induced BMP2 expression. Indeed, gene expression confirmed increasing osteogenic gene expression over time, with the constitutive BMP-2-expressing group having the largest increase in most

osteogenic genes. Interestingly, very little Col10a1 expression is present in any of these constructs.

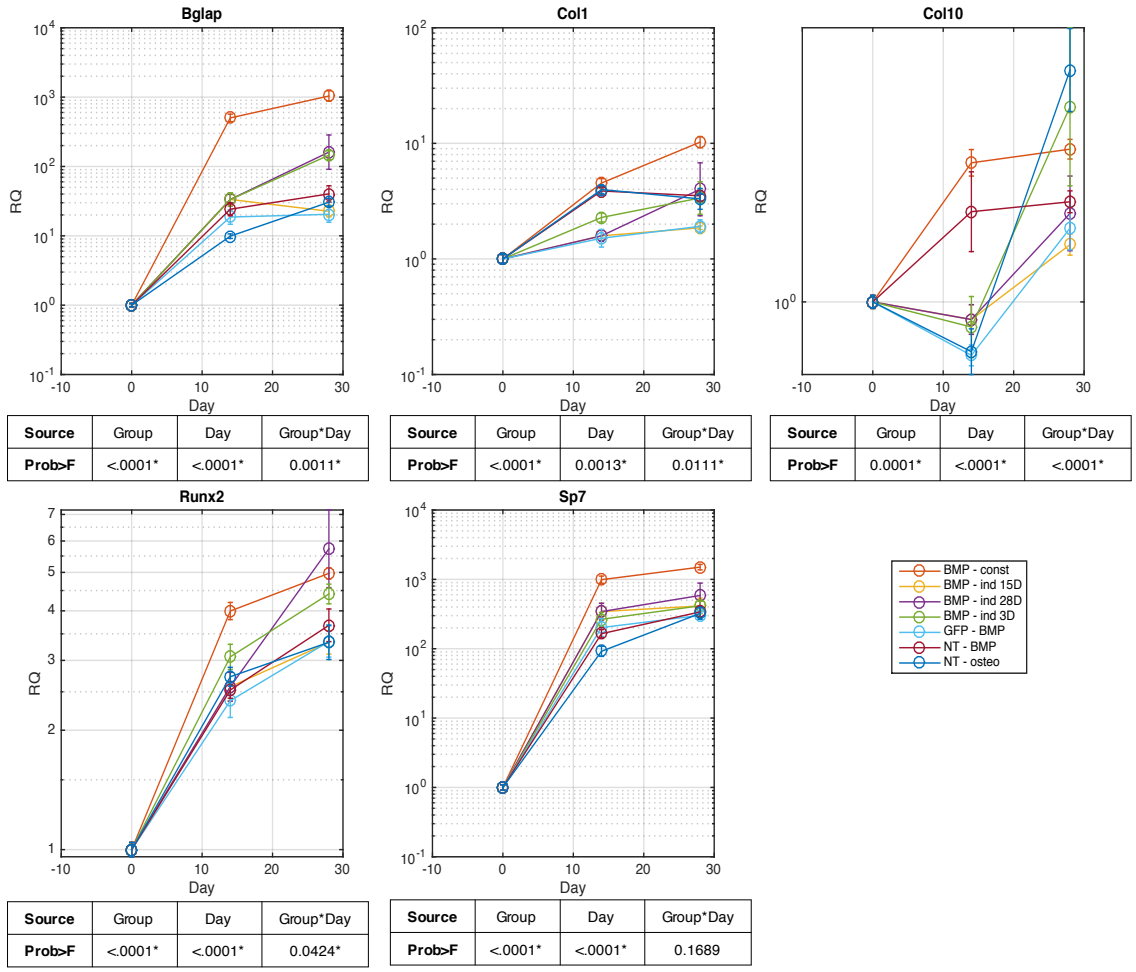


**Figure 4.5 qPCR shows expected increase in osteogenic gene expression during osteogenic induction.** Data points and error bars demonstrate mean  $\pm$  SEM. RQ = Relative Quantification, or fold change. The reference gene is GAPDH. Effects tests shown below each gene after two-way ANOVA analysis. Effects with \* are significant with  $p < 0.05$ . Const = constitutive; ind = inducible; NT = non-transduced.

Cells transduced with BMP-2 vectors, whether in a constitutive or an inducible manner, consistently showed expression of BMP-2, and constructs that were not transduced with BMP-2 did not produce this gene. Note that since there was no amplification of this gene in the Day 0 group, as expected, the groups that did amplify could not be normalized to the Day 0 group, so this graph is presented as  $\Delta$ CT values. (Figure 4.6)

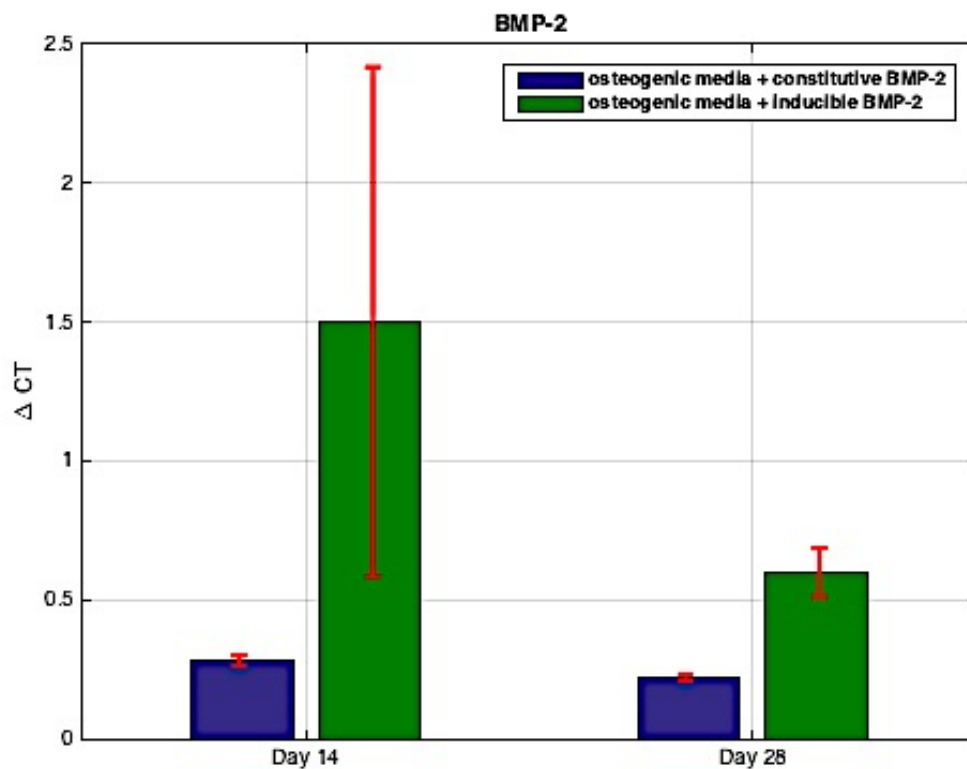


**Figure 4.6 qPCR of hBMP2 shows expression in groups transduced with hBMP2, and no amplification in non-transduced groups.** Probing for human BMP2 gene expression yielded no amplification in day 0 cells, nor in groups that were not constitutively or inducibly transduced with the gene; thus, the  $\Delta$ CT values are plotted. Data points and error bars demonstrate mean  $\pm$  SEM. The reference gene is GAPDH.

As expected, chondrogenic gene expression in osteogenic groups increases from day 0, but are at lower levels than chondrogenic groups. Note that all PCR for this study was run in parallel, with samples from each group run on different plates. Therefore, although the data is divided by groups for different figures, the fold changes can be compared to each other.

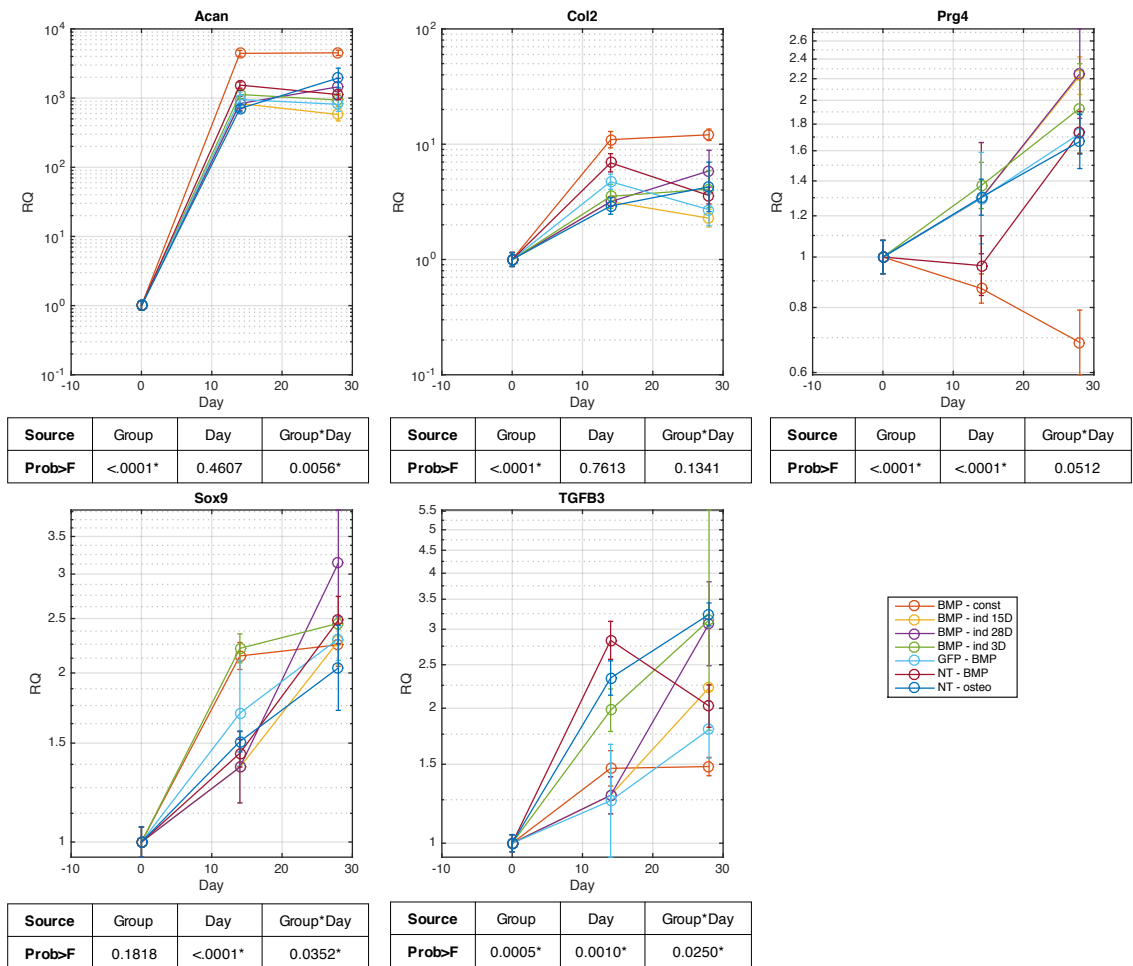


**Figure 4.7** qPCR shows increase in chondrogenic gene expression from day 0 during osteogenic induction, with smaller increases than in chondrogenic groups, as expected. Data points and error bars demonstrate mean  $\pm$  SEM. RQ = Relative Quantification, or fold change. The reference gene is GAPDH. Effects tests shown below each gene after two-way ANOVA analysis. Effects with \* are significant with  $p < 0.05$ . Const = constitutive; ind = inducible; NT = non-transduced.

MicroCT imaging illustrates mineralized tissue distributed through the scaffold construct, and a larger amount of mineralization in the osteochondral groups and in the constitutively-expressing-BMP-2 group, (Figure 4.8) which is confirmed in bone volume (Figure 4.9) and BV/TV (Figure 4.10) measurements. Interestingly, in the inducible expression system, more mineralization occurred in the group given doxycycline for 3 days than for 15 days or 28 days. Although these differences were not statistically significantly different from each other, the trend suggests a pulse with BMP-2 might be better than sustained release of BMP-2 over time.

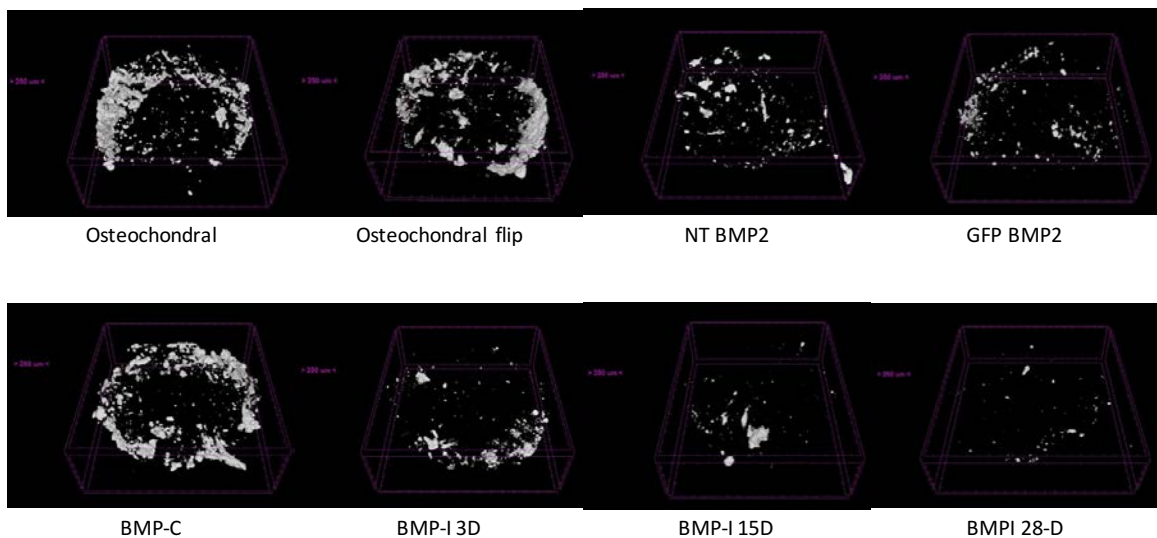


**Figure 4.8 MicroCT imaging demonstrates mineralized tissue distributed through the scaffold.** Calcification of bone volume shown in grayscale. Threshold for mineralization was set with calibration phantoms.

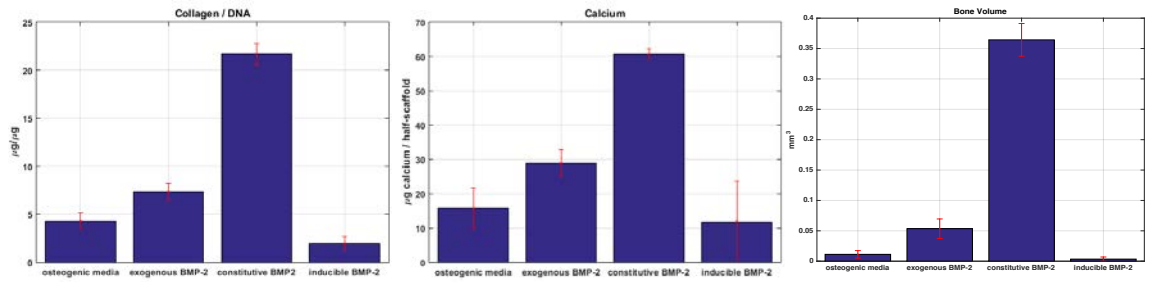


**Figure 4.9 Biochemical and microCT evaluation of collagen content, calcium content, and bone volume demonstrated collagen, calcium, and mineralization in all osteo groups, with significantly higher values in the BMP-2 constitutive groups.** The inducible group here was given dox for 28 days. N=3-6 per group. Data points and error bars demonstrate mean  $\pm$  SEM.

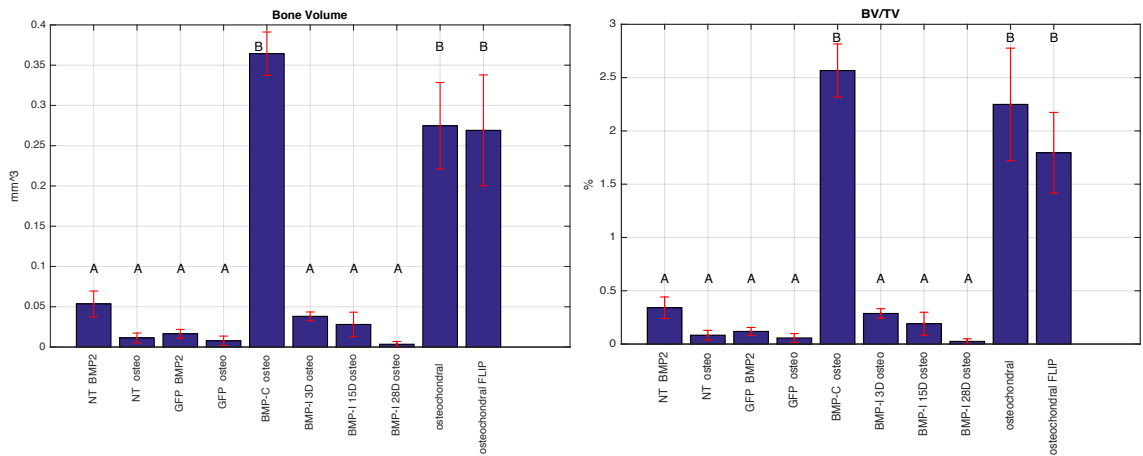


**Figure 4.10 MicroCT evaluation of bone volume (BV) and bone volume over tissue volume (BV/TV) demonstrated mineralization in all osteo groups, with significantly higher bone volumes in the BMP-2 constitutive and the osteochondral groups.** N=3-6 per group. Data points and error bars demonstrate mean  $\pm$  SEM. Groups not labelled with the same letter are significantly different by one-way ANOVA with post-hoc Tukey-Kramer analysis with  $p < 0.05$ .

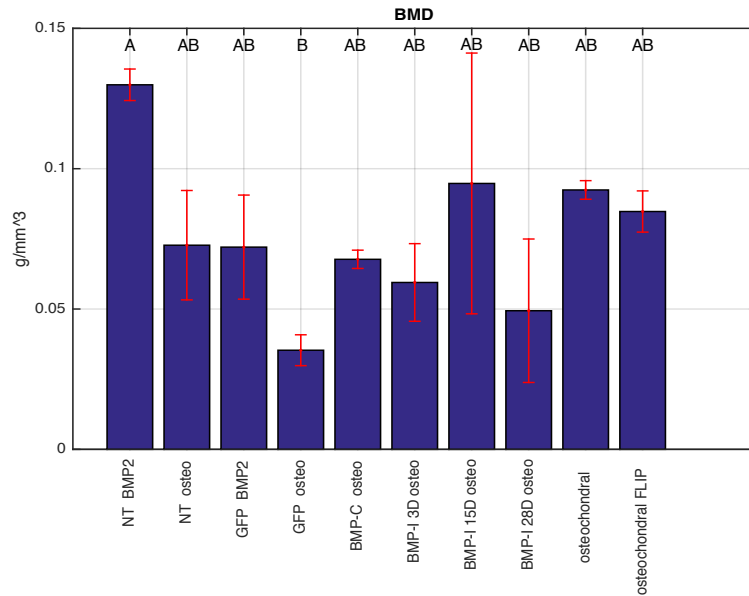


**Figure 4.11 MicroCT evaluation of bone mineral density demonstrated mineralization in all osteo groups.** N=3-6 per group. Data points and error bars demonstrate mean  $\pm$  SEM. Groups not labelled with the same letter are significantly different by one-way ANOVA with post-hoc Tukey-Kramer analysis with  $p < 0.05$ .

The constitutive expression of BMP-2 released more BMP-2 into the media than the inducible expression in this system. Both systems decreased their protein expression over time, (Figure 4.12) but their gene expression was maintained through the study.

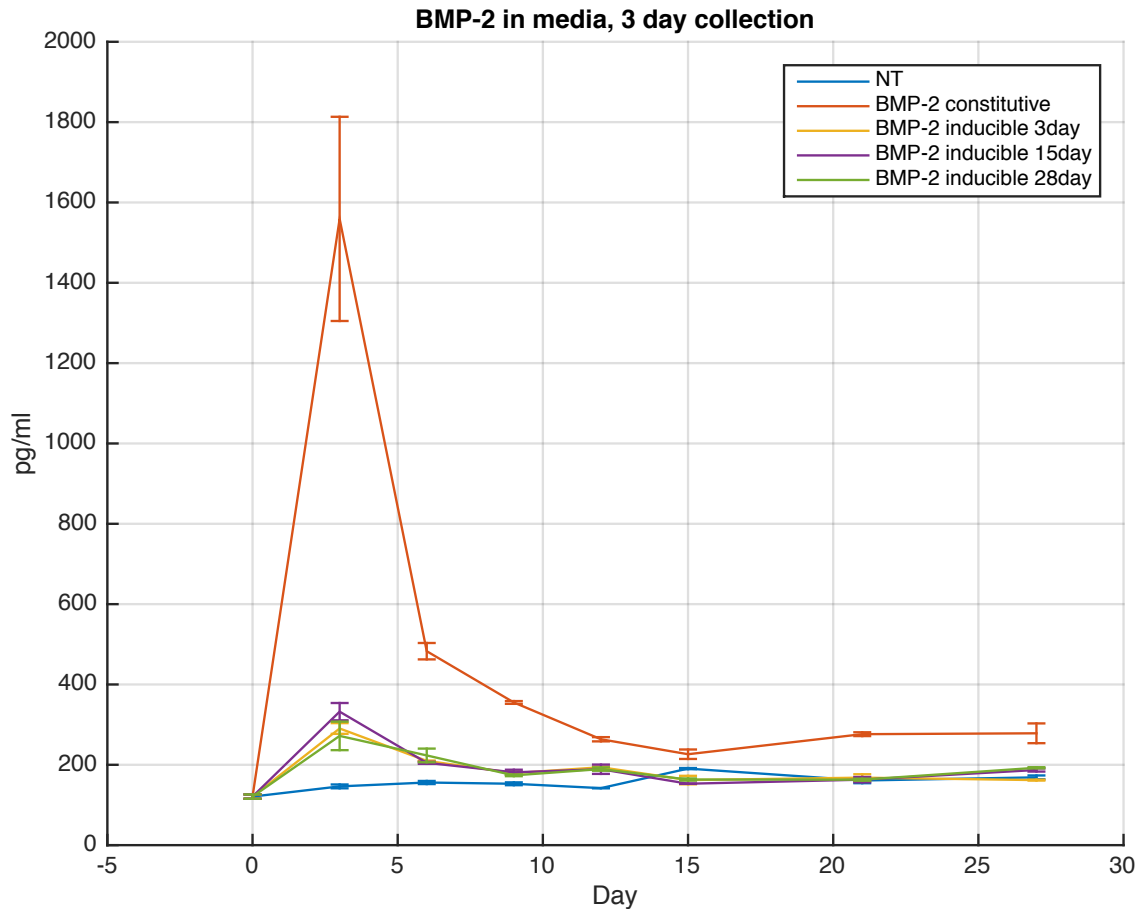


**Figure 4.12 ELISA assay demonstrates early expression of BMP-2 from constitutive and inducible constructs, which tapers off over time.** Half media changes were performed every three days. Connected lines are sampled from the same wells over time. N=3 per group. Data points and error bars demonstrate mean  $\pm$  SEM.

### 3.3.2 Chondrogenic scaffold constructs

After chondrogenic induction in scaffold constructs, qPCR confirmed increasing chondrogenic gene expression over time. Interestingly, very little Col10a1 expression is present in any of these constructs. Cells transduced with TGF- $\beta$ 3 vectors, whether in a constitutive or an inducible manner, consistently

showed expression of TGF- $\beta$ 3, and constructs that were not transduced with TGF- $\beta$ 3 produced very little of this gene. (Figure 4.13)

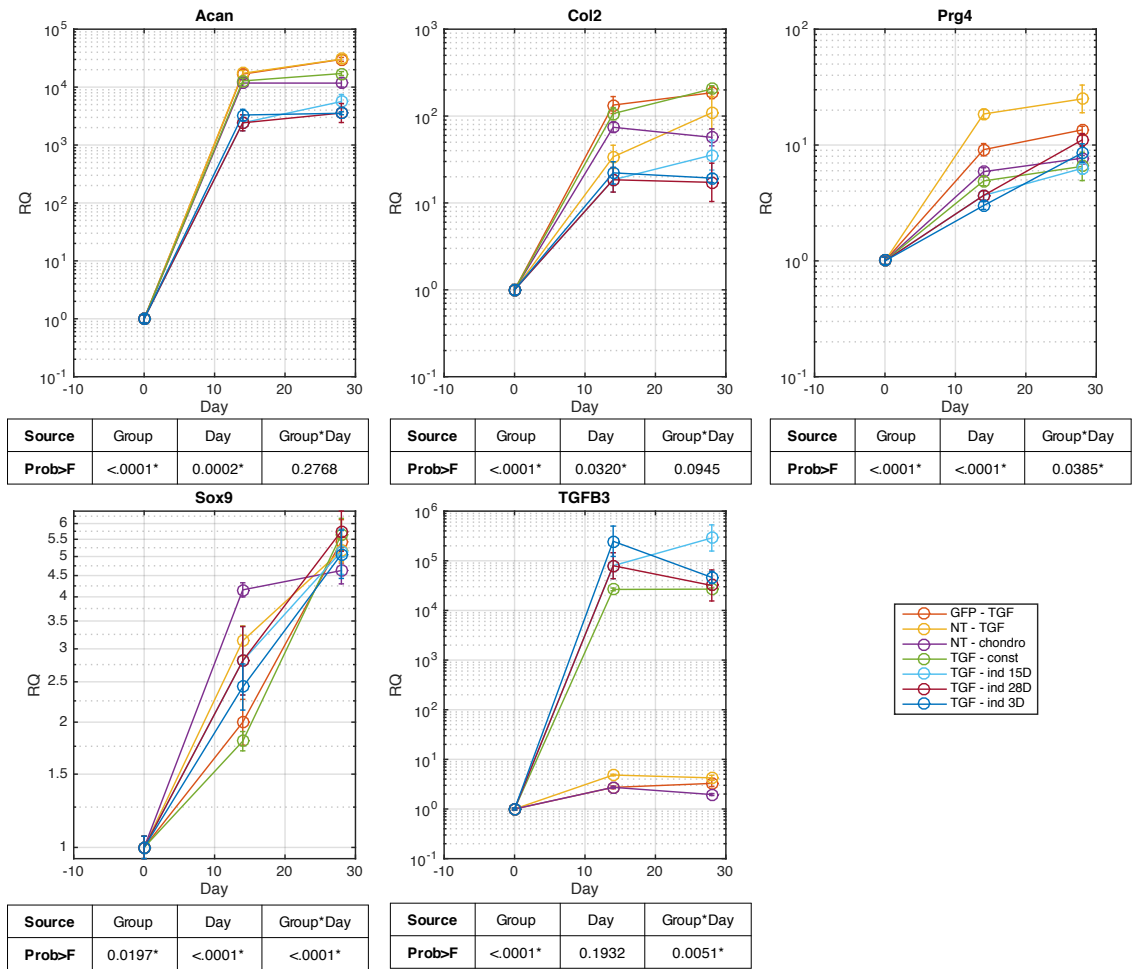


**Figure 4.13** qPCR shows increase in chondrogenic gene expression during chondrogenic induction, with smaller increases than in chondrogenic groups, as expected. TGF- $\beta$ 3 expression is significantly higher in groups transduced with TGF- $\beta$ 3 either constitutively or inducibly. Data points and error bars demonstrate mean  $\pm$  SEM. RQ = Relative Quantification, or fold change. The reference gene is GAPDH. Effects tests shown below each gene after two-way ANOVA analysis. Effects with \* are significant with  $p < 0.05$ . Const = constitutive; ind = inducible; NT = non-transduced.

As expected, osteogenic gene expression in chondrogenic groups increases from day 0, but are at lower levels than osteogenic groups. Note that all

PCR for this study was run in parallel, with samples from each group run on different plates; although the data is divided by groups for different figures, the fold changes can be compared to each other.

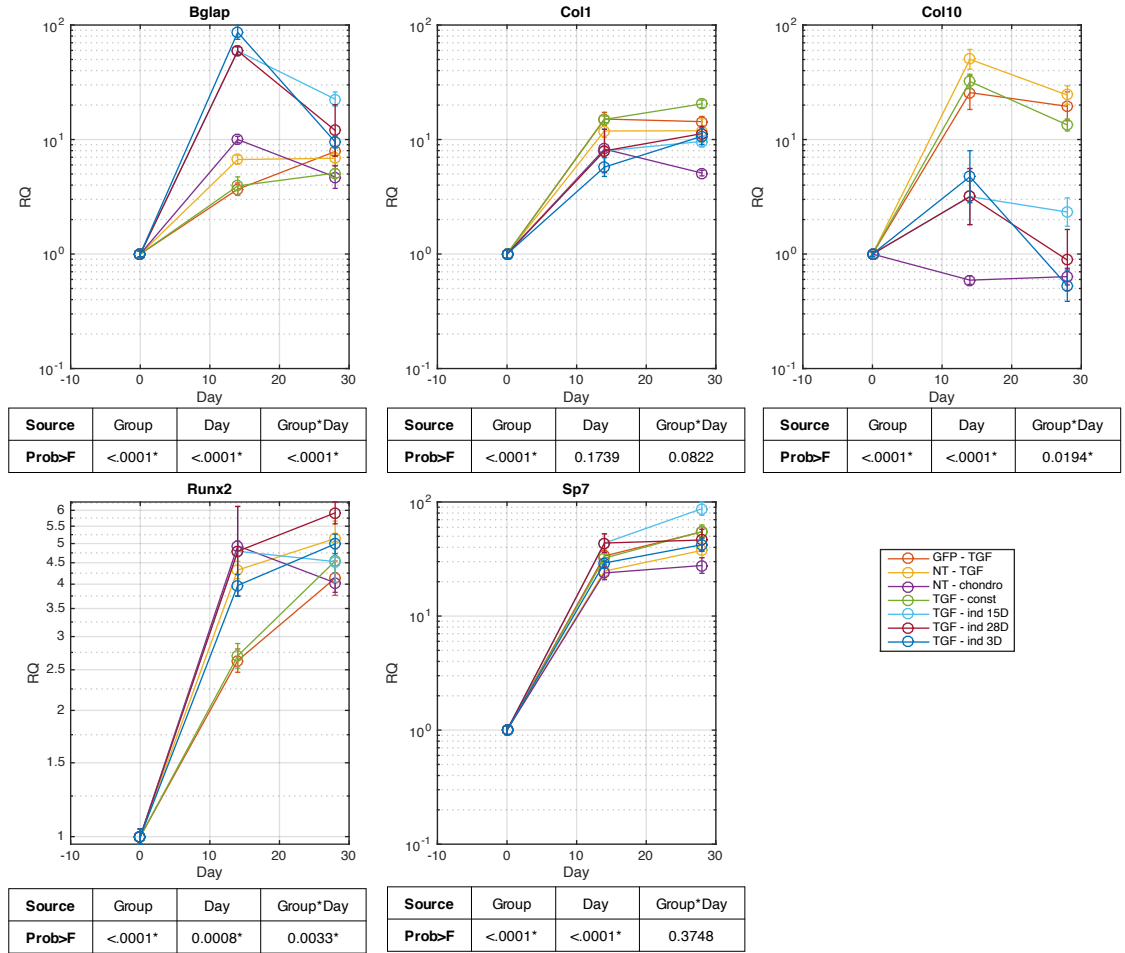


**Figure 4.14 qPCR shows increase in osteogenic gene expression from day 0 during chondrogenic induction, with smaller increases than in chondrogenic groups, as expected.** Data points and error bars demonstrate mean  $\pm$  SEM. RQ = Relative Quantification, or fold change. The reference gene is GAPDH. Effects tests shown below each gene after two-way ANOVA analysis. Effects with \* are significant with  $p < 0.05$ . Const = constitutive; ind = inducible; NT = non-transduced.

The constitutive expression of TGF- $\beta$ 3 released more TGF- $\beta$ 3 into the media than the inducible expression in this system. Both systems decreased their protein expression over time, (Figure 4.15) but their gene expression was maintained through the study. Active TGF- $\beta$ 3 was measured from each media sample; media samples were also activated, in order to indirectly measure the inactive (latent) form of the growth factor that was released in this system. Far more of the latent form of TGF- $\beta$ 3 was present in the media samples than the active form.

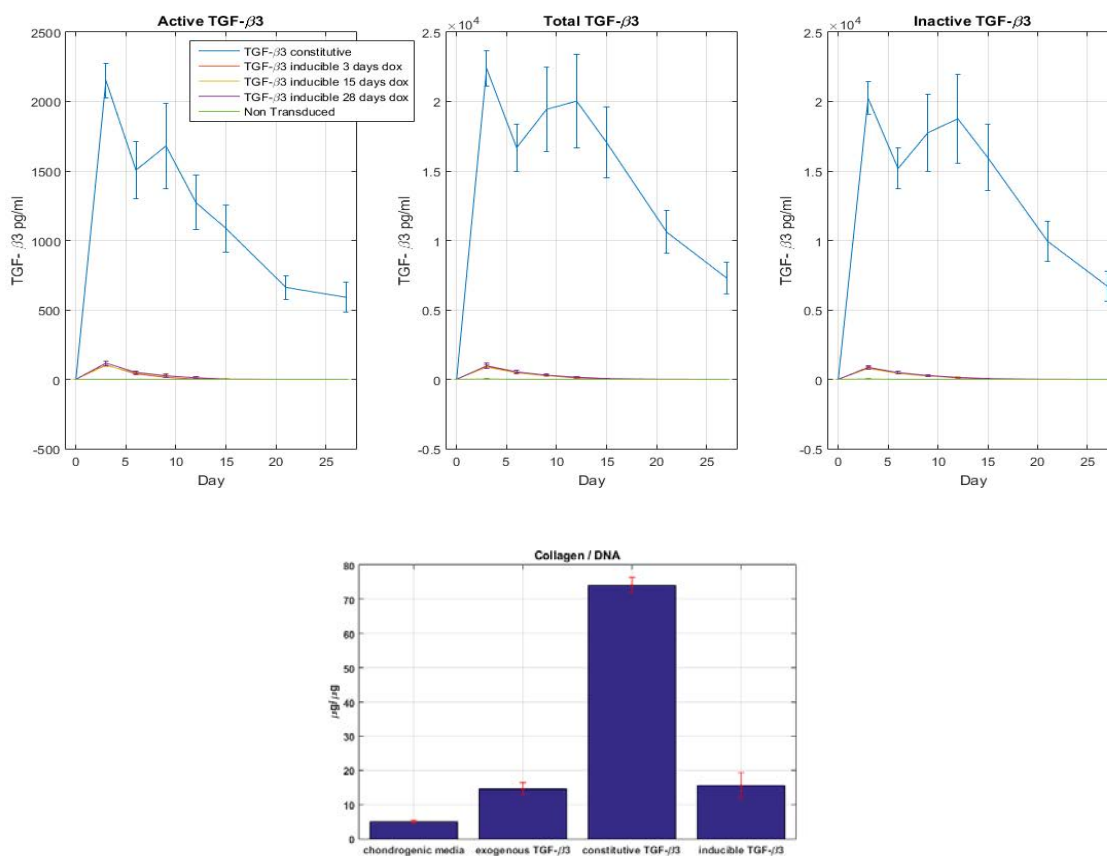


**Figure 4.15 Biochemical analysis: ELISA assay demonstrates early expression of TGF- $\beta$ 3 from constitutive and inducible constructs, which tapers off over time. Collagen content shows significantly higher values in the TGF- $\beta$ 3 constitutive groups.** Half media changes were performed every three days. Connected lines are sampled from the same wells over time. N=3 per group. Data points and error bars demonstrate mean  $\pm$  SEM. Active TGF- $\beta$ 3 was measured directly from sampled media. Media was activated to measure total TGF- $\beta$ 3, and inactive TGF- $\beta$ 3 was calculated from the first two measurements.

Fluorescence microscopy of the surface of these constructs demonstrates cells with a rounded morphology, similar to chondrocyte morphology. Furthermore, confocal microscopy demonstrates co-localization of cells expressing GFP via the Col2-GFP reporter system and cells expressing DsRed through the TGF- $\beta$ 3-IRES-dsRed system. Since these proteins have short half lives in cell expression systems, these images demonstrate healthy cells in these constructs.

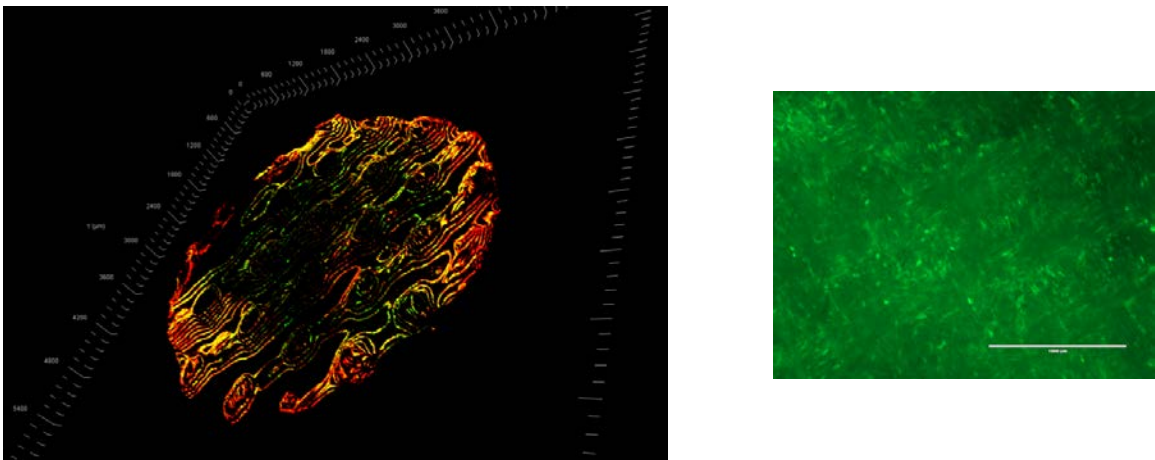


**Figure 4.16 Confocal microscopy (left) and fluorescence microscopy (right) demonstrates surface topology of fluorescent cells on the scaffold after 28 days of culture.** Chondrogenic construct with scaffold-mediated virally transduced constitutive TGF- $\beta$ 3-IRES-DsRed shows co-localization with cells expressing GFP via the Col2-GFP reporter construct (left). Chondrogenic construct with scaffold-mediated virally transduced constitutive GFP virus and given exogenous TGF- $\beta$ 3 shows healthy GFP-producing cells with rounded morphology, indicative of chondrocyte-like cells.

Scaffolds for histological analysis have been processed and sectioned, and staining has begun for glycosaminoglycans, collagen, and mineralization, and immunohistochemistry for Type I Collagen, Type II Collagen, Type VI Collagen,

Type X Collagen. This data is still being processed and, thus, is not presented here.

#### **4.4 Discussion: conclusions, limitations, and implications**

In this study, chondrogenic and osteogenic tissue was grown on a 3D-woven PCL scaffold with miPSCs for the first time. These tissue constructs incorporate the main components of an optimal osteochondral graft: a strong, biocompatible scaffold; a pluripotent, non-immunogenic cell source; endogenous delivery of growth factors for tissue differentiation and maintenance; and the presence of cartilage-like and mineralized tissues. Furthermore, both of these tissue types were created with the exogenous supplementation of growth factors, as well as via scaffold-mediated lentiviral delivery of genes encoding these growth factors under constitutive promoter expression and under an inducible expression system. Additionally, a new Col2-GFP reporter cell line was engineered and screened for chondrogenic potential, made from miPSCs generated with transient expression of the Yamanaka factors. Others in the Guilak lab have already started using this cell line to examine additional dox-inducible expression systems. Gene expression and microCT data have further confirmed osteogenic potential of this cell line. Also, gene expression and microCT data suggest we have created a biphasic osteochondral construct.

Of note, these results to-date do not include histology data, as histological processing is still being completed. Thus, confirmation of these findings will be

forthcoming via histological analysis. Additional limitations include the result the inducible groups underperformed relative to the constitutive groups. It must also be highlighted that this inducible system of expression, the TetOn doxycycline inducible expression vector, has been shown to be immunogenic, and therefore is not directly translational for human treatment. This TotOn system is an excellent tool for modelling outcomes of gene expression manipulation *in vitro* and in small animal models, however, and CRISPR technology provides an invaluable subsequent tool for using knowledge gained from these studies and propelling them into the translational realm when appropriate. Before such a transition, however, more work needs to be done in a mouse model, to determine the minimum culture time needed prior to *in vivo* implantation. Additionally, this platform would need to be reproduced with human iPSCs.

#### **4.4.1 Applications of bone, cartilage, and osteochondral tissue grafts**

Several recent studies have utilized the biocompatible, durable, and strong properties of polycaprolactone in creating musculoskeletal tissue engineered constructs, including for cartilage,<sup>116, 117</sup> tendon,<sup>118</sup> and bone.<sup>119</sup> Most of these studies have used hMSCs, a cell type already clinically used in bone regeneration for surgical repair of nonunions and osteonecrosis.<sup>56, 57</sup> After cell culture manipulation and culture, though, MSC-derived tissue transplanted *in vivo* has shown unstable, transient characteristics.<sup>120, 121</sup> Interestingly, chondrogenically-induced iPSCs have expressed very little collagen type X during differentiation,<sup>50,</sup>

<sup>51</sup> suggesting the that tissue formed from chondrogenically-induced murine iPSCs might remain chondrogenic after *in vitro* culture and subsequent implantation. This study demonstrates the ability of miPSCs to chonrogenically and osteogenically differentiate on a polycaprolactone scaffold. Although for this study, mechanical properties were not directly tested, this 3D-woven scaffold seeded with cell types such as MSCs and ASCs has been extensively tested with consistent results demonstrating comparable strength testing to native articular cartilage.<sup>37, 38, 122</sup> Thus, the scaffolds created in this study would likely have similar mechanical properties. An osteochondral construct with the strength of the surrounding cartilage and having the ability to anchor into the subchondral bone layer could be the next step to creating an osteochondral graft that would promote articular cartilage regeneration, without fibrous tissue formation, that would remain in the defect site well after implantation.

#### **4.4.2 Applications of tissue constructs created without exogenous growth factor delivery**

Although these constructs were grown *in vitro*, a future clinically-applicable, implantable graft would ideally be cultured for as little time as possible prior to implantation. Thus, a polymer-based scaffold with tethered lentivirus for the scaffold-mediated transduction of genes encoding chondrogenic and osteogenic growth factor expression is appealing, to decrease time to implantation. Additionally, with recent debate on the effects of long term growth factor delivery,<sup>123-125</sup> local paracrine delivery and signaling of growth factors would

minimize off-target effects. The utilization of an inducible expression system, with the option to withdraw doxycycline stimulation once a stable, mature osteochondral tissue has been formed, would further improve the safety profile of such a therapy. The results in this study demonstrate an exciting platform to grow osteochondral tissue constructs with iPSCs, and serve as the next step toward an implantable construct to treat osteochondral defects.

## **5. Conclusions and future applications**

The first study presented in this work demonstrates the creation of an iPSC-derived osteochondral organoid construct. Constructs of neocartilage were subsequently osteogenically differentiated via endochondral ossification. We also showed that the presence of a cartilaginous extracellular matrix (ECM) can prevent re-induction of iPSC pluripotency. The impact of this study is two-fold: for translational tissue engineering applications, it implies that a robust chondrogenic matrix may prevent dedifferentiation upon implantation, which has been a critical barrier to iPSC implantation in patients. Additionally, the creation of this novel iPSC-derived osteochondral organoid has great potential for studying normal and pathological interactions between bone and cartilage at the osteochondral junction, as well as for therapeutic screening in disease models of osteochondral disorders.

In the second study presented in this work, chondrogenic and osteogenic tissue was grown on a 3D-woven PCL scaffold with miPSCs for the first time. Both of these tissue types were created with the exogenous supplementation of growth factors, as well as via scaffold-mediated lentiviral delivery of genes encoding these growth factors under constitutive promoter expression and under an inducible expression system. Gene expression and microCT data have further confirmed osteogenic potential of this cell line. Confirmation of these findings will be forthcoming via histological analysis. Additionally, a new Col2-GFP reporter cell line was engineered which demonstrated both chondrogenic and osteogenic

potential, made from miPSCs generated with transient expression of the Yamanaka factors, lending itself to us with additional inducible gene expression studies.

While the work shows great promise in the field of osteochondral tissue engineering, more work needs to be done to realize the goal of treating patients with debilitating arthropathies.

## **5.1 Disease modeling in a dish**

These studies investigate an exciting platform for studying normal biology and pathological disease affecting the osteochondral junction. Several disease-in-a-dish models have been created to study disease models for chondrogenic and osteogenic applications, even in iPSCs.<sup>1</sup> Studying the osteochondral junction in this manner, however, has not been done, and the distinct interplay between these tissue types may help further elucidate the mechanism of arthropathies such as rheumatoid arthritis and osteoarthritis; there is great debate as to whether the bone or the cartilage is the first tissue to trigger pathology, but it is accepted that both are important.<sup>68</sup> Thus, the organoid created here would be an excellent platform for high-throughput screening of small molecules and biologics that could help treat arthropathies, and especially for testing pharmaceuticals that are good candidates for treating cartilage but known to affect bone, such as steroid and hormone-based therapies. By using iPSC-derived cells for this study, the platform lends itself to growing constructs from iPSCs derived from patients with rare musculoskeletal disorders, in order to discern better treatments for these patients. Chondrogenesis

of hiPSCs in multiple cell lines is being investigated currently in our lab, and the application of the methods described here applied to an hiPSC-derived model system could have incredible potential for the study of rare diseases affecting cartilage and bone, such as osteochondritis dessicans, osteogenesis imperfecta, juvenile idiopathic arthritis, and hundreds of other genetically-linked arthropathies.

## **5.2 Implantation of functional osteochondral grafts in animal models**

In the first study presented here, we demonstrated that a robust cartilaginous extracellular matrix (ECM) can prevent re-induction of iPSC pluripotency. This conclusion has exciting potential, but needs further examination in other systems before this conclusion can be applied to any clinical applications. The study here focused on murine iPSCs. Many questions would invite additional follow-up: Does the protection against re-induction of pluripotency in these constructs extend to *in vivo* implantation? Would this protection occur in a human system with hiPSCs? Are there other tissues, in addition to cartilage and bone, that have extracellular matrix properties that could also protect cells from re-induction of pluripotency? What are the specific mechanisms that convey this protection, and can those be harnessed to protect iPSC-derived cells in other tissue constructs from de-differentiating? Could those mechanisms eventually be harnessed to protect cells even without a strong surrounding matrix, for future cell-based therapies, in addition to tissue-based therapies?

Since pellet-based engineered constructs would be less conducive to implantation than scaffold-based systems, many of these questions might be better suited to being answered with the platform developed in the second study: on a biocompatible 3D-woven PCL scaffold. 3D-woven PCL scaffold-based dox-inducible expression vectors have already been demonstrated to show promise when seeded with hASCs in a rabbit model in our lab.<sup>126</sup> The successful osteochondral induction of miPSCs in the system studied here would be an excellent platform for *in vivo* studies in mouse models. Many of the previous questions could be answered in a subcutaneous implantation mouse model,<sup>127, 128</sup> in addition to answering temporal questions regarding the length of time necessary for local growth factor expression for developing stable osteogenesis and chondrogenesis *in vivo*. This study takes exciting steps toward a functional iPSC-based osteochondral graft, and further development in animal models is necessary before bringing this technology from the bench to the bedside.

## References

1. Willard VP, Diekman BO, Sanchez-Adams J, Christoforou N, Leong KW and Guilak F. Use of cartilage derived from murine induced pluripotent stem cells for osteoarthritis drug screening. *Arthritis Rheumatol*. 2014;66:3062-72.
2. Praemer A, S. Furner, and D.P. Rice. *Musculoskeletal Conditions in the United States* Rosemont, IL: American Academy of Orthopaedic Surgeons; 1999.
3. Prevalence of doctor-diagnosed arthritis and arthritis-attributable activity limitation--United States, 2010-2012. *MMWR Morb Mortal Wkly Rep*. 2013;62:869-73.
4. Brundtland GH. A WHO Scientific Group on the Burden of Musculoskeletal Conditions at the Start of the New Millennium met in Geneva from 13 to 15 January 2000. *Burden of Musculoskeletal Conditions at the Start of the New Millennium*. 2003;919:1-218.
5. Lawrence RC, Felson DT, Helmick CG, Arnold LM, Choi H, Deyo RA, Gabriel S, Hirsch R, Hochberg MC, Hunder GG, Jordan JM, Katz JN, Kremers HM and Wolfe F. Estimates of the prevalence of arthritis and other rheumatic conditions in the United States. Part II. *Arthritis Rheum*. 2008;58:26-35.
6. Hunziker EB. Articular cartilage repair: basic science and clinical progress. A review of the current status and prospects. *Osteoarthritis Cartilage*. 2002;10:432-63.
7. Schinhan M, Gruber M, Vavken P, Dorotka R, Samouh L, Chiari C, Gruebl-Barabas R and Nehrer S. Critical-size defect induces unicompartmental osteoarthritis in a stable ovine knee. *J Orthop Res*. 2012;30:214-20.
8. Brittberg M, Lindahl A, Nilsson A, Ohlsson C, Isaksson O and Peterson L. Treatment of deep cartilage defects in the knee with autologous chondrocyte transplantation. *N Engl J Med*. 1994;331:889-95.
9. Hunziker EB. Tissue engineering of bone and cartilage. From the preclinical model to the patient. *Novartis Found Symp*. 2003;249:70-8; discussion 78-85, 170-4, 239-41.
10. Pavesio A, et al. *Hyaluronan-based scaffolds in the treatment of cartilage defects of the knee: Clinical results*. Rosemont, IL: American Academy of Orthopaedic Surgeons; 2004.
11. Lee CR, Grodzinsky AJ, Hsu HP, Martin SD and Spector M. Effects of harvest and selected cartilage repair procedures on the physical and biochemical properties of articular cartilage in the canine knee. *J Orthop Res*. 2000;18:790-9.
12. Harris JD, Siston RA, Brophy RH, Lattermann C, Carey JL and Flanigan DC. Failures, re-operations, and complications after autologous chondrocyte implantation--a systematic review. *Osteoarthritis Cartilage*. 2011;19:779-91.

13. Lee CR, Grodzinsky AJ, Hsu HP, Martin SD and Spector M. Effects of harvest and selected cartilage repair procedures on the physical and biochemical properties of articular cartilage in the canine knee. *Journal of Orthopaedic Research*. 2000;18:790-799.
14. Wouters E, Bassett FH, 3rd, Hardaker WT, Jr. and Garrett WE, Jr. An algorithm for arthroscopy in the over-50 age group. *Am J Sports Med*. 1992;20:141-5.
15. Denoncourt PM, Patel D and Dimakopoulos P. Arthroscopy update #1. Treatment of osteochondrosis dissecans of the knee by arthroscopic curettage, follow-up study. *Orthop Rev*. 1986;15:652-7.
16. Aichroth PM, Patel DV and Moyes ST. A prospective review of arthroscopic debridement for degenerative joint disease of the knee. *Int Orthop*. 1991;15:351-5.
17. Baumgaertner MR, Cannon WD, Jr., Vittori JM, Schmidt ES and Maurer RC. Arthroscopic debridement of the arthritic knee. *Clin Orthop Relat Res*. 1990:197-202.
18. Johnson LL. Arthroscopic abrasion arthroplasty: a review. *Clin Orthop Relat Res*. 2001:S306-17.
19. Friedman MJ, Berasi CC, Fox JM, Del Pizzo W, Snyder SJ and Ferkel RD. Preliminary results with abrasion arthroplasty in the osteoarthritic knee. *Clin Orthop Relat Res*. 1984:200-5.
20. Steadman JR, Briggs KK, Rodrigo JJ, Kocher MS, Gill TJ and Rodkey WG. Outcomes of microfracture for traumatic chondral defects of the knee: average 11-year follow-up. *Arthroscopy*. 2003;19:477-84.
21. Steadman JR, Rodkey WG and Rodrigo JJ. Microfracture: surgical technique and rehabilitation to treat chondral defects. *Clin Orthop Relat Res*. 2001:S362-9.
22. Kish G, Modis L and Hangody L. Osteochondral mosaicplasty for the treatment of focal chondral and osteochondral lesions of the knee and talus in the athlete. Rationale, indications, techniques, and results. *Clin Sports Med*. 1999;18:45-66, vi.
23. Aubin PP, Cheah HK, Davis AM and Gross AE. Long-term followup of fresh femoral osteochondral allografts for posttraumatic knee defects. *Clin Orthop Relat Res*. 2001:S318-27.
24. Emmerson BC, Gortz S, Jamali AA, Chung C, Amiel D and Bugbee WD. Fresh osteochondral allografting in the treatment of osteochondritis dissecans of the femoral condyle. *Am J Sports Med*. 2007;35:907-14.
25. Ghazavi MT, Pritzker KP, Davis AM and Gross AE. Fresh osteochondral allografts for post-traumatic osteochondral defects of the knee. *J Bone Joint Surg Br*. 1997;79:1008-13.
26. Gudas R, Kalesinskas RJ, Kimtys V, Stankevicius E, Toliulis V, Bernotavicius G and Smailys A. A prospective randomized clinical study of mosaic osteochondral

autologous transplantation versus microfracture for the treatment of osteochondral defects in the knee joint in young athletes. *Arthroscopy : the journal of arthroscopic & related surgery : official publication of the Arthroscopy Association of North America and the International Arthroscopy Association*. 2005;21:1066-75.

27. Mithoefer K, McAdams T, Williams RJ, Kreuz PC and Mandelbaum BR. Clinical efficacy of the microfracture technique for articular cartilage repair in the knee: an evidence-based systematic analysis. *Am J Sports Med*. 2009;37:2053-63.

28. Gobbi A, Nunag P and Malinowski K. Treatment of full thickness chondral lesions of the knee with microfracture in a group of athletes. *Knee surgery, sports traumatology, arthroscopy : official journal of the ESSKA*. 2005;13:213-21.

29. Kon E, Gobbi A, Filardo G, Delcogliano M, Zaffagnini S and Marcacci M. Arthroscopic second-generation autologous chondrocyte implantation compared with microfracture for chondral lesions of the knee: prospective nonrandomized study at 5 years. *Am J Sports Med*. 2009;37:33-41.

30. Blevins FT, Steadman JR, Rodrigo JJ and Silliman J. Treatment of articular cartilage defects in athletes: an analysis of functional outcome and lesion appearance. *Orthopedics*. 1998;21:761-7; discussion 767-8.

31. Mithoefer K, Williams RJ, 3rd, Warren RF, Wickiewicz TL and Marx RG. High-impact athletics after knee articular cartilage repair: a prospective evaluation of the microfracture technique. *Am J Sports Med*. 2006;34:1413-8.

32. Shapiro F, Koide S and Glimcher MJ. Cell origin and differentiation in the repair of full-thickness defects of articular cartilage. *J Bone Joint Surg Am*. 1993;75:532-53.

33. Tew SR, Kwan AP, Hann A, Thomson BM and Archer CW. The reactions of articular cartilage to experimental wounding: role of apoptosis. *Arthritis Rheum*. 2000;43:215-25.

34. Nehrer S, Spector M and Minas T. Histologic analysis of tissue after failed cartilage repair procedures. *Clin Orthop Relat Res*. 1999:149-62.

35. Valonen PK, Moutos FT, Kusanagi A, Moretti MG, Diekman BO, Welter JF, Caplan AI, Guilak F and Freed LE. In vitro generation of mechanically functional cartilage grafts based on adult human stem cells and 3D-woven poly(epsilon-caprolactone) scaffolds. *Biomaterials*. 31:2193-200.

36. Moutos FT and Guilak F. Functional properties of cell-seeded three-dimensionally woven poly(epsilon-caprolactone) scaffolds for cartilage tissue engineering. *Tissue Eng Part A*. 16:1291-301.

37. Moutos FT, Freed LE and Guilak F. A biomimetic three-dimensional woven composite scaffold for functional tissue engineering of cartilage. *Nature Materials*. 2007;6:162-167.

38. Moutos F and Guilak F. Functional properties of cell-seeded three-dimensionally woven poly(epsilon-caprolactone) scaffolds for cartilage tissue engineering. *Tissue Eng Part A*. 2009.
39. Abrahamsson CK, Yang F, Park H, Brunger JM, Valonen PK, Langer R, Welter JF, Caplan AI, Guilak F and Freed LE. Chondrogenesis and mineralization during in vitro culture of human mesenchymal stem cells on three-dimensional woven scaffolds. *Tissue Eng Part A*. 16:3709-18.
40. Gersbach CA, Guldberg RE and Garcia AJ. In vitro and in vivo osteoblastic differentiation of BMP-2- and Runx2-engineered skeletal myoblasts. *J Cell Biochem*. 2007;100:1324-36.
41. Gersbach CA, Le Doux JM, Guldberg RE and Garcia AJ. Inducible regulation of Runx2-stimulated osteogenesis. *Gene Ther*. 2006;13:873-82.
42. Gersbach CA, Byers BA, Pavlath GK, Guldberg RE and Garcia AJ. Runx2/Cbfa1-genetically engineered skeletal myoblasts mineralize collagen scaffolds in vitro. *Biotechnol Bioeng*. 2004;88:369-78.
43. Gersbach CA, Byers BA, Pavlath GK and Garcia AJ. Runx2/Cbfa1 stimulates transdifferentiation of primary skeletal myoblasts into a mineralizing osteoblastic phenotype. *Exp Cell Res*. 2004;300:406-17.
44. Gersbach CA, Coyer SR, Le Doux JM and Garcia AJ. Biomaterial-mediated retroviral gene transfer using self-assembled monolayers. *Biomaterials*. 2007;28:5121-7.
45. Phillips JE, Gersbach CA and Garcia AJ. Virus-based gene therapy strategies for bone regeneration. *Biomaterials*. 2007;28:211-29.
46. Gersbach CA, Phillips JE and Garcia AJ. Genetic engineering for skeletal regenerative medicine. *Annu Rev Biomed Eng*. 2007;9:87-119.
47. Diekman BO, Estes BT and Guilak F. The effects of BMP6 overexpression on adipose stem cell chondrogenesis: Interactions with dexamethasone and exogenous growth factors. *J Biomed Mater Res A*. 2010;93:994-1003.
48. Takahashi K and Yamanaka S. Induction of pluripotent stem cells from mouse embryonic and adult fibroblast cultures by defined factors. *Cell*. 2006;126:663-76.
49. Yu J, Vodyanik MA, Smuga-Otto K, Antosiewicz-Bourget J, Frane JL, Tian S, Nie J, Jonsdottir GA, Ruotti V, Stewart R, Slukvin, II and Thomson JA. Induced pluripotent stem cell lines derived from human somatic cells. *Science*. 2007;318:1917-20.
50. Diekman BO, Christoforou N, Willard VP, Sun H, Sanchez-Adams J, Leong KW and Guilak F. Cartilage tissue engineering using differentiated and purified induced pluripotent stem cells. *Proc Natl Acad Sci U S A*. 2012;109:19172-7.

51. Diekman BO, Thakore PI, O'Connor SK, Willard VP, Brunger JM, Christoforou N, Leong KW, Gersbach CA and Guilak F. Knockdown of the cell cycle inhibitor p21 enhances cartilage formation by induced pluripotent stem cells. *Tissue Eng Part A*. 2015;21:1261-74.
52. Bernhardt A, Paul B and Gelinsky M. Biphasic Scaffolds from Marine Collagens for Regeneration of Osteochondral Defects. *Mar Drugs*. 2018;16.
53. Gonzalez-Fernandez T, Tierney EG, Cunniffe GM, O'Brien FJ and Kelly DJ. Gene Delivery of TGF-beta3 and BMP2 in an MSC-Laden Alginate Hydrogel for Articular Cartilage and Endochondral Bone Tissue Engineering. *Tissue Eng Part A*. 2016;22:776-87.
54. Levingstone TJ, Ramesh A, Brady RT, Brama PAJ, Kearney C, Gleeson JP and O'Brien FJ. Cell-free multi-layered collagen-based scaffolds demonstrate layer specific regeneration of functional osteochondral tissue in caprine joints. *Biomaterials*. 2016;87:69-81.
55. Kanatli U, Eren A, Eren TK and Vural A. Treatment of Osteochondral Lesions of the Talus With Cell-free Polymer-based Scaffold in Single-Step Arthroscopic Surgery. *Arthrosc Tech*. 2017;6:e1727-e1734.
56. Hernigou P, Dubory A, Flouzat Lachaniette CH, Khaled I, Chevallier N and Rouard H. Stem cell therapy in early post-traumatic talus osteonecrosis. *Int Orthop*. 2018.
57. Schottel PC and Warner SJ. Role of Bone Marrow Aspirate in Orthopedic Trauma. *Orthop Clin North Am*. 2017;48:311-321.
58. Guzzo RM, Gibson J, Xu RH, Lee FY and Drissi H. Efficient differentiation of human iPSC-derived mesenchymal stem cells to chondroprogenitor cells. *J Cell Biochem*. 2013;114:480-90.
59. Chen YS, Pelekanos RA, Ellis RL, Horne R, Wolvetang EJ and Fisk NM. Small molecule mesengenic induction of human induced pluripotent stem cells to generate mesenchymal stem/stromal cells. *Stem Cells Transl Med*. 2012;1:83-95.
60. Umeda K, Zhao J, Simmons P, Stanley E, Elefanty A and Nakayama N. Human chondrogenic paraxial mesoderm, directed specification and prospective isolation from pluripotent stem cells. *Sci Rep*. 2012;2:455.
61. Yamashita A, Morioka M, Yahara Y, Okada M, Kobayashi T, Kuriyama S, Matsuda S and Tsumaki N. Generation of scaffoldless hyaline cartilaginous tissue from human iPSCs. *Stem Cell Reports*. 2015;4:404-18.
62. Craft AM, Rockel JS, Nartiss Y, Kandel RA, Alman BA and Keller GM. Generation of articular chondrocytes from human pluripotent stem cells. *Nat Biotechnol*. 2015;33:638-45.

63. Driessen BJH, Logie C and Vonk LA. Cellular reprogramming for clinical cartilage repair. *Cell Biol Toxicol.* 2017;33:329-349.
64. Lozito TP, Alexander PG, Lin H, Gottardi R, Cheng AW and Tuan RS. Three-dimensional osteochondral microtissue to model pathogenesis of osteoarthritis. *Stem Cell Res Ther.* 2013;4 Suppl 1:S6.
65. Lin H, Lozito TP, Alexander PG, Gottardi R and Tuan RS. Stem cell-based microphysiological osteochondral system to model tissue response to interleukin-1beta. *Mol Pharm.* 2014;11:2203-12.
66. Alexander PG, Gottardi R, Lin H, Lozito TP and Tuan RS. Three-dimensional osteogenic and chondrogenic systems to model osteochondral physiology and degenerative joint diseases. *Exp Biol Med (Maywood).* 2014;239:1080-95.
67. Lancaster MA and Knoblich JA. Organogenesis in a dish: modeling development and disease using organoid technologies. *Science.* 2014;345:1247125.
68. Zhen G, Wen C, Jia X, Li Y, Crane JL, Mears SC, Askin FB, Frassica FJ, Chang W, Yao J, Carrino JA, Cosgarea A, Artemov D, Chen Q, Zhao Z, Zhou X, Riley L, Sponseller P, Wan M, Lu WW and Cao X. Inhibition of TGF-beta signaling in mesenchymal stem cells of subchondral bone attenuates osteoarthritis. *Nat Med.* 2013;19:704-12.
69. Pitt CG. Poly-epsilon-caprolactone and its copolymers. In: M. Chasin and R. Langer, eds. *Biodegradable polymers as drug delivery systems* New York: Marcel Dekker; 1990: 71-120.
70. Sinha VR, Bansal K, Kaushik R, Kumria R and Trehan A. Poly-epsilon-caprolactone microspheres and nanospheres: an overview. *International Journal of Pharmaceutics.* 2004;278:1-23.
71. Li WJ, Danielson KG, Alexander PG and Tuan RS. Biological response of chondrocytes cultured in three-dimensional nanofibrous poly(epsilon-caprolactone) scaffolds. *Journal of Biomedical Materials Research.* 2003;67A:1105-1114.
72. Huang MH, Li SM, Hutmacher DW, Coudane J and Vert M. Degradation characteristics of poly(epsilon-caprolactone)-based copolymers and blends. *Journal of Applied Polymer Science.* 2006;102:1681-1687.
73. Sun H, Mei L, Song C, Cui X and Wang P. The in vivo degradation, absorption and excretion of PCL-based implant. *Biomaterials.* 2006;27:1735-1740.
74. Pannier AK and Shea LD. Controlled release systems for DNA delivery. *Mol Ther.* 2004;10:19-26.
75. Han S, Mahato RI, Sung YK and Kim SW. Development of biomaterials for gene therapy. *Mol Ther.* 2000;2:302-17.

76. Phillips JE, Burns KL, Le Doux JM, Guldborg RE and Garcia AJ. Engineering graded tissue interfaces. *Proc Natl Acad Sci U S A*. 2008;105:12170-5.
77. Shea LD, Smiley E, Bonadio J and Mooney DJ. DNA delivery from polymer matrices for tissue engineering. *Nat Biotechnol*. 1999;17:551-4.
78. Fang J, Zhu YY, Smiley E, Bonadio J, Rouleau JP, Goldstein SA, McCauley LK, Davidson BL and Roessler BJ. Stimulation of new bone formation by direct transfer of osteogenic plasmid genes. *Proc Natl Acad Sci U S A*. 1996;93:5753-8.
79. Koefoed M, Ito H, Gromov K, Reynolds DG, Awad HA, Rubery PT, Ulrich-Vinther M, Soballe K, Guldborg RE, Lin AS, O'Keefe RJ, Zhang X and Schwarz EM. Biological effects of rAAV-caAlk2 coating on structural allograft healing. *Mol Ther*. 2005;12:212-8.
80. Ito H, Koefoed M, Tiyyapatanaputi P, Gromov K, Goater JJ, Carmouche J, Zhang X, Rubery PT, Rabinowitz J, Samulski RJ, Nakamura T, Soballe K, O'Keefe RJ, Boyce BF and Schwarz EM. Remodeling of cortical bone allografts mediated by adherent rAAV-RANKL and VEGF gene therapy. *Nat Med*. 2005;11:291-7.
81. Salvay DM, Zelivyanskaya M and Shea LD. Gene delivery by surface immobilization of plasmid to tissue-engineering scaffolds. *Gene Ther*.
82. Shin S, Tuinstra HM, Salvay DM and Shea LD. Phosphatidylserine immobilization of lentivirus for localized gene transfer. *Biomaterials*. 2010;31:4353-9.
83. Shin S and Shea LD. Lentivirus immobilization to nanoparticles for enhanced and localized delivery from hydrogels. *Mol Ther*. 2010;18:700-6.
84. Shin S, Salvay DM and Shea LD. Lentivirus delivery by adsorption to tissue engineering scaffolds. *J Biomed Mater Res A*. 2010;93:1252-9.
85. Hu WW, Wang Z, Hollister SJ and Krebsbach PH. Localized viral vector delivery to enhance in situ regenerative gene therapy. *Gene Ther*. 2007;14:891-901.
86. Hu WW, Lang MW and Krebsbach PH. Development of adenovirus immobilization strategies for in situ gene therapy. *J Gene Med*. 2008;10:1102-12.
87. Hu WW, Elkasabi Y, Chen HY, Zhang Y, Lahann J, Hollister SJ and Krebsbach PH. The use of reactive polymer coatings to facilitate gene delivery from poly (epsilon-caprolactone) scaffolds. *Biomaterials*. 2009;30:5785-92.
88. Zhang Y, Deng X, Scheller EL, Kwon TG, Lahann J, Franceschi RT and Krebsbach PH. The effects of Runx2 immobilization on poly (epsilon-caprolactone) on osteoblast differentiation of bone marrow stromal cells in vitro. *Biomaterials*. 2010;31:3231-6.
89. Brunger JM, Huynh NP, Guenther CM, Perez-Pinera P, Moutos FT, Sanchez-Adams J, Gersbach CA and Guilak F. Scaffold-mediated lentiviral transduction for functional tissue engineering of cartilage. *Proc Natl Acad Sci U S A*. 2014.

90. Moutsatsos IK, Turgeman G, Zhou S, Kurkalli BG, Pelled G, Tzur L, Kelley P, Stumm N, Mi S, Muller R, Zilberman Y and Gazit D. Exogenously regulated stem cell-mediated gene therapy for bone regeneration. *Mol Ther.* 2001;3:449-61.
91. Peng H, Usas A, Hannallah D, Olshanski A, Cooper GM and Huard J. Noggin improves bone healing elicited by muscle stem cells expressing inducible BMP4. *Mol Ther.* 2005;12:239-46.
92. Urlinger S, Baron U, Thellmann M, Hasan MT, Bujard H and Hillen W. Exploring the sequence space for tetracycline-dependent transcriptional activators: novel mutations yield expanded range and sensitivity. *Proc Natl Acad Sci U S A.* 2000;97:7963-8.
93. Zhu Z, Ma B, Homer RJ, Zheng T and Elias JA. Use of the tetracycline-controlled transcriptional silencer (tTS) to eliminate transgene leak in inducible overexpression transgenic mice. *J Biol Chem.* 2001;276:25222-9.
94. Rendahl KG, Quiroz D, Ladner M, Coyne M, Seltzer J, Manning WC and Escobedo JA. Tightly regulated long-term erythropoietin expression in vivo using tet-inducible recombinant adeno-associated viral vectors. *Hum Gene Ther.* 2002;13:335-42.
95. Barde I, Zanta-Boussif MA, Paisant S, Leboeuf M, Rameau P, Delenda C and Danos O. Efficient control of gene expression in the hematopoietic system using a single Tet-on inducible lentiviral vector. *Mol Ther.* 2006;13:382-90.
96. Glass KA, Link JM, Brunger JM, Moutos FT, Gersbach CA and Guilak F. Tissue-engineered cartilage with inducible and tunable immunomodulatory properties. *Biomaterials.* 2014;35:5921-31.
97. Grant TD, Cho J, Ariail KS, Weksler NB, Smith RW and Horton WA. Col2-GFP reporter marks chondrocyte lineage and chondrogenesis during mouse skeletal development. *Dev Dyn.* 2000;218:394-400.
98. Carey BW, Markoulaki S, Hanna J, Saha K, Gao Q, Mitalipova M and Jaenisch R. Reprogramming of murine and human somatic cells using a single polycistronic vector. *Proc Natl Acad Sci U S A.* 2009;106:157-62.
99. Morris SA, Grewal S, Barrios F, Patankar SN, Strauss B, Buttery L, Alexander M, Shakesheff KM and Zernicka-Goetz M. Dynamics of anterior-posterior axis formation in the developing mouse embryo. *Nat Commun.* 2012;3:673.
100. Morris SA, Guo Y and Zernicka-Goetz M. Developmental plasticity is bound by pluripotency and the Fgf and Wnt signaling pathways. *Cell Rep.* 2012;2:756-65.
101. Morris SA, Teo RT, Li H, Robson P, Glover DM and Zernicka-Goetz M. Origin and formation of the first two distinct cell types of the inner cell mass in the mouse embryo. *Proc Natl Acad Sci U S A.* 2010;107:6364-9.

102. Torres-Padilla ME and Zernicka-Goetz M. Role of TIF1alpha as a modulator of embryonic transcription in the mouse zygote. *J Cell Biol.* 2006;174:329-38.
103. Estes BT, Diekman BO, Gimble JM and Guilak F. Isolation of adipose-derived stem cells and their induction to a chondrogenic phenotype. *Nat Protoc.* 2010;5:1294-311.
104. Hu DP, Ferro F, Yang F, Taylor AJ, Chang W, Miclau T, Marcucio RS and Bahney CS. Cartilage to bone transformation during fracture healing is coordinated by the invading vasculature and induction of the core pluripotency genes. *Development.* 2017;144:221-234.
105. Mandai M, Watanabe A, Kurimoto Y, Hirami Y, Morinaga C, Daimon T, Fujihara M, Akimaru H, Sakai N, Shibata Y, Terada M, Nomiya Y, Tanishima S, Nakamura M, Kamao H, Sugita S, Onishi A, Ito T, Fujita K, Kawamata S, Go MJ, Shinohara C, Hata KI, Sawada M, Yamamoto M, Ohta S, Ohara Y, Yoshida K, Kuwahara J, Kitano Y, Amano N, Umekage M, Kitaoka F, Tanaka A, Okada C, Takasu N, Ogawa S, Yamanaka S and Takahashi M. Autologous Induced Stem-Cell-Derived Retinal Cells for Macular Degeneration. *N Engl J Med.* 2017;376:1038-1046.
106. Engler AJ, Sen S, Sweeney HL and Discher DE. Matrix elasticity directs stem cell lineage specification. *Cell.* 2006;126:677-89.
107. Wen JH, Vincent LG, Fuhrmann A, Choi YS, Hribar KC, Taylor-Weiner H, Chen S and Engler AJ. Interplay of matrix stiffness and protein tethering in stem cell differentiation. *Nat Mater.* 2014;13:979-87.
108. Marturano JE, Schiele NR, Schiller ZA, Galassi TV, Stoppato M and Kuo CK. Embryonically inspired scaffolds regulate tenogenically differentiating cells. *J Biomech.* 2016;49:3281-3288.
109. McNary SM, Athanasiou KA and Reddi AH. Transforming growth factor beta-induced superficial zone protein accumulation in the surface zone of articular cartilage is dependent on the cytoskeleton. *Tissue Eng Part A.* 2014;20:921-9.
110. Murphy WL, McDevitt TC and Engler AJ. Materials as stem cell regulators. *Nat Mater.* 2014;13:547-57.
111. Wiznerowicz M and Trono D. Conditional suppression of cellular genes: lentivirus vector-mediated drug-inducible RNA interference. *J Virol.* 2003;77:8957-61.
112. Hotta A, Cheung AY, Farra N, Vijayaragavan K, Seguin CA, Draper JS, Pasceri P, Maksakova IA, Mager DL, Rossant J, Bhatia M and Ellis J. Isolation of human iPS cells using EOS lentiviral vectors to select for pluripotency. *Nat Methods.* 2009;6:370-6.
113. Szulc J, Wiznerowicz M, Sauvain MO, Trono D and Aebischer P. A versatile tool for conditional gene expression and knockdown. *Nat Methods.* 2006;3:109-16.

114. Gossen M, Freundlieb S, Bender G, Muller G, Hillen W and Bujard H. Transcriptional activation by tetracyclines in mammalian cells. *Science*. 1995;268:1766-9.
115. Salmon P and Trono D. Production and titration of lentiviral vectors. *Curr Protoc Neurosci*. 2006;Chapter 4:Unit 4 21.
116. Bean AC and Tuan RS. Fiber diameter and seeding density influence chondrogenic differentiation of mesenchymal stem cells seeded on electrospun poly(epsilon-caprolactone) scaffolds. *Biomed Mater*. 2015;10:015018.
117. Li WJ, Chiang H, Kuo TF, Lee HS, Jiang CC and Tuan RS. Evaluation of articular cartilage repair using biodegradable nanofibrous scaffolds in a swine model: a pilot study. *J Tissue Eng Regen Med*. 2009;3:1-10.
118. Yang G, Lin H, Rothrauff BB, Yu S and Tuan RS. Multilayered polycaprolactone/gelatin fiber-hydrogel composite for tendon tissue engineering. *Acta Biomater*. 2016;35:68-76.
119. Zheng P, Yao Q, Mao F, Liu N, Xu Y, Wei B and Wang L. Adhesion, proliferation and osteogenic differentiation of mesenchymal stem cells in 3D printed poly-epsilon-caprolactone/hydroxyapatite scaffolds combined with bone marrow clots. *Mol Med Rep*. 2017;16:5078-5084.
120. Pelttari K, Winter A, Steck E, Goetzke K, Hennig T, Ochs BG, Aigner T and Richter W. Premature induction of hypertrophy during in vitro chondrogenesis of human mesenchymal stem cells correlates with calcification and vascular invasion after ectopic transplantation in SCID mice. *Arthritis Rheum*. 2006;54:3254-66.
121. Chen FH and Tuan RS. Mesenchymal stem cells in arthritic diseases. *Arthritis Res Ther*. 2008;10:223.
122. Moutos FT, Estes BT and Guilak F. Multifunctional hybrid three-dimensionally woven scaffolds for cartilage tissue engineering. *Macromol Biosci*. 2010;10:1355-64.
123. Tian H, Zhao J, Brochmann EJ, Wang JC and Murray SS. Bone morphogenetic protein-2 and tumor growth: Diverse effects and possibilities for therapy. *Cytokine Growth Factor Rev*. 2017;34:73-91.
124. McCollum PT, Bush JA, James G, Mason T, O'Kane S, McCollum C, Krievins D, Shiralkar S and Ferguson MW. Randomized phase II clinical trial of avotermin versus placebo for scar improvement. *Br J Surg*. 2011;98:925-34.
125. So K, McGrouther DA, Bush JA, Durani P, Taylor L, Skotny G, Mason T, Metcalfe A, O'Kane S and Ferguson MW. Avotermin for scar improvement following scar revision surgery: a randomized, double-blind, within-patient, placebo-controlled, phase II clinical trial. *Plast Reconstr Surg*. 2011;128:163-72.

126. Moutos FT, Glass KA, Compton SA, Ross AK, Gersbach CA, Guilak F and Estes BT. Anatomically shaped tissue-engineered cartilage with tunable and inducible anticytokine delivery for biological joint resurfacing. *Proc Natl Acad Sci U S A*. 2016;113:E4513-22.
127. Paige KT, Cima LG, Yaremchuk MJ, Schloo BL, Vacanti JP and Vacanti CA. De novo cartilage generation using calcium alginate-chondrocyte constructs. *Plast Reconstr Surg*. 1996;97:168-78; discussion 179-80.
128. Erickson GR, Gimble JM, Franklin DM, Rice HE, Awad H and Guilak F. Chondrogenic potential of adipose tissue-derived stromal cells in vitro and in vivo. *Biochem Biophys Res Commun*. 2002;290:763-9.

## Biography

Shannon Kathleen O'Connor was born in Billings, Montana. She earned her B.S. in Biomedical Engineering from the Johns Hopkins University in May 2009, and began in the Medical Scientist Training Program at Duke University in the summer of 2009. Her PhD advisor is Dr. Farshid Guilak, formerly at Duke University, and currently in the Department of Orthopaedics at Washington University and Shriner's Hospital for Children in St. Louis, MO.

### **Shannon has received the following educational fellowships / scholarships:**

1. Medical Scientist Training Program, Duke University: T32GM007171
  - NIH supported grant to support MD/PhD training
2. Graduate Student Fellowship, Duke University: F31ARQ68217
  - NIH supported grant to support PhD training
3. R. Sanders Williams Summer Research Fellowship, Duke University
  - Duke fellowship to support summer research before med school
4. Charles R. Westgate Scholarship, Johns Hopkins University
  - 4-year merit scholarship awarded in undergraduate engineering
5. Davis Scholarship, United World College, USA
  - 2-year merit scholarship for the IB diploma program

### **Shannon has published the following articles:**

1. Diekman BO, Thakore PI, **O'Connor SK**, Willard VP, Brunger JD, Christoforou N, Leong KW, Gersbach CA, and Guilak F. Modulating the expression of the cell cycle inhibitor p21 to enhance cartilage formation by

iPSCs. Tissue Engineering Part A. 2014.

2. Varadraj V, Wallace C, Wu M, Chao J, **O'Connor SK**, Raleigh A, Liu X, Haugh J, Reichert W. Bioactive Surfaces with Oriented and Patterned Protein for Real-Time Tracking of Cell Migration. Colloids Surf B Biointerfaces. 2014. Nov;123:225-35.
3. McNulty A, Miller M, **O'Connor SK**, Guilak F. The effects of adipokines on cartilage and meniscus catabolism. Connective Tissue Research. 2011. Jul;52(6):523-33.
4. **O'Connor S**, Li E, Majors BS, He L, Placone J, Baycin D, Betenbaugh MJ, Hristova K. Increased expression of the integral membrane protein ErbB2 in Chinese hamster ovary cells expressing the anti-apoptotic gene Bcl-xL. Protein Expr Purif. 2009. Sep;67(1):41-7.

**Shannon has presented the following posters:**

1. **O'Connor SK**, Katz D, Oswald S, Guilak F. Chondrogenic differentiation of induced pluripotent stem cells and formation of cartilaginous extracellular matrix prevents re-induction of pluripotency. The Orthopaedic Research Society Annual Meeting: New Orleans, LA. 2018.
2. **O'Connor SK**, Willard VP, Brunger J, Moutos F, Guilak F. Cartilage and bone tissue engineering on 3D-woven scaffolds with induced pluripotent stem cells. The Gordon Research Conference, Musculoskeletal Biology and Bioengineering: Andover, NH. 2016.

3. **O'Connor SK**, Willard VP, Diekman BO, Moutos F, Christoforou N, Leong KW, Guilak F. Cartilage tissue engineering with induced pluripotent stem cells on 3-dimensional woven scaffolds. The 29th Annual MD/PhD Student Keystone Conference: Keystone, CO. 2014.
4. Willard VP, Diekman BO, Sanchez-Adams J, **O'Connor SK**, Christoforou N, Leong KW, Guilak F. An induced pluripotent stem cell-based model of osteoarthritis for therapeutic screening. North Carolina Tissue Engineering and Regenerative Medicine Society conference: Winston-Salem, NC. 2013.
5. Diekman BO, Willard VP, Sanchez-Adams J, Sun H, Christoforou N, **O'Connor SK**, Leong KW, Guilak F. Tissue engineered cartilage using induced pluripotent stem cells for in vitro modeling of osteoarthritis. World iPS Cell Summit: Boston, MA. 2012.
6. He L, **O'Connor SK**, Shobnam N, Hristova K. Effect of short transmembrane peptides on the activation and dimerization of an FGFR3 pathogenic mutant. Experimental Biology Conference: New Orleans, LA. 2009.
7. **O'Connor SK**, Taboas J, Tuan R. Protecting against arthritis with physiologic loading and gene therapy. Biomedical Engineering Summer Internship Program: Bethesda, MD 2008.
8. **O'Connor SK**, He L, Li E, Placone J, Betenbaugh M, Hristova K. Membrane protein expression in anti- apoptotic mammalian cells. Biophysical Society's 51st Annual Meeting: Baltimore, MD. 2007.

9. He L, Li E, **O'Connor SK**, Placone J, Hristova K. Probing the biophysical and molecular mechanism of pathogenic mutations in the transmembrane domain of Fibroblast Growth Factor Receptor 3. Biophysical Society's 51st Annual Meeting: Baltimore, MD. 2007.
10. Aleem A, Corcoran-Schwartz I, Stellmach B, Suvarna N, Bararpour L, Mallipudi R, **O'Connor SK**, Soumare A, Xiao A, Young D. Detection of Airborne *mycobacterium Tuberculosis*. Biomedical Engineering Design Team presentation: Baltimore, MD. 2006.

**Shannon has given the following research talks:**

1. Bridging Engineering and Medicine: a Duke MSTP Student's Perspective. Medical Alumni Council meeting. Durham, NC. April 2015.
2. Linking the School of Medicine to the School of Engineering: an MSTP Student's Perspective. Medical Center Academic Affairs Committee of the Board of Trustees. September 2014.
3. IPSCs, Elastin-Like Peptide, and 3D Woven PCL Scaffolds for Cartilage Tissue Engineering Applications. MSTP lunch talk. Durham, NC. April 2014.
4. Induced pluripotent stem cells for cartilage tissue engineering applications. Duke MSTP retreat. Wilmington, NC. September 2012.